2018

# Reliability and Resiliency Driven Solutions for Electric Power Systems Operation and Planning

Kwami Senam Afenefa Sedzro
*Lehigh University*

# RELIABILITY AND RESILIENCY DRIVEN SOLUTIONS FOR ELECTRIC POWER SYSTEMS OPERATION AND PLANNING

by

KWAMI SENAM A. SEDZRO

Presented to the Graduate and Research Committee

of Lehigh University

in Candidacy for the Degree of

Doctor of Philosophy

in

Electrical Engineering

Lehigh University

May, 2018

Approved and recommended for acceptance as a dissertation in partial fulfillment of the requirements for the degree of Doctor of Philosophy.

_____
Date

_____
Date Accepted

_____
Dissertation Advisor

Committee Members:

_____
Prof. Shalinee Kishore
(Committee Chair)

_____
Prof. Alberto Lamadrid

_____
Prof. Wenxin Liu

_____
Prof. Lawrence V. Snyder

# Acknowledgements

At the very outset of this dissertation, I would like to extend my sincere and heartfelt thanks to the many people who have given me their unfailing support and greatly contributed towards my development and success. The completion of this undertaking could not be possible without them. Many may not find their names in this section, but their contributions are highly appreciated and acknowledged.

Above all, all thanks to Jehovah God the Almighty who has never let us down.

I would like to thank my dear wife Perla for her unconditional love, patience, understanding and unequivocal support. Likewise, I am deeply grateful to our children Othniel, Nathan, Ethan and Alva. Their being well-behaved and orderly has minimized my fathering time and energy for the benefit of my research projects.

To my advisor and "elder sister", Prof. Shalinee Kishore, I owe my utmost gratitude for her continuous support and encouragement. Without her expertise, tactful leadership and boundless kindness, I could not carry out this endeavor. Her enduring support, selflessness and belief in my abilities enabled me to explore the different research topics in this dissertation with confidence and resolve. At a time of our journey when thick shadows of sorrow overcast our horizon, she did not hesitate to undertake the role of a sister. May she find throughout these lines my family's deepest recognition.

Before the start of my PhD journey, I was fortunate enough to meet Prof. Alberto J. Lamadrid to whom I am extremely grateful for his leadership, trust, unending support and outstanding contribution to the success of this work. His unique knowledge in power systems, economics and operations research has shaped this dissertation. His dedication and incredible work ethic are priceless qualities I will continue match. Above all, my family will always remember his personal help beyond the research meeting rooms.

I would like to thank Prof. Wenxin Liu for his insightful advice, his power systems expertise

and his kindness. I will not forget our many ad-hoc meetings, thanks to his availability and unconditional willingness to help. My wife still remembers the day he gave me a ride to the LVHN Cedar Crest hospital when Ethan was born.

I owe a deep sense of gratitude to Prof. Larry V. Snyder for his trust, knowledge and contributions. I had the privilege to have this world-class OR expert as my M.Eng. capstone project mentor. Without a doubt, this project is the one that set the tone for my PhD research interest. I want to express my sincere thanks for his help in reviewing my personal statement and statement of purpose, critical parts of a PhD application.

I would like to thank Prof. Luis F. Zuluaga for his advice and contributions to this work. His qualitative reviews of my research articles are very much appreciated. His priceless professional advice will continue to shape my career path.

It is a great pleasure for me to express my heartfelt gratitude and genuine admiration for Prof. Mooi C. Chuah for her trust, abnegation, contributions and direction. I started this journey under her leadership. Her genuine and relentless dedication is a unique gem in the treasure I found at Lehigh University.

This endeavor could not be possible without the strategic planning of my Director and "mother" Martha Dodge, past Director of the ESEI program. I very much appreciate her direction towards the PhD program and connecting me with the appropriate resources. Many thanks to Eileen Kaplan, past ESEI program coordinator, for her time and advice.

To the current ESEI staff, Dr Rudy Shankar and Wendy Vohar, I express my deep appreciation for giving me so many opportunity to talk about my research and personal technology interests. I am also thrilled to serve on the program's Strategic Advisory Council.

I extend my appreciation to my colleagues Parth Pradhan, Kostas Hatalis and Xin Shi for their countless discussions and insightful collaboration on our joint projects. Xin's contribution to Chapter 7 is significant.

To my 2014 ESEI graduate friends of all times, Dean Weng, Sarah Conde and Lauren Strella, I express my heartfelt gratitude for their unconditional and faithful friendship.

My thanks go to my industry mentors, friends and colleagues at PJM Interconnection for their support, camaraderie, and enjoyable conversations: David Hislop, David Schweizer, Jason Sexauer, Joseph Mulhern, Wayne Moodie, Elizabeth Anastasio. I am also grateful for our staff members David Morrisette, Diane Hubinsky, Ruby Scott, Jessica Berton and Shakuntala Jain-Cocks who were always very helpful and caring.

These acknowledgements would not be complete without the mention of the Assistant Dean and personal friend Donna Mohr for her unconditional support. I will not forget her umbrella.

I owe a deep recognition to Prof. John Coulter, Associate Dean for Graduate Studies, for his mentorship through the P.C. Rossin Fellows' program. Many thanks to Brianne Lisk for her assistance in the program and her help at the different administrative stages of the graduate program.

I am indebted to Erin Kintzer and Cathy Albertson of the Real Estate Office, for offering us a safe, affordable and convenient housing conditions that reduced my stress and worries.

I would like to express my appreciation to Kathleen S. Hutnik, Associate Dean and Director of Graduate Student Life and to Dr Henry U. Odi, Deputy Vice President for Equity and Community and Associate Provost for Academic Diversity, for their encouragement.

To my friends and Fulbright brothers, Brad Hounkpati, Tete Tevi and Pimam Manzi, I extend my cordial gratitude for their faithful support throughout these years. I would also like to express my sincere and special appreciation to my friend and former student Maskana Adedjouman, M.Eng. student in Structural Engineering at Lehigh, for his company.

To the Public Affairs Section of the US Embassy in Togo and the board of the Fulbright Program, I am forever indebted. I could not have afforded my studies at Lehigh without their support.

I am specially grateful to all funding agencies (U.S. Department of Energy, National Science Foundation, PITA Grants, etc.) that supported our projects.

The importance of the support and encouragement I received from my father could not be overstated. His life is a living example for me, even though he is currently resting in death. The education he gave me is an active inheritance share. Many thanks to my mom for instilling in me the tenacity needed to complete this journey.

# Contents

# List of Tables

# List of Figures

# Abstract

The presented research entails three critical areas of the electric power systems that can significantly impact its reliability and resiliency: retail market design (Chapters 2 - 4), renewable integration (Chapter 5) and post-disturbance grid recovery (Chapter 6).

With the increase of intermittent renewable resource on the electric grid, comes the potential for more reliability issues. To increase reliability and efficient operation of the electric grid in presence of renewables, a novel retail electricity pricing scheme (GenMinimax) is introduced. The scheme incentivizes end-users to efficiently follow system operators/utilities optimal supply signals while shaping their demand for lower energy bills. The presentation will highlight the performance of GenMinimax compared to that of Time-of-Use and Real-time pricing. GenMinimax is preceded by Minimax pricing, which helps improve the load factor.

Next, the work focuses on renewable market integration modeling. To increase renewable energy farms marketability and integration while interfacing the grid from the inherent volatility of their output, we devised optimal storage-based reliability-aware portfolio bidding strategies that enable them to participate in multiple markets and play an active role in grid reliability. A short-term reserve market was proposed and proved beneficial for both renewable farms and grid operation.

The third solution area aims at devising post-disturbance restoration strategies for resilient power systems. For an efficient recovery after large disturbances such as weather-related power outages, a post-disaster microgrid formation model is proposed. The model applies to any type of network topology and accommodates demand-responsive loads and fixed or mobile distributed black-start resources for grid recovery operation and planning. A heuristic approach introduced, proves to reduce the CPU time.

# Chapter 1

# Introduction

## 1.1 Minimax pricing, providing incentives to improve the load factor

Over the past 5 years, the average price of electricity for residential consumers in US has increased by 29% [3]. Over the last 20 years, the residential electricity demand in US has increased 49% due to increasing number of energy-consuming household devices [4]. As a result, the average home electricity bill now accounts for 2.8% of household income [4, 5]. The most direct way for consumers to reduce their electricity bills is to simply use less electricity but this is not realistic since each household has more and more energy-consuming devices e.g. more smartphones and laptops. Another way to reduce the cost is to reduce demand peaks since a significant fraction of the electric grid's capital and operational expenses is incurred for satisfying its peak power demands. The marginal cost for generating electricity is non-linear and increases rather exponentially as more costly generators are used to meet peak demands [4]. Utilities have also explored using large-scale centralized energy storage systems at strategic points within the grid to reduce peak demands [6]. Consumers too are incentivized to install and control their own small-scale energy storage systems [7,8] to reduce peak demands. In addition, to reduce peak demands, many utilities have explored using market-based charging schemes instead of the conventional fixed-rate pricing model. For example, Time of Use (TOU) pricing scheme which charges more during peak hours and less during off-peak hours is being used in Ontario [9]. Three different price tiers (off-, mid- and peak) are used. Similarly, Illinois already requires utilities to provide residential consumers the option of using day-ahead wholesale hourly electricity prices [10]. However, such pricing schemes

put too much burden on consumers to continuously monitor their usage to reduce costs. Consumers may need to install batteries to allow them to use less energy during peak hours and re-charge the batteries during off-peak hours. Such installation costs them money and hence not many are willing to respond to price changes and hence the grid operators may not see any cost-saving benefits of peak reduction. Furthermore, there is a possibility of increasing grid peaks if demand is highly elastic and responsive to price changes [4]. The authors in [4] show that the peak demand will migrate to the previously off-peak period and might increase peak demand by nearly 120% if TOU pricing scheme is used. With Real-Time Pricing, peak demand might decline and off-peak demand might increase, so the price difference between peak and off-peak prices narrows and hence the benefits of energy storage might also decrease which discourages consumers from adopting the RTP.

The present work designs a new pricing scheme called the *Minimax* scheme which incentivizes consumers to schedule their deferrable demands such that they can see reduction in energy bills without causing the system to experience increase in peak load demands.

## 1.2 The Value of Aggregation Under Minimax

Responsiveness of demand is key in any efficient energy management program [11]. Price has been extensively used as a management tool to incentivize end-users [12]. Witness, most demand response (DR) programs are either cost reduction based or reward based [13]. However, for consumers to participate in DR programs, they must have DR resources available [14]. These are deferrable loads whose start-up can be shifted to another time, curtailable loads which can be simply kept off-line, and interruptible loads which can be turned off if needed. Even if DR programs encounter success in industry [15], they hardly write the same succes story in residential settings due to small amount of deferrable load at individual end-user premises [16] The more DR resource one has available, the more flexible his demand is in adjusting to different DR signals. By pooling their individual DR resources, aggregate consumers can unleash the market power of the load. Indeed, few works discussed the benefits of load aggregation benefits of demand aggregation in the context of deregulated power industry. For instance Barsali et al. in [17] point out that load aggregation provides simplified balancing procedures, helps achieve consumption thresholds and provides consumers with contractual power which makes them non-negligible players in the power and energy market. In fact, Kirby [18] showed that loads can even provide more reliable

contingency reserves than generators.

In this work, we explore both economical and technical benefits of load aggregation under the electricity retail pricing scheme, Minimax, introduced in 2.

## 1.3 GenMinimax pricing, a market tool for reliable electric grids

In electricity wholesale markets, producers, utilities, aggregators and load serving entities (LSE), amongst others, trade energy under the management of a system operator (SO). The wholesale price, set frequently (e.g., every 15 minutes), is settled by the dynamic equilibrium of supply and demand. It is under such dynamic pricing situation that retailers buy electricity and resell it to consumers who cannot directly participate in the wholesale market. The retail pricing design is based on how much uncertainty or risk end-users are willing to face, and the availability of both long and short-term contracts.[1] There are two major forms of tariffs found in literature: static and dynamic pricing.

In the case of static pricing, consumers are isolated from the wholesale dynamics, leading to perfectly inelastic demands with respect to prices [14]. In compensation, as part of the flat rate, consumers pay an insurance premium against the risk of price spikes [14, 19, 20].

In dynamic pricing, a measure of wholesale market uncertainties is passed onto end-users, taking advantage of the price elasticity of demand. The contracts offered to consumers are generally based on the uncertainty level in wholesale markets, sometimes with provisions included to take advantage of the consumer's willingness to pay for coverage against price spikes.The most common forms of dynamic pricing include time-of-use (TOU), critical peak pricing (CPP), peak time rebate (PTR), variable peak pricing (VPP), real time pricing (RTP) [13, 21–23].

Faruqui et al. observed in 34 projects across seven countries that TOU contracts induce 3 to 6% drop in peak demand, while CPP led to a 13 - 20% drop [22], with differences driven by the heterogeneities in rates. The authors in [4] show that the peak demand may migrate to the previous off-peak period and might be increased by nearly 120% if TOU is used. In our previous work [24], we also showed through simulation that TOU might result in a higher peak demand if a consider-

[1] In this work, we focus on short-term contracts.

able number of consumers simultaneously shift their flexible loads to off-peak hours. Even if RTP tends to be the most efficient retail pricing scheme [25–27], it does not guarantee peak demand reduction as proven in [24]. McDonald & Lo point to social welfare as a fundamental basis for retail pricing design [28]. However, the communication technology and automation requirements of RTP along with the uncertainty related anxiety caused to consumers seems to be far greater than any potential bill reduction. Therefore, there are challenges associated with TOU and RTP in terms of consumers' incentives to follow the wholesale optimal energy profile. These schemes do not ensure peak demand reduction, which is crucial for a more economical management of the installed capacity. As Triki and Violi in [29] show, even customers with low consumptions during peak periods are charged the same high rates caused by those who contribute more significantly to the high peak demands [30], which is not fair. Hence, there is a pressing need to rethink retail electricity pricing so as to achieve price responsive demands through price signals, while ensuring reasonable peak demands. For DR resources to trigger the demand to follow the supply [31] in a price-based DR environment, every participant should be encouraged to follow the supply signals. To this end, [29] proposed a hybrid two-component pricing scheme made of a flat tariff followed by a recourse dynamic price that captures the stochasticity of supply and demand. By combining static and dynamic pricing, the authors in [29] aimed to flexibly compensate the shortcomings of both pricing types with their benefits. The only challenge for the customers is that they do not know their energy price until their demand is realized. To address uncertainty and reduce end-users' anxiety while enabling price responsiveness of demand and achieving lower peak loads, we introduced in Chapter 2 [24]. The presented research formulates the interaction between the players in the framework of our proposed reliability-driven pricing scheme as a bilevel (or more accurately, two-stage) optimization problem.

Previous works on bilevel optimization [32, 33] usually have decision variables between inner and outer problems depending on each other. In this work we propose an approximation method to decouple these decisions. We measure the performance of the consumers' decisions given the load aggregator signal. In our model, the follower's decision mostly affects her own payoff, contrasting with models where the leader has to readjust his strategy depending on the follower's response (see e.g., [34–36]). We solve first the inner problem, and the optimal solution is used as input to the outer problem. This approximation improves computational tractability while maintaining the salient features of the model. A strand of the literature studies the incentives to manipulate the

market prices to their own advantage [37–39]. We impose incentive compatibility conditions for the consumer group to modify their behavior in response to the aggregator's signal and remediate this issue. Further, more sophisticated and intelligent energy consumption management approach exists in the literature (e.g. [40]) but most of them may not be readily applicable due to their complexity for customers or their cost compared to their potential benefits. We propose a day-ahead scheduling model that produces a schedule any commercially available energy management system can implement. Finally, there is a growing body of literature [41–44] showing that load aggregation is beneficial to both consumers and the grid due to its potential to reduce electricity market average prices, provide more flexibility in shaping demand profiles and achieve greater savings for customers.

In this work, we generalize the approach introduced in Chapter 2 [24] to any reference supply curve having in mind the high renewable penetration expected worldwide by 2020 [45].

## 1.4 Reliabilty-aware Renewable Integration: Introduction of a Short-term Reserve Market

The first and most daunting enemy of renewable energy integration into the electric grid remains its inherent intermittency. This poses a reliability threat to the electric grid in addition to demand variability and the unpredictable contingencies related to generation, transmission and distribution. Reserves are needed to balance supply-demand mismatches. The reserve market constitutes a critical asset for reliable and economic system operation in providing, whenever necessary, the missing portion of needed energy at an acceptable cost. Thus, with high renewable penetration, the capacity of reserve (as an insurance premium) is expected to increase [46]. This can prove to be a handicap for renewable integration since reserve costs may increase as well, limiting the achievable percentage of renewable penetration for a reliable grid. To mitigate this reliability issue, it is reasonable to involve renewable farms in the grid reliability efforts. In the attempt of making renewable farms responsible for any mismatch between their day-ahead commitment and their actual power output, some market policies impose supply shortfall penalties [47].
The focus of a significant amount of research in the literature is on devising better methods of integrating renewable energy converters (REC) into the existing power grid. A first category of work seeks solution in more accurate short-term (24-36 hours) forecasting techniques [48–50]. Neverthe-

less, forecasting errors cannot be completely eliminated. Thus, even though improving forecasting accuracy could significantly contribute to reliability, the research community have sought after other renewable integration strategies. Bathurst et. all [48] evaluated several market structures in order to suggest to policy makers and market operators the one that promotes a fair and reliable wind power integration. They came to the conclusion that the market clearing price calculation should not account for wind generation. Makarov et al. [51] contemplate intra-day markets as critical to improving reliability of offered wind contracts given that short term forecasts tend to be more accurate. Castronuovo and Lopes [52] designed a combined wind and hydro system where the pump hydro is aimed at shifting the output of the wind energy converter (WEC) in time.

In the specific scope of this work, Dukpa et al. proposed an optimal participation strategy for a WEC coupled with an energy storage system (ESS) that maximizes profit and mitigate the risk of supply shortfalls. The authors confirm that it is imperative to combine a REC with an ESS to increase reliability and profitability. Bathurst et al. [48], Matevosyan and Soder [53], and Morales et al. [54] studied the wind farm profit maximization problem in a stochastic programing approach. Botterud et al. [55], and Morales et al. [54] further added a risk sensitivity term, the conditional value at risk (CVaR) to the objective in order to control the variability of the expected profit. Pinson et al. [56] proved that the optimal day-ahead bid can be expressed as a probabilistic quantile on prices as in the newsvendor problem, a classic problem in inventory theory [57]. Dent et al. [58] allow wind and imbalance prices to be correlated, taking into account the practical impacts of wind power injection on system balance. Moreover, Bitar et al. [59] derived an explicit formulae for optimal contract offering and the corresponding optimal expected wind farm profit in a competitive two-settlement market settings.

In this work, we exploit the analytical results of [59] to derive a criterion for renewable farms' participation in the grid reliability efforts.The renewable energy farms' bidding strategy is formulated as a portfolio optimization problem assuming a storage system. The portfolio is made of the day-ahead, real-time and short-term reserve offers. We first start by analyzing the renewable day-ahead bidding problem as a newsvendor one. We formulate the farm's intra-day strategy as a two-stage stochastic optimization problem. Next we evaluate the impact of the short-term reserve market opportunity on the farm's profitability, at different levels of risk aversion. The main contribution of this chapter is the assessment of potential benefits, if any, renewable energy resources

would have in participating in short-term reserve markets with both capacity and energy offers. The study also presents the change in risk range and profit reduction that result from the reserve market. By separating the day-ahead and intra-day strategies, we aim to emphasize the corrective nature of the intra-day market.

## 1.5 Post-disaster Grid Recovery Through Optimal Microgrid Formation

The socio-economic losses due to power outages during the last decades are evidence that enhancing the ability to rapidly restore the functionality of the power system is a fundamental concern for operators and planners. According to the Executive Office of the President, weather-related outages are estimated to have cost the U.S. economy an inflation-adjusted annual average of $18 to $33 billion over the period from 2008 to 2012 [1]. Campbell estimates that weather-related outages cost the U.S. between $20 and $55 billion annually [60], and superstorm Sandy, the second most costly storm in US history, left 8.5 million customers without electricity across 15 U.S. states [61]. The National Centers for Environmental Information (NCEI) [62] reports 196 weather and climate disasters from 1980 to 2016 in the U.S., with related costs of approximately $1 billion, adjusted by the consumer price index (CPI). Further, according to NERC, all of the top-10 most severe power outages (ranked based on the severity risk index - SRI) in 2014 were initiated or aggravated by weather events [63].

Even though operational reliability and the effects of events with low impact but medium to high probability of occurrence have long been in the realm of system operators [64], the capacity to restore the functionality of the system after a low probability, high impact event, what we define as *grid resilience*, is garnering increasing attention. The severe impact of natural disasters on the electric power system and the increasing trend of power outages has been considered in [1]. The criticality of resiliency in grid modernization efforts has been considered in [65]. Descriptive studies, such as [66], examine the resiliency of the power network by developing spatial and non-spatial econometric models to estimate factors affecting the restoration time, including the restoration priority, infrastructure characteristics and weather related variables. Generally, strategies to deal with extreme event disruptions can be grouped into two broad categories: preventive and corrective actions. The objective of preventive pre-disaster strategies is to find the most potentially vulnerable components in order to replace or upgrade them before any potential disturbance. Preventive

actions include but are not limited to installing power lines underground, reinforcement of poles, management of vegetation and stockpiling of power lines [67]. However, strategies such as installing lines underground cost two to ten times as much as overhead lines [68], and create issues with restoration [69]. Other works, such as Ma et al. [70], approach the grid resilience enhancement problem from a preventive viewpoint by proposing an optimal hardening strategy that finds critical components (lines, poles, etc.). This is done through a greedy search that minimizes the hardening investment cost.

Corrective strategies are scenario-based backup plans designed to reduce the impact of a disaster, if any, and recover from disruptions as quickly as possible. In a corrective approach, Sarkar et al. [71] propose an adaptive distribution grid restoration method based on tie-line switching that is formulated as a non-linear mixed-integer program (MIP) that is solved by a greedy search algorithm to reduce the combinatorial search space. Choobineh and Mohagheghi [72] propose a non-linear MIP to optimally dispatch energy resources within a microgrid subject to capacity and fuel availability constraints, in the aftermath of a natural disaster. However, [72] does not address how the post-disaster microgrids are formed.

Several system restoration models have been proposed in the literature to circumvent either reliability or resiliency disrupting events (see, e.g., [73]). Ren et al. [74] develop a multi-agent system with a dynamic agent team forming mechanism for interconnected power systems restoration. Nagata et al. [75] propose a multi-agent framework for power system restoration in which bus agents are coordinated by a facilitator agent in order to reach a suboptimal system configuration after fault events, ten years before the work in [74]. Kirschen and Volkmann [76] introduce a hierarchically structured expert system that separates strategic and tactical reasonings in order to minimize the restoration time. The same grid resiliency is the subject of Z. Wang and J. Wang [77], formulating a stochastic self-healing model, that accounts for intermittent energy resources. Farzin et al. [78] devise a two-stage hierarchical outage management scheme to enhance the resilience of a multi-microgrid distribution system as a mixed-integer linear program (MILP) using the total energy curtailment as a resiliency index. In [78] the authors assume that the distribution grid is designed as a collection of microgrids with a known structure prior to the events. In fact, microgrids are considered as key assets in improving grid resilience and studies to validate them as a viable grid hardening solution are being conducted by New York, Connecticut and California as well as the U.S. Department of Energy. One of the most attractive features of microgrids is their ability to operate in island and grid-connected modes [79]. Tan et al. [80] propose a grid recovery

scheme based on a black-start sequence algorithm and spanning tree search, assuming that a fixed distributed generator (DG) with black-start capability is available after the disaster. Microgrids are first formed around the DG units without including any load. Loads belonging to microgrids are picked up according to Kirchhoff's laws and other critical isolated loads are connected through a spanning tree search. Gao et al. [81] introduce a critical load restoration method using microgrids and considering generation resource availability as well as uncertainties associated to intermittent energy sources and loads in a continuous operation time mode. Guidelines on microgrid operation and system restoration dynamics can be found in [82, 83].

Most of the existing methods based on topological control seek to isolate the faulted line or area by reconfiguring the feeder to allow as much load as possible to be served. A general assumption when these strategies are applied to the distribution grid is that the substation (the interface between the transmission and distribution systems) is healthy after the fault. Recent work by Chen et. al [84] relaxes this assumption in the context of *chaotic* weather events where the only supply solutions available following the disaster might be DG units arbitrarily positioned. The problem then transitioned from a topological structure alteration to a network partitioning problem where each partition, called a *microgrid*, is supplied by a DG. However, the MILP model proposed applies only to radial distribution grids, in which there is only one generation bus. In [84], the DG units are prepositioned, possibly precluding to reach maximum load pick-up. In [85], the authors address this DG location constraint by dynamically allocating DG units to candidate nodes. They assumed DG units to be mobile emergency generators (e.g., truck-mounted), a conjecture consistent with overall restoration efforts. In fact, amongst the lessons learned after the severe ice storm that affected eastern Canada and the northeastern US from 20 to 23 December 2013, the use of large-scale portable Diesel generators comes out as recommended in the preparedness process [86]. These emergency generators can be placed in any location where there may be a need to support the microgrid formation. However, the distribution system model considered in [85] is still one with a single microgrid root.

In this work, we extend the previous work, particularly [84],[2] to account for a future grid, where the direction of flows on a given branch is not necessarily known beforehand. We focus on resiliency events assuming reliability as a prerequisite [87–89]. Our main contributions are (1) we do not assume a radial network, allowing distribution systems where consumers may have energy sources on their premises, in which case the direction of the flow on a given branch is not predetermined,

[2]See the Appendix for a detailed discussion.

that is, the relationship parent-child nodes is reversible because there are potentially multiple root nodes; (2) we account for both fixed and mobile DG units that can be optimally placed in the system, and evaluate the benefits that this optimal location has on the objective function, a proxy for social welfare.

Throughout this chapter, it is assumed that the state of the network (after a possible disruption) is known before designing the microgrids. For articles in which the state of the network is not known in advance, but a much simpler microgrid design problem is required to be solved, we direct the reader to Eskandarpour et al. [90] and the references therein.

## 1.6 A Heuristic Approach to the Post-disturbance Microgrid Formation Problem

The dependence of humanity on electricity renders its unavailability truly handicapping, making the electric power systems extremely critical. Nevertheless, disruptions are becoming more frequent due to extreme weather events such as floods, tsunamis, hurricanes, earthquakes and ice storms. Between 2009 and 2014, the number of power outages has increased by more than 200% (see Fig. 1.1). During Hurricane Sandy, 8.5 million people were left without electricity [61]. The Executive Office of the President estimates the inflation-adjusted annual average cost of weather-caused power outages to be between 18 and 33 billion dollars over the period from 2008 to 2012 [1]. According to Campbell [60], weather-related grid disruptions cost the U.S. economy between 20 and 55 billion dollars annually. At 2:30 pm EDT 09/11/2017, hurricane Irma caused loss of power to more than 7 million customers in Florida, Georgia and South Carolina [91]. In addition to weather events, the increasing use of information technology in power system operation makes cyber-physical attacks a real resiliency threat to the electric grid.

Due to the high impact of the above-mentioned disruptions, their mitigation strategies are garnering increasing attention [65]. Prevention and corrective solutions have been widely proposed and explored in the literature. In particular, preventive action plans include revising design, siting and construction standards, promoting systematic inspection and maintenance schedules, developing best operating practices, and implementing cyber and physical security measures such as system hardening, component upgrades, pole reinforcement, vegetation management, and stockpiling of power lines [67, 70]. Corrective plans focus on how to ensure basic urgent levels of service (survivability) and how to recover from a forced outage as quickly as possible. This article is

a contribution to the body of literature on post-disaster grid recovery and, in particular, to the microgrid formation and resource allocation literature. In fact, due to their ability to operate in island and grid-connected modes [79], microgrids are widely viewed as a viable grid resiliency solution, and validation projects are being completed by New York, Connecticut and California as well as the U.S. Department of Energy.

The literature is rich in interesting grid restoration approaches. In previous work, Choobineh and Mohagheghi [72], and Sarkar [71] formulate the restoration problem as a non-linear mixed-integer program (NLMIP). The model in [71] seeks to optimally reconfigure the distribution grid by switching tie-lines. A proposed greedy search algorithm avoids the computational complexity of solving the NLMIP by approximately solving the model. Reference [72] focuses on the optimal dispatch of energy resources within supply capacity and fuel availability limits. In [78], the authors assume the distribution system to be an interconnection of multiple preformed microgrids, within which, a two-stage hierarchical outage management scheme maximizes the total load served following a disruption.

The microgrid based grid restoration approach also received much attention in [80], [81] and [84]. The scheme in [81] considers intermittent energy resource availability and uncertainties in a continuous operation time mode. Reference [80] assumes that fixed distributed generation (DG) units with black-start capability are available, and proposes a black-start sequence algorithm using a spanning tree search for an efficient grid restoration. Chen et. al [84] present a mixed integer linear program (MILP) formulation with fixed DG units. In [85], the authors relaxed the fixed DG unit location constraint by optimally allocating mobile emergency DG units to candidate nodes. The concept of mobile DG units is justified by the recommendations derived from the severe ice storm that affected Eastern Canada and the Northeastern US in December 2013 [86]. Most of

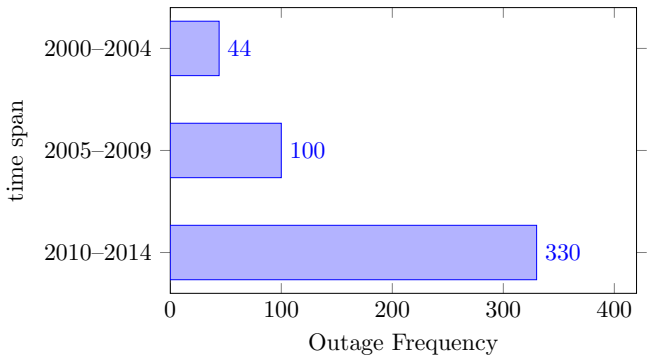


Figure 1.1: Outage frequency increase between 2000 and 2014 [1]

the aforementioned models only apply to the traditional radial distribution networks with directed flows. The work in [92] extends the model in [84] to general network architectures (both radial and meshed) while allowing both fixed and mobile DG units. The proposed model also accounts for demand responsive loads. As in [84], each load is assigned a criticality factor to model the utility or comfort level that a given load provides when served. However, the computation time of the corresponding MILP models increases significantly with the network size and the number of microgrids. This computational complexity is a major challenge when it comes to large electric networks. Given that time is a critical factor in post-disturbance grid restoration, and due to the fact that many instances of the problem with different parameter settings might have to be considered to reach a microgrid formation policy for the network, it is important to devise solution approaches for the problem that would provide answers in as reasonable a time as possible, as well as using moderate memory resources.

In this work we propose an approximate solution approach for the model in [92] that solves the microgrid formation problem in reasonable times and using moderate computational resources, even in large network test cases. Specifically, we propose a 3-stage solution method that decouples the DG unit placement and the associated grid partitioning problems. The first stage consists of locating DG units. The second stage uses the DG unit location results from the first stage as centroids to form corresponding microgrid partitions. The third stage assesses the feasibility of the microgrids formed in the second stage within the power systems operation constraints.

Furthermore, the modeling of microgrids along with prevailing uncertainties is also critical in achieving satisfactory microgrid formation plans in light of potential catastrophes. Such an idea has been discussed in [93], [94], [95] and [96]. In [95], the author presented a two-stage stochastic programing approach to minimize the expected social cost of microgrids and enhance the resilience of microgrids in natural disasters. The authors in [94] propose a stochastic programming approach for increasing resiliency of a distribution system exposed to an approaching wildfire. Also, [96] and [97] focus on the microgrid energy scheduling and management using stochastic programming techniques. However, in these works, stochastic programming techniques are not used to address the crucial problem of microgrid formation under uncertainty on the potential failure scenarios faced by the electrical grid. To our knowledge, this problem has received little attention in the literature due to the numerical complexity associated with its solution.

More specifically, we consider a situation under which the uncertain failures that can affect a power system are given in the form of a finite number of scenarios, together with their probability of

occurrence. In this case one is interested in deciding where to increase the generation capacity of the network (within resource constraints) so that, in expectation, the network load served is maximized once microgrids are formed after the failure, based on the placement of the additional generation capacity. This stochastic problem can be formulated as a two-stage stochastic program. Even more dramatically than in the deterministic failure case, as the size of the network, or the number of failure scenarios considered increases, this problem becomes too complex to solve to optimality using MILP solvers. In this case too, the heuristic solution approach for the deterministic failure case, proposed here, can be used to approximately solve the problem.

## 1.7 Outline of The Dissertation

The reset of this dissertation is organized as follows. Chapter 2 presents our work on improving load factor through adoption of Minimax, our proposed retail electricity pricing scheme. Next, Chapter 3 establishes the importance of load aggregation in achieving grid reliability under Minimax, and shows how the pricing scheme encourages consumers to pool their deferrable loads. Chapter 4 describes our work on the Generalized Minimax pricing mechanism, a scheme that incentivizes consumer groups to follow a predetermined optimal supply profile for a reduced energy bill and an improved grid reliability. Chapter 5 describes our work on renewable integration in which it is demonstrated that introducing a short-term reserve market would increase reliability in a system with high penetration of renewable energy resources and provide market opportunities for renewable farm owners. Chapter 6 presents our work on post-disturbance grid recovery through optimal microgrid formation and resource allocation. Finally, Chapter 7 describes our work on reducing computation time when solving the grid restoration problem discussed in Chapter 6 using a heuristic approach. This work also extends the boundaries of the solution to resiliency-aware generation siting problems which, in nature, are planning problems. Chapter 8 concludes the dissertation.

# Chapter 2

# Minimax Pricing, Providing Incentives to Consumers to Improve their Load Factor

## 2.1 Introduction

Reducing peak demand is critically important in smartgrid as a significant fraction of the electric grid's capital and operational expenses is affected by the peak power demands. Time of Use (ToU) and Real Time Pricing (RTP) pricing schemes have been used by power system operators to incentivize customers to reduce their peak energy demands during peak hours. However, ToU only provides a weak incentive for customers and does not promote adoption at scale. Similarly, day-ahead Real-Time Pricing (RTP) scheme might create peaks in previoulsy off-peak periods and causes some ping-pong effect in next day prices. In this chapter, we introduce a new incentive-driven scheme called Minimax which encourages customers to flatten their daily load profiles such that they can reduce their electricity bill and help lowering the aggregate peak power demands. Using two real life energy usage datasets, we show via simulations how the peak energy usage and load factor vary with different choices of parameter values we select for the Minimax scheme. In addition, we present our optimal scheduling policy which yields the minimum energy bill assuming a certain percentage of load demands is schedulable. Our results using energy usage data of 100 homes from the UMASS dataset show that customers can save 13-17% of their electricity bills if

the Minimax scheme is used but only about 2-3% if RTP or TOU scheme is used. Furthermore, the power system operators see a 10% reduction in peak power demand if appropriate parameter values are used for the Minimax scheme while the peak demands increase by more than 70% using RTP or TOU schemes.

The Minimax scheme charges consumers at a $C_{\text{base}}$ rate if a consumer's demand is at a certain $base_{\text{thrsh}}$ but charges higher if his demand exceeds or drops below $base_{\text{thrsh}}$. If the consumer demand exceeds $base_{\text{thrsh}}$, he will pay at a rate $C_{\text{high}}$ while if his demand drops below $base_{\text{thrsh}}$, he will pay at a rate $C_{\text{low}}$ where typically $C_{\text{high}} > C_{\text{low}}$. We show via analysis and simulation studies how appropriate choice of parameter values allow the Minimax scheme to achieve both goals of reducing consumers' energy bills while reducing peak load demand. In addition, we show how elastic or scheduable loads can be scheduled to achieve these two goals using the Minimax scheme. Using two real life energy usage datasets, one from UMASS researchers [98] and another from a Lehigh residential building, we show the benefits of the Minimax pricing scheme over the two existing pricing schemes, namely TOU and RTP schemes.

In the remainder of this chapter, we first introduce the novel retail pricing scheme. Section 2.3 presents the proposed deferrable load scheduling optimization model. Simulation case studies are found in Section 2.4 and Section 2.5 highlights the main concluding remarks.

## 2.2 Minimax Pricing Scheme

In this section, we first present an overview of Minimax, our proposed pricing scheme. Then, we present design guidelines by discussing how its parameter settings can be chosen to meet certain goals.

### 2.2.1 Minimax Description

Minimax is a pricing scheme where the rate $C^t$ at any time $t$ depends on the amount of the power request $p^t_{\text{dem}}$. Equation (2.1) presents the pricing schedule.

$$C^t = \begin{cases} C_{\text{low}} & \text{if } p^t_{\text{dem}} < B, \\ C_{\text{base}} & \text{if } p^t_{\text{dem}} = B, \\ C_{\text{high}} & \text{if } p^t_{\text{dem}} > B. \end{cases} \tag{2.1}$$

where $C_{\text{low}}$ in (2.1) is the applied rate if the realized demand is less than a pre-determined

baseline threshold $B$. $C_{\text{base}}$ is the rate applied if the demand is equal to the threshold, and $C_{\text{high}}$ is the rate applied if the demand is above $B$.

Let us define the tuning parameters $k_1, k_2$ as follows: $k_1 = \frac{C_{\text{low}}}{C_{\text{base}}}$, and $k_2 = \frac{C_{\text{high}}}{C_{\text{base}}}$. Furthermore, let us denote $k = \frac{B}{P_{\text{avg}}}$ where $P_{\text{avg}}$ is the daily average power request. Next, we will discuss how these three parameters should be chosen to motivate consumers to flatten their load profiles.

### 2.2.2 Minimax Design

The performance metrics targeted in a peak load management program are (i) a lower energy bill (customers' benefit) and (ii) a higher load factor (utility companies' benefit). The load factor $LF$, equation (2.2), is defined as the average-to-peak load ratio within the considered time horizon [99]. In this paper, we base our analysis on a 24-hour time horizon.

$$LF = \frac{P_{\text{avg}}}{P_{\text{max}}} \tag{2.2}$$

where $P_{\text{avg}}$ is the average power request and $P_{\text{max}}$ the peak load. The daily bill is the sum of all energy costs incurred by end-user throughout the day based on her/his power request and the rate(s) charged by the utility company.

#### $k_1$ and $k_2$ Settings

We refer to $k_1$ and $k_2$ as the differential pricing parameters. One of the goals of designing Minimax is to ensure a higher load factor or a lower peak-to-average load ratio. It means that we want to reduce the variability of the demand. To incentivize end-users, the three rates presented in equation (2.1) should satisfy the following inequality

$$C_{\text{base}} < C_{\text{low}} < C_{\text{high}} \tag{2.3}$$

$$1 < k_1 < k_2 \tag{2.4}$$

$$k = \frac{B}{P_{\text{avg}}} \tag{2.5}$$

Equation (2.3) encourages consumers to flatten their load profiles as much as possible. In addition, it is better for a consumer to keep his demand below the threshold than above the threshold. From (2.3), we see that $1 < k_1 < k_2$.

Let us break down a daily load profile into three components $E_{(+)}$, $E_{(-)}$ and $E_{(0)}$ defined by equations (2.6) through (2.8).

$$E_{(+)} = \sum_{t}^{|T|} p_{\text{dem}}^{t} | p_{\text{dem}}^{t} > B \tag{2.6}$$

$$E^{(-)} = \sum_{t}^{|T|} p_{\text{dem}}^{t} | p_{\text{dem}}^{t} < B \tag{2.7}$$

$$E_{(0)} = \sum_{t}^{|T|} p_{\text{dem}}^{t} | p_{\text{dem}}^{t} = B \tag{2.8}$$

where $E^{(+)}$ is the total power requests above the baseline threshold $B$, $E_{(-)}$ the total power requests below the baseline threshold $B$ and $E_{(0)}$ is the total power requests equal to the baseline threshold B; $p_{\text{dem}}^{t}$ is the power request at time t. Thus, according to equation (2.1), $E_{(+)}$ is charged at a rate $C_{\text{high}}$, $E_{(-)}$ is charged at a rate $C_{\text{low}}$, and $E_{(0)}$ is charged at a rate $C_{base}$ respectivley. It follows that the daily bill can be expressed by

$$Bill = \left( \frac{k_2}{k_1} E_{(+)} + E_{(-)} + \frac{1}{k_1} E_{(0)} \right) C_{\text{low}} \tag{2.9}$$

Once the power system operators have fixed $C_{\text{low}}, C_{\text{high}}, C_{\text{base}}$, given equation (2.9), reducing the quantity $E_{(+)}$ (meaning lesser power request above B) has the highest impact on decreasing the customer's bill because $k_2 > k_1$. $E_{(+)}$ can be reduced by either (i) scheduling deferrable loads such that the peak demand is below B if feasible, or (ii) a larger B can be negotiated.

### $k$ Settings

We refer to $k$ as the threshold parameter. According to equations (2.4) and (2.9), a consumer would schedule his deferrable load to reach a peak demand as high as the baseline threshold B to enjoy the lowest rate $C_{\text{base}}$. Thus, from a customer prospective, the ideal peak demand under Minimax is the threshold $B$. $B$ has to satisfy equation (2.10)

$$k > 1 \tag{2.10}$$

Just as a utility may set a minimum power factor of 0.9, a system operator may set a load factor minimum target $LF_0$ to meet in order to ensure reliability. In other words, all allowable peak demands should be less than a certain maximum defined by $LF_0$ and the average demand $P_{\text{avg}}$. The baseline threshold $B$ must be defined in a way that satisfies the minimum load factor target. Because the end-user under Minimax is likely to peak at the threshold $B$, the condition of

equation (2.11) should be satisfied

$$B \leq \frac{P_{avg}}{LF_0} \tag{2.11}$$

We derive (2.12) from (2.11) and $k = \frac{B}{P_{\text{avg}}}$, which serves as a design principle for the threshold parameter $k$.

$$k \leq \frac{1}{LF_0} \tag{2.12}$$

In practice, however, the design principle (2.12) does not guarantee the minimum load factor. Before we present how the minimum load factor can be guaranteed, we first describe the assumption made of a user's energy load profile in this paper. Given that in reality, not all power requests are deferrable, the load profile considered in this paper consists of a non-deferrable load profile which we call base load and a deferrable load profile which we call schedulable load. The amount of schedulable load and the relative position of the baseline threshold compared to the maximum power request of the base load profile are just as important as the choice of $k$ in achieving the target load factor. If an end-user has more schedulable load, then he can more easily improve the load factor of his load profile. However, if the peak demand (the maximum power request) of the non-deferrable load profile is higher than the baseline threshold, then this peak demand cannot be changed no matter how the end-user dispatches its schedulable load. For the consumer to have the opportunity to improve his load factor and achieve the target $LF_0$, the condition (2.13) must be satisfied.

$$B \geq P_{\text{max,BL}} \tag{2.13}$$

where $P_{\text{max,BL}}$ is the peak demand of the base load profile. Given $SL$, the sum of the available schedulable loads and $BL$, the sum of all non-deferrable loads, equations (2.5) and (2.13) lead to.

$$k\frac{BL + SL}{24} \geq P_{\text{max,BL}} \tag{2.14}$$

We transform (2.14) by algebraic manipulation to express the minimum fraction of schedulable load needed in order to satisfy the condition (2.13) for a given k and load factor of the non-deferrable load profile $LF_{BL}$ as follows.

$$\frac{SL}{BL} \geq \frac{1}{k} \times \frac{24.P_{\text{max,BL}}}{BL} - 1 \tag{2.15}$$

$$\frac{SL}{BL} \geq \frac{1}{k} \times \frac{1}{LF_{\text{BL}}} - 1 \tag{2.16}$$

The load factor minimum target $LF_0$ can be guaranteed only if equations (2.12) and (2.16) hold simultaneously. We validate this claim in section 2.4.

## 2.3 Optimal Load Scheduling

In this section, we formulate the load scheduling problem and propose an optimization model under each pricing scheme (ToU and Minimax). To assess the performance of the Minimax pricing scheme, we assume that an end-user has a load scheduler with perfect pricing information. The customer' reaction to a particular pricing scheme is evaluated via the scheduling decisions made by the scheduler. The main concern for an end-user is the minimization of her/his daily bill, given the available deferrable power requests and the pricing policy designed by the utility company. The problem which needs to be considered is the scheduling of the deferrable power request(s) which achieves the lowest possible daily bill.

### 2.3.1 Problem Formulation under ToU and RTP

Under time-based pricing schemes such as Time-of-Use and Real-Time Pricing, the rate applied at every hour is known beforehand. Hence, there is no issue with non-linearity in the objective function. In equations (2.17) through (2.21), we formulate the load scheduling problem which minimizes the energy bill under ToU and RTP as a Mixed Integer Linear Problem (MILP).

$$\min : \text{Bill} = \sum_{t}^{|T|} p^t_{\text{dem}} \times C^t \tag{2.17}$$

Subject to:

$$p^t_{\text{dem}} = \textstyle\sum_{i=1}^{|I|} z^{it} \times P^i + BL^t, \quad \forall t \in T \tag{2.18}$$

$$\textstyle\sum_{t=1}^{|T|} z^{it} = D^i, \quad \forall i \in I \tag{2.19}$$

$$\textstyle\sum_{t=1}^{|T|-1} z^{it} \times (1 - z^{i(t+1)}) = 1, \quad \forall i \in I \tag{2.20}$$

$$z^{it} \in \{0,1\}, \quad \forall i \in I, \quad \forall t \in T \tag{2.21}$$

where:

$T$, the set of time (we assume 24 hours)

$I$, the set of schedulable loads

$p^t_{\text{dem}}$ the demand in time $t$

$C^t$, the energy price in time t

$z^{it}$, the decision variable equals 1 if load $i$ is scheduled in time t and 0 otherwise

$P^i$, power rating for load $i$

$D^i$, duration of load $i$

$BL^t$, the base load demand in time $t$.

Constraint (2.18) defines the resulting power request as a combination of a known demand $BL^t$ and potential scheduled load(s). Constraints (2.19) and (2.20) ensure that once load $i$ starts being served, it stops to be served only after its operating time $D^i$ is over. Constraint (2.20) guarantees that a deferrable power request cannot be fractioned.

### 2.3.2 Problem Formulation under Minimax

Under Minimax, $C^t$ is a function of $p^t_{\text{dem}}$ (equation (2.1)), and $p^t_{\text{dem}}$ itself is function of $z^{it}$, the decision variable (equation (2.18)). To linearize the objective function (2.17), we reformulate the problem as follows.

$$\min : \sum_{t=1}^{|T|} \left[ \frac{1}{k_1} \left(1 + Q^t_{\text{low}} + Q^t_{\text{high}}\right) \times B + \frac{k_2}{k_1} \times p^t_{\text{high}} - p^t_{\text{low}} \right] \times C_{\text{low}} \tag{2.22}$$

with:

$$\begin{aligned} Q^t_{\text{low}} &= (k_1 - 1) X^t_{\text{low}} \\ Q^t_{\text{high}} &= (k_2 - 1) X^t_{\text{high}} \end{aligned} \tag{2.23}$$

Subject to:

$$p^t_{\text{dem}} = \textstyle\sum_{i=1}^{|I|} z^{it} \times P^i + BL^t, \quad \forall t \in T \tag{2.24}$$

$$p^t_{\text{high}} - p^t_{\text{low}} = p^t_{\text{dem}} - B, \quad \forall t \in T \tag{2.25}$$

$$M \times (1 - X^t_{\text{low}}) + B \geq p^t_{\text{dem}} + \varepsilon, \quad \forall t \in T \tag{2.26}$$

$$M \times X^t_{\text{high}} + B \geq p^t_{\text{dem}} + \varepsilon, \quad \forall t \in T \tag{2.27}$$

$$X^t_{\text{low}} + X^t_{\text{high}} \leq 1, \quad \forall t \in T \tag{2.28}$$

$$\sum_{t=1}^{|T|} z^{it} = D^i, \quad \forall i \in I \tag{2.29}$$

$$z^{i0} = 0, \quad \forall i \in I \tag{2.30}$$

$$M \times (1 - y^{it}) + z^{it} \geq z^{i(t-1)} + \varepsilon, \quad \forall i \in I, \quad \forall t \in T \tag{2.31}$$

$$M \times y^{it} + z^{i(t-1)} \geq z^{it} - \varepsilon, \quad \forall i \in I, \quad \forall t \in T \tag{2.32}$$

$$\sum_{t=1}^{|T|} y^{it} = 1, \quad \forall i \in I \tag{2.33}$$

$$y^{it} \in \{0, 1\}, \quad \forall i \in I, \quad \forall t \in T \tag{2.34}$$

$$z^{it} \in \{0, 1\}, \quad \forall i \in I, \quad \forall t \in T \tag{2.35}$$

where:

$T$, the set of time (we assume 24 hours)

$I$, the set of schedulable loads

$p^t_{\text{dem}}$ the demand in time $t$

$C^t$, the energy price in time t

$z^{it}$, the decision variable equals 1 if load $i$ is scheduled in time t and 0 otherwise

$P^i$, power rating for load $i$

$D^i$, duration of load $i$

$BL^t$, the base load demand in time $t$;

$X^t_{\text{low}}$, a decision variable, is equal to 1 if $p^t_{\text{dem}}$ is less than $B$ and 0 otherwise

$X^t_{\text{high}}$, a decision variable, is equal to 1 if $p^t_{\text{dem}}$ is greater than B and 0 otherwise

$p^t_{\text{low}}$, the gap between $p^t_{\text{dem}}$ and $B$ if $p^t_{\text{dem}}$ is less than $B$ and 0 otherwise

$p^t_{\text{high}}$, the gap between $p^t_{\text{dem}}$ and $B$ if $p^t_{\text{dem}}$ is greater than $B$ and 0 otherwise

$y^{it}$, a binary decision variable, is equal to 1 if load $i$ comes online in time $t$ after being offline in time $t-1$

$M$, a large number (big M method)

$\varepsilon$, an infinitesimal number (the inverse of $M$ for example) used to enforce strict inequalities in (32) and (33).

Equations (2.22) through (2.35) present the optimization problem which yileds minimum energy bill under Minimax. We introduce new variables and used the "big M" method to reformulate the problem as an MILP. In the next section we used real life energy usage datasets to compare the effectiveness of the three pricing schemes in achieving (a) the minimum energy bill for a consumer and (b) to reduce the peak load demands. Furthermore, we also validate the few Minimax design principles discussed above.

## 2.4 Case Study

To compare how the different pricing schemes incentivize consumers in scheduling their elastic load demands, we built a simulator which can schedule elastic load demands using the scheme described in Section 3.2 under the following three pricing schemes, namely the (i) Minimax, (ii) ToU, and (iii) RTP schemes. Our RTP pricing data is obtained from the Illinois energy price clearing house website [10]. The RTP price we have chosen was the one used for Aug 20th, 2013. The TOU price was based on Ontario's rates [9], specifically, \$0.063 per kWh from 11pm to 6 am(off-peak period); \$0.118 per kWH between 6 am to 10 am and 4pm to 11 pm (peak periods), and \$0.099 per kWh from 10 am to 4pm (mid-peak period). For the Minimax scheme, we use $k = 1.05, k_1 = 1.1, k_2 = 1.3$ unless otherwise specified. Figure 3 shows the price signals we used for ToU and RTP.

### 2.4.1 Comparison of Minimax, TOU and RTP

To compare the impact of the three different pricing schemes on two important metrics, namely (i) the load factor achieved after scheduling all the deferrable loads, (ii) the resulting customer daily energy bill, we used two real energy usage datasets. The first one (Dataset 1) is the energy usage dataset released by UMASS researchers [4, 98], and the second one (Dataset 2) is an energy usage dataset of a 30-bed student residential building at Lehigh University.

In dataset 1, we aggregated the energy usage from 100 homes to create our base load profile. The total base load energy usage amounts to 6546.3 kWh for the entire day and has a load factor of 91%. We added 100 deferrable power requests ranging from 1 to 5 kW each to this base load profile. The schedulable load amounts to 307 kWh total. These deferrable requests reflect schedulable loads e.g. washer, dryer, dishwasher, etc, that other researchers have studied [100].Fig. 1 plots the hourly base load, the hourly schedulable load and the original hourly load profile which is the sum of the hourly base and schedulable loads . The average, standard deviation and load factor of this daily load profile is tabulated in Table 1.

In dataset 2, we pick the daily usage of a 30-bed Lehigh residential building on Aug 20, 2013 which has a load factor of 90%. This daily load of 1955.88 kWH will be our base load. Then, we add an additional 30 scheduable loads, each of size 3 or 5 kW representing a cloth washer or a dryer. The total schedulable loads amounts to 120 kWh. Figure 2 shows the load profile, the base load and the schedulable load for Dataset 2. The average, standard deviation and load factor of this load profile is tabulated in Table 1.

Table 2.1: Load profile characteristics

| Datasets | Average demand (kW) | Standard deviation (kW) | Load factor |
|---|---|---|---|
| Dataset 1 | 285.55 | 16.53 | 0.85 |
| Dataset 2 | 86.49 | 12.76 | 0.74 |

-

To ensure a fair comparison between Minimax and ToU, we choose $C_{\text{low}}$ such that the energy bills yielded by both schemes are equal if we have an ideal flat load profile where the power request at any time is equal to the average demand. In this case, because of (2.13), the Minimax rate applied is $C_{\text{low}}$. For both bills to be equal, $C_{\text{low}}$ must be equal to the average of the ToU pricing vector. Next, let us assume that we want the load factor minimum target $LF_0$ of 95%, hence, we can select k using (2.15). Next, we verified that the available schedulable loads for both datasets

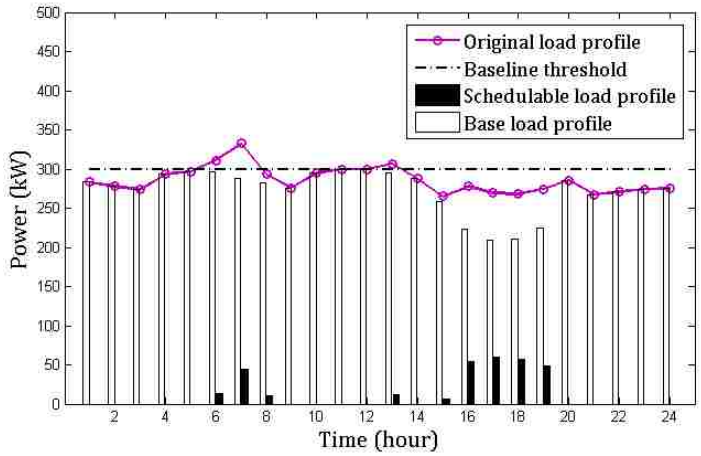


Figure 2.1: Base Load and Schedulable Load Profile of dataset 1

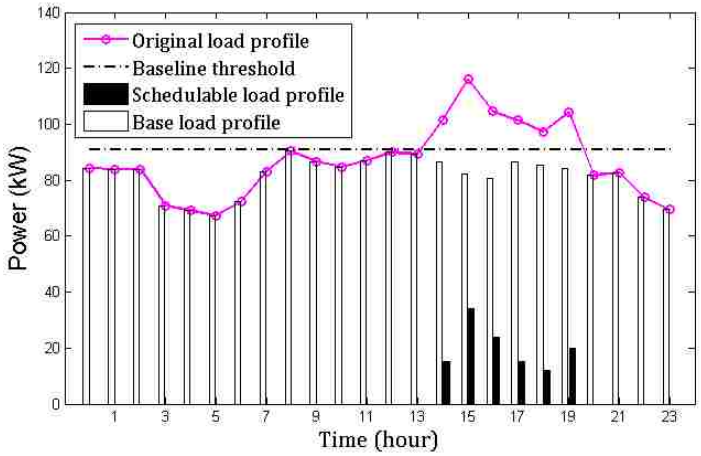


Figure 2.2: Base Load and Schedulable Load Profile of dataset 2

satisfy the condition expressed in (2.19). In fact, the ratio $\frac{SL}{BL}$ is 0.0469 while the right hand side of the inequality, $\frac{1}{k}\frac{1}{LF_{\mathrm{BL}}} - 1$, is 0.0466. Both $k_1$ and $k_2$ satisfy (2.8). With the above presented data and parameter settings, we solved the MILP problems formulated in section III using AMPL and CPLEX. The results are presented next.

**Simulation Results**

For both datasets, we first applied ToU, RTP and Minimax to the original load profile. Second, we simulated the customers' reaction to the pricing schemes and computed the energy bills incurred using the optimal profiles obtained after load scheduling. Table 2 presents the load factors and energy bills before and after scheduling.

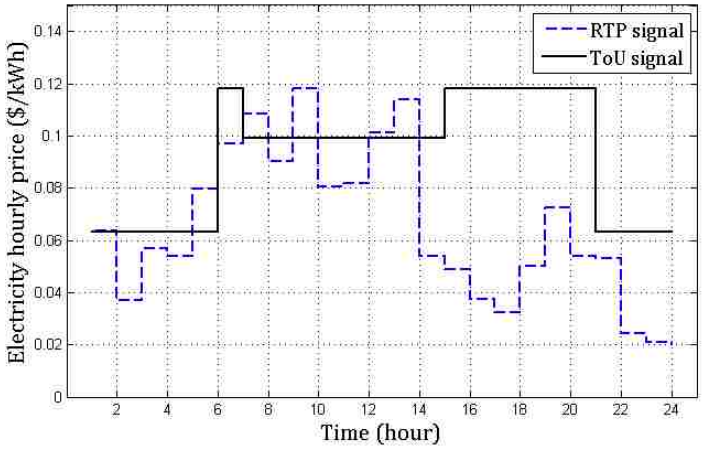


Figure 2.3: ToU and RTP pricing signals

Table 2.2: Load factor and bill comparison before and after load scheduling

| | | LFBS[1] (%) | LFAS[2] (%) | PDV[3] (%) | EBBS[4] ($) | EBAS[5] ($) | EBR[6] (%) |
|---|---|---|---|---|---|---|---|
| Dataset 1 | ToU | 85 | 48 | +77 | 625.10 | 609.47 | 2.5 |
| | RTP | | 49 | +73 | 450.09 | 437.10 | 2.9 |
| | Minimax | | 95 | -10 | 649.60 | 564.12 | 13.0 |
| Dataset 2 | ToU | 74 | 42 | +76 | 193.50 | 186.80 | 3.5 |
| | RTP | | 45 | +64 | 132.54 | 129.45 | 2.3 |
| | Minimax | | 95 | -22 | 206.00 | 170.80 | 17.1 |

[1] Load factor before scheduling
[2] Load factor after scheduling
[3] Peak demand variation, (+): increase, (-): decrease
[4] Energy bill before scheduling
[5] Energy bill after scheduling
[6] Energy bill reduction EBR $= \frac{\text{EBAS}-\text{EBBS}}{\text{EBBS}} \times 100\%$

The simulation results presented in figures 4, 5 and Table 2 show that the load factor improves under the Minimax scheme while it worsens under ToU and RTP for both datasets 1 and 2. In fact, we observe about 12% load factor increase for dataset 1, an equivalent 22% peak demand reduction when Minimax is applied. In contrary, ToU and RTP led to 43% and 42% load factor decrease respectively, meaning 77% peak demand increase for ToU and 73% peak demand increase for RTP. Using dataset 2, the load factor increases by 28% under Minimax and decreases by 43% and 39% for ToU and RTP respectively. From a Load Serving Entity (LSE)'s standpoint, an increased load factor and thus a reduced peak demand is equivalent, in the long run, to less commitment in the capacity market. Hence, Minimax has proven to meet LSE's interest.

In addition, even though all three schemes led to a reduced customer electricity bill, Minimax

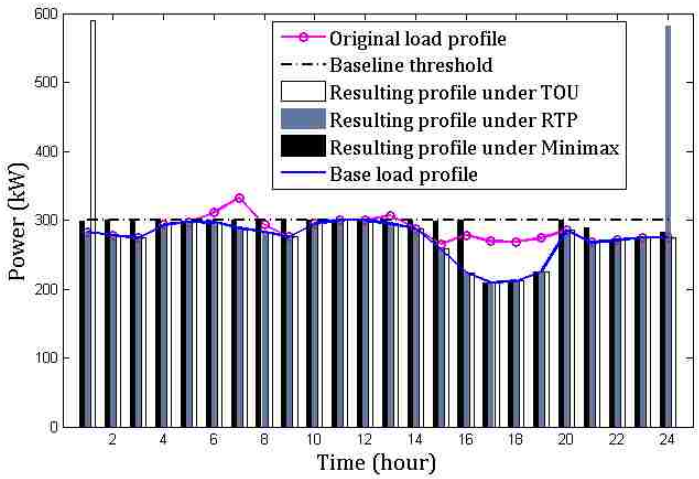


Figure 2.4: Optimal Scheduled Load profiles under ToU, RTP and Minimax for dataset 1

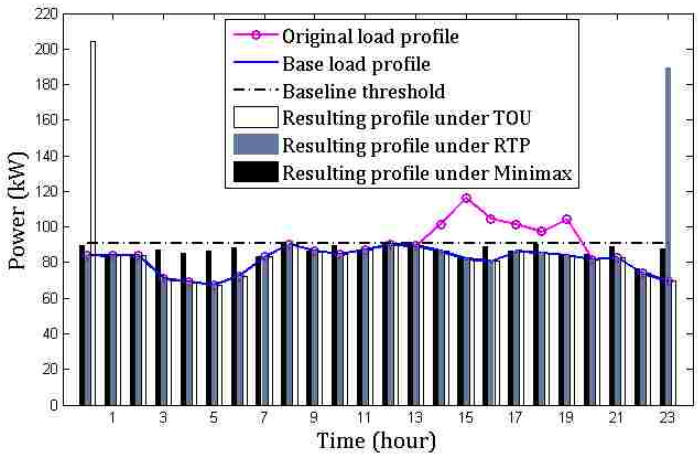


Figure 2.5: Optimal Scheduled Load profiles under ToU, RTP and Minimax for dataset 2

induced the highest bill reduction. In fact, considering dataset 1, ToU and RTP helped reduce the energy bill by less than 3% while the bill reduction is 13% under Minimax. When applied to dataset 2, the load scheduling models yielded less than 4% energy bill savings with ToU and less than 3% with RTP while Minimax helped save 17% on the electricity bill. Even in energy bill savings, Minimax outperforms ToU and RTP and hence meets consumers' interest as well. Since the rates in Minimax are not time-based but rather quantity-based, profile flattening and bill reduction are achieved simultaneously, given a set of well-designed pricing and threshold parameters.

Note that for this set of experiments, the load factor minimum target of 0.95 is achieved. However, we want to derive more insights as to the sensitivity of Minimax's performance with regards to the threshold parameter $k$. We explore this in the next subsection.

### 2.4.2 Minimax Design Validation

Three main parameters, namely $k_1$, $k_2$ and $k$, characterize the Minimax pricing scheme . The validation of the design principle (2.8) of the pricing parameters $k_1$ and $k_2$ is straightforward. (2.12) along with the discussion of its detailed implications provided in section II-B is sufficient to prove that the necessary and sufficient conditions expressed by (2.8). Therefore, in this subsection, we will concentrate on the sensitivity of Minimax with regards to the threshold parameter $k$. We will first present the data and parameters used in this experiment. -

#### Simulation Setup

In this experiment, we use the daily energy usage data (dataset 2) presented in figure 2 and table 1. For Minimax, we set $k_1 = 1.1, k_2 = 1.3$ and vary k from 1.01 to 1.10 with an increment of 0.01.

#### Simulation Results

Table 3 tabulates how the left and right hand-side of (2.16) vary as k changes from 1.01 to 1.10. It also tabulates how the target load factor $LF_0$ as k changes using (2.12). In fact, for each value of the threshold parameter k, (2.12) assigns a target minimum load factor $LF_0$ which can be achieved under Minimax if (a) an end-user reacts perfectly as the optimal load scheduling model developed in Section 2.3, and (ii) he has sufficient amount of schedulable loads. We also plot the achievable load factor and the daily bill as k varies in Fig. 2.6 and 2.7.

Table 2.3: Sensitivity analysis and design validation

| $k$ | Ratio $\frac{SL}{BL}$ | $\frac{1}{k} \times \frac{1}{LF_{\text{BL}}} - 1$ | $LF_0$[1] | ALF[2] | Daily bill ($) |
|---|---|---|---|---|---|
| 1.01 | | 0.10001 | 0.99 | 0.9572 | 178.20 |
| 1.02 | | 0.0893 | 0.98 | 0.9572 | 178.04 |
| 1.03 | | 0.0787 | 0.97 | 0.9572 | 177.89 |
| 1.04 | | 0.0684 | 0.96 | 0.9572 | 175.52 |
| 1.05 | 0.06135 | 0.0582 | 0.95 | 0.9572 | 170.87 |
| 1.06 | | 0.0482 | 0.94 | 0.9463 | 170.70 |
| 1.07 | | 0.0384 | 0.93 | 0.9377 | 170.52 |
| 1.08 | | 0.0288 | 0.92 | 0.9265 | 170.36 |
| 1.09 | | 0.0194 | 0.91 | 0.9293 | 170.19 |
| 1.10 | | 0.0101 | 0.90 | 0.9124 | 170.02 |

[1] Target load factor
[2] Achieved load factor

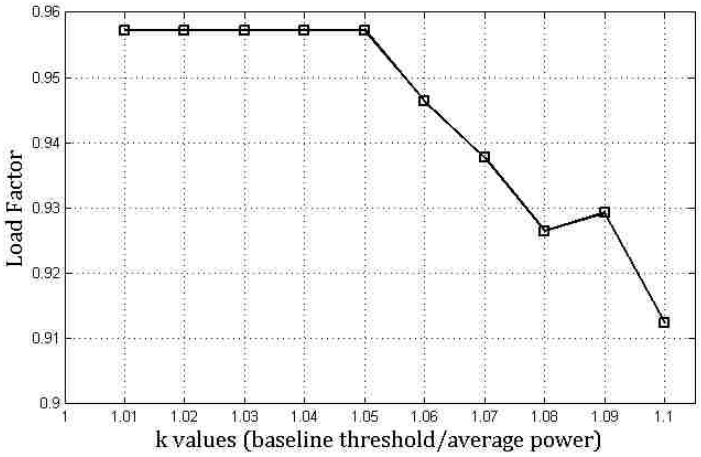


Figure 2.6: Impact of the threshold parameter k on the load factor

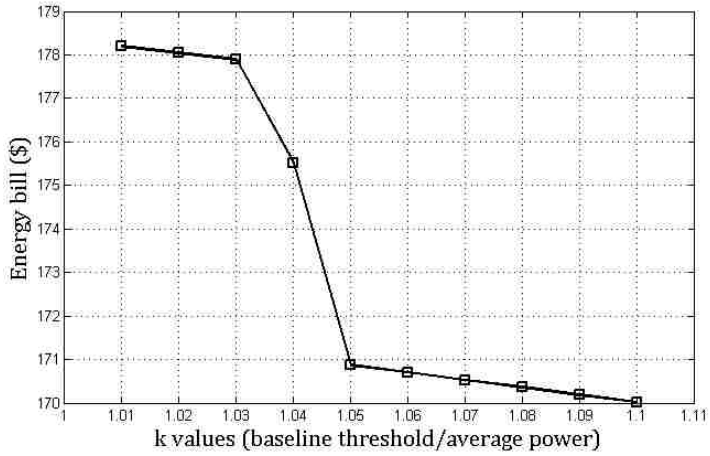


Figure 2.7: Impact of the threshold parameter k on the energy bill

We observe that from $k = 1.01$ to $k = 1.04$, the condition in (2.16) is not satisfied, meaning that the available schedulable load is not enough to empower the end-user to reach the target load factor. The direct consequence is that for these values of $k$, the load factors achieved are consistently less than their corresponding targets $LF_0$. In fact, the achieved load factors remain the same for these 4 $k$ values because the baseline threshold $B$ is below the base load maximum $P_{\text{max,BL}}$. Since the average load demand and the peak demand, $P_{\text{max,BL}}$, are fixed, we have the same load factor of 0.9572 for these 4 cases. From $k = 1.05$ to $k = 1.10$, (2.16) holds and the target load factors defined in (2.15) can be achieved.

From Fig. 2.6, we see that the load factor in general decreases with increasing values of $k$. However, we note a little increase (0.9265 to 0.9293) of load factor from $k = 1.08$ to $k = 1.09$.

This is because when k=1.09, the maximum load demand after optimal scheduling is below the baseline threshold B which causes the load factor to decrease below the Pmax value obtained for k=1.08. Fig. 2.7 and column 6 of Table 2.3 show that the energy bill incurred is also decreasing with increasing threshold parameter $k$.

## 2.5 Conclusion

Our proposed Minimax pricing scheme has much potential for electricity peak demand management. In addition to improving the load factor and reducing the peak demand, it lowers the consumers's daily bill, providing enough incentive for consumers to adopt it. Contrary to the Time-of-use and Real-time pricing schemes under which customers tend to shift schedulable loads to off-peak hours and thus create new peak hours, the Minimax scheme encourages an even distribution of loads. In addition, we explored the sensitivity of our chosen parameters and validated our design principles. The pricing parameters are chosen in order to provide incentives to customers and the threshold parameter is designed based on a load factor target set by the utility company or system operator and on the available deferrable loads. The target load factor can be achieved only if the schedulable load is a certain percentage of the overall load demand.

# Chapter 3

# The Value of Aggregation Under Minimax

## 3.1 Introduction

The electric grid's capital and operational expenses are significantly affected by the system's peak. In an effort to reduce peak electricity demands, electricity market analysts and researchers have designed different pricing schemes that provide a certain incentive to end-users to reduce their usage during what are considered peak consumption periods. Among those schemes, Time of Use (ToU) and Real Time Pricing (RTP) have been well researched and implemented. However, it became apparent that there are incentive compatibility issues with both. In addition, it has been reported that they can even lead to peak migration instead of reduction. Recently, we introduced a new incentive-driven scheme named Minimax whose objective is to incentivize customers to flatten their daily load profiles and help lower the aggregate peak power demands. Simulation studies showed that customers can save 13-17% of their electricity bills if the Minimax scheme is used but only 2-3% if RTP or ToU scheme is used. In addition, Minimax can save 10% of the generation cost. The benefits of Minimax are threefold: consumer bill reduction, peak power reduction, and generation cost reduction. In our previous work related to Minimax, we used aggregated household energy data. In this chapter, we are interested in exploring the value of aggregation under the Minimax pricing mechanism. We evaluate the impact of aggregation on energy bill reduction, power factor, voltage profile and generation cost reduction using the IEEE 33-bus distribution system. Our studies based on piece-wise linear generation cost function show that, for the same

total load, larger aggregate groups achieve lower energy bill, lower generation cost, lower aggregate peak demand and better voltage profile. Aggregation results in 40% peak power reduction, 6% consumers' bill reduction, 13% supply cost reduction and no voltage bound violation.

The rest of this chapter is organized as follows. Section 3.2 gives a brief overview of Minimax, followed by section 3.3 which presents the consumers' reaction model to a Minimax price signal. Next, we discuss the DSO's problem in section 3.4. Section 3.5 exposes the load aggregation evaluation framework while section 3.6 discusses the results. We conclude the chapter in section 3.7.

## 3.2 The Pricing Scheme

In this section, we present an overview of Minimax (cf., 2). Minimax is a pricing scheme which aims to incentivize end-users to reduce their peak power demand [24]. It is a 3-rate scheme with an attractive low rate $C_{\text{base}}$ offered to consumers when they reach a threshold level $B$ (see equation (3.2)). Below and above $B$, higher rates $C_{\text{low}}$ and $C_{\text{high}}$ are respectively charged. Note that $C_{\text{low}}$ is less than $C_{\text{high}}$. Equation (3.1) presents the pricing schedule $C^t$ as a function of the power request $p^t$. See [24] for more detail about Minimax.

$$C^t = \begin{cases} C_{\text{low}} & \text{if } p^t < B, \\ C_{\text{base}} & \text{if } p^t = B, \\ C_{\text{high}} & \text{if } p^t > B. \end{cases} \tag{3.1}$$

with

$$B = k.\text{mean}(p^t) \tag{3.2}$$

## 3.3 Optimal Consumer Response Model

In this section, we summarize the load scheduling problem formulation under Minimax [24]. To simulate consumer's response to Minimax, we assume the ideal case where any end-user has a load scheduler with perfect pricing information. His/her main concern is the minimization of her/his daily bill. We adopt the load model made of base load (non-deferrable) and deferrable load. The end-user is interested in how to schedule the deferrable loads in order to achieve the lowest possible daily bill (see equations (3.3) through (3.16)).

$$\min : \sum_{t=1}^{|T|} P_{\mathrm{b}}^{t} C_{\mathrm{base}} \tag{3.3}$$

s.t.:

$$P_{\mathrm{b}}^{t} = \left[1 + (k_1 - 1)X_{-}^{t} + (k_2 - 1)X_{+}^{t}\right] B + k_2 p_{+}^{t} - k_1 p_{-}^{t} \tag{3.4}$$

$$p^t = \textstyle\sum_{i=1}^{|I|} z^{i,t} SL^i + BL^t, \quad \forall t \in T \tag{3.5}$$

$$p_{+}^{t} - p_{-}^{t} = p^t - B, \quad \forall t \in T \tag{3.6}$$

$$M.X_{-}^{t} + p_{+}^{t}\varepsilon \geq B, \quad \forall t \in T \tag{3.7}$$

$$M.X_{+}^{t} + B \geq p^t + \varepsilon, \quad \forall t \in T \tag{3.8}$$

$$X_{-}^{t} + X_{+}^{t} \leq 1, \quad \forall t \in T \tag{3.9}$$

$$\textstyle\sum_{t=1}^{|T|} z^{i,t} = D^i, \quad \forall i \in I \tag{3.10}$$

$$z^{i,0} = 0, \quad \forall i \in I \tag{3.11}$$

$$M.(1 - y^{i,t}) + z^{i,t} \geq z^{i,t-1} + \varepsilon, \quad \forall i \in I, \quad \forall t \in T \tag{3.12}$$

$$M.y^{i,t} + z^{i,t-1} \geq z^{i,t} - \varepsilon, \quad \forall i \in I, \quad \forall t \in T \tag{3.13}$$

$$\textstyle\sum_{t=1}^{|T|} y^{i,t} = 1, \quad \forall i \in I \tag{3.14}$$

$$y^{i,t} \in \{0,1\}, \quad \forall i \in I, \quad \forall t \in T \tag{3.15}$$

$$z^{i,t} \in \{0,1\}, \quad \forall i \in I, \quad \forall t \in T \tag{3.16}$$

where:

$T$, the set of time (we assume 24 hours); $I$, the set of schedulable loads; $p^t$ the demand in time $t$; $C^t$, the energy price in time t; $z^{i,t}$, the decision variable equals 1 if load $i$ is scheduled in time t and 0 otherwise; $SL^i$, power rating for the schedulable load $i$; $D^i$, duration of load $i$; $BL^t$, the base load demand in time $t$; $X^t_-$, a decision variable, is equal to 1 if $p^t$ is less than $B$ and 0 otherwise; $X^t_+$, a decision variable, is equal to 1 if $p^t$ is greater than B and 0 otherwise; $p^t_-$, the absolute deviation of $p^t$ from $B$ when $p^t$ is less than $B$ and 0 otherwise; $p^t_+$, the absolute deviation of $p^t$ from $B$ when $p^t$ is greater than $B$ and 0 otherwise; $k_1$ and $k_2$ define the ratios $C_{\text{low}}/C_{\text{base}}$ and $C_{\text{high}}/C_{\text{base}}$ respectively; $y^{i,t}$, a binary decision variable, is equal to 1 if load $i$ comes online in time $t$ after being offline in time $t-1$; $M$, a relatively large number (big M method); $\varepsilon$, a small number used here to enforce strict inequalities.

In the following section we describe the distribution system operator's problem.

## 3.4 The Distribution System Operator's (DSO) Problem

Once the consumers determine their optimal load schedules, the DSO's responsibility is to keep the electric system stable, reliable and at a low cost while end-users enjoy the service of their appliances. We will model in this chapter the DSO's role as an optimal AC power flow (OPF) problem presented in equations (3.17) through (3.21).

$$\min : \sum_{j=1}^{n_{\text{g}}} f^j_{\text{P}}(p^j_{\text{g}}) + f^j_{\text{Q}}(q^j_{\text{g}}) \tag{3.17}$$

s.t.:

$$\theta^k_{\min} \leq \theta^k \leq \theta^k_{\max}, \quad \forall k = 1, 2, ...n_b \tag{3.18}$$

$$v^k_{\min} \leq v^k \leq v^k_{\max}, \quad \forall k = 1, 2, ...n_b \tag{3.19}$$

$$p^j_{\mathrm{g,min}} \leq p^j_{\mathrm{g}} \leq p^j_{\mathrm{g,max}}, \quad \forall j = 1, .., n_g \tag{3.20}$$

$$q^j_{\mathrm{g,min}} \leq q^j_{\mathrm{g}} \leq q^j_{\mathrm{g,max}}, \quad \forall j = 1, .., n_{\mathrm{g}} \tag{3.21}$$

where the decision variables $\theta^k$, $v^k$, $p^j_{\mathrm{g}}$ and $q^j_{\mathrm{g}}$ stand for voltage angle, voltage magnitude, active power output and reactive power output respectively; $n_{\mathrm{g}}$ and $n_{\mathrm{b}}$ are respectively the number of generation units and number of buses; $f^j_{\mathrm{P}}$ and $f^j_{\mathrm{Q}}$ are the active and reactive power cost functions. In the case of a conventional distribution system where we assume power is being supplied from only one bus $n_{\mathrm{g}} = 1$.

## 3.5 Case Study Setup

Our objective is to compare how the total energy bill, generation cost and peak power differs when customers react to Minimax signals locally as an aggregate group (bus level coalition) and when they are in a much larger aggregate group.

The flow chart of the aggregation value evaluation can be summarized as follows: $(i)$ the DSO sends a price signal made of pricing parameters $C_{base}$, $k_1$, $k_2$ and $k$; $(ii)$ consumers form coalition(s) and react to the pricing signal by shifting the available deferrable loads and submit the resulting demand profile(s) to the DSO who solves his OPF problem assess the steady-state operation of his system. At this point the DSO is concerned about not only the supply cost but also the constraint violations if any.

We first used a simulator we built to schedule elastic load demands based on the optimal response model of section 3.3. The pricing parameters we used for the Minimax scheme are $k = 1.05,\ k_1 = 1.1,\ k_2 = 1.3$ and $C_{\mathrm{base}} = \$0.05/\mathrm{kWh}$.

As test power system, we use the IEEE 33-bus distribution system [2] shown in Fig. 3.1. This system consists of 33 buses. We hypothetically place a 10 MW generator at bus 01. We consider a piece-wise linear generation cost function presented in Fig.3.2.

We use the energy usage data set released by UMASS researchers [4, 98]. We select 40 homes from this dataset and then add additional schedulable load such as 40 space heaters, 20 large and 10 small EVs to these homes. We assume each space heater consumes 10 kW with 1 hour operation time. The large fast-charging EV can be charged in 2 hours at a charging rate of 12.5 kW while

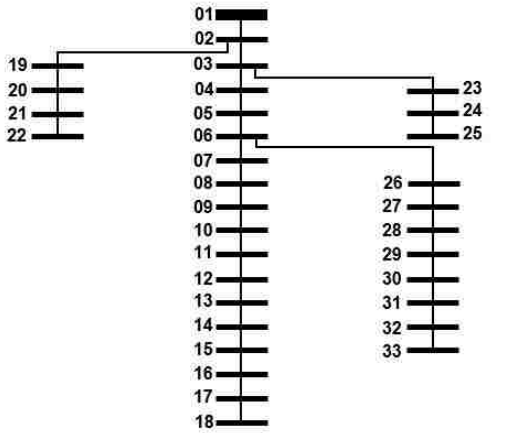


Figure 3.1: IEEE 33-bus System [2]

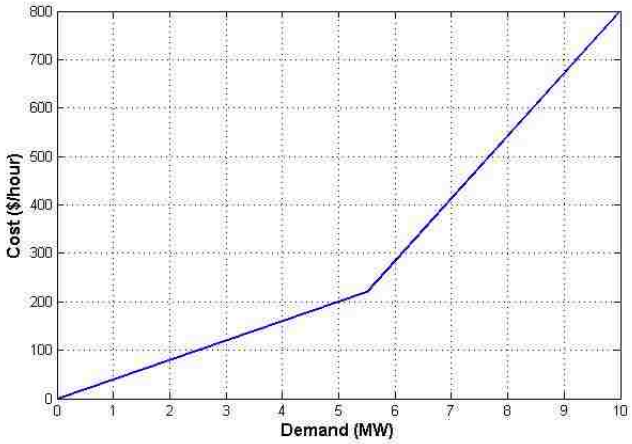


Figure 3.2: Generation cost function

the small EV can be charged at a rate of 3.5 kW for 4 hours [101]. We then form 10 groups of 4 homes each. Each group is allocated the same deferrable load i.e 4 space heaters, 2 large EVs and 1 small EV. At buses 18, 6, 29, 33, 25, 22, 15, 9, 21 and 8 of the IEEE 33-bus system we add the loads of these 10 groups. To keep the same order of magnitude as in the original "case33", the original loads at these buses were scaled down by half and the added loads up by ten. The 23 other buses were kept intact.

We then construct three different demand scenarios: $(i)$ in Scenario 0, we generate base case load schedule and derive for each bus, the demand profile; $(ii)$ in Scenario 1, the consumers serviced by the same bus put their deferrable loads together and react to the DSO's price signal by optimally shifting them in a way that minimize their daily bill; $(iii)$ in Scenario 2, all consumers pool their

deferrable resources and centrally optimize their demand schedule so as to reduce their daily bill, and the central schedule obtained is then dispatched among consumers according to their respective loads.

We solved the consumers' MILP formulated in Section 3.3 using AMPL and CPLEX. We solved the DSO's problem formulated in section 3.4 using MATPOWER [102]. The results are presented in the next section.

## 3.6 Results and Discussion

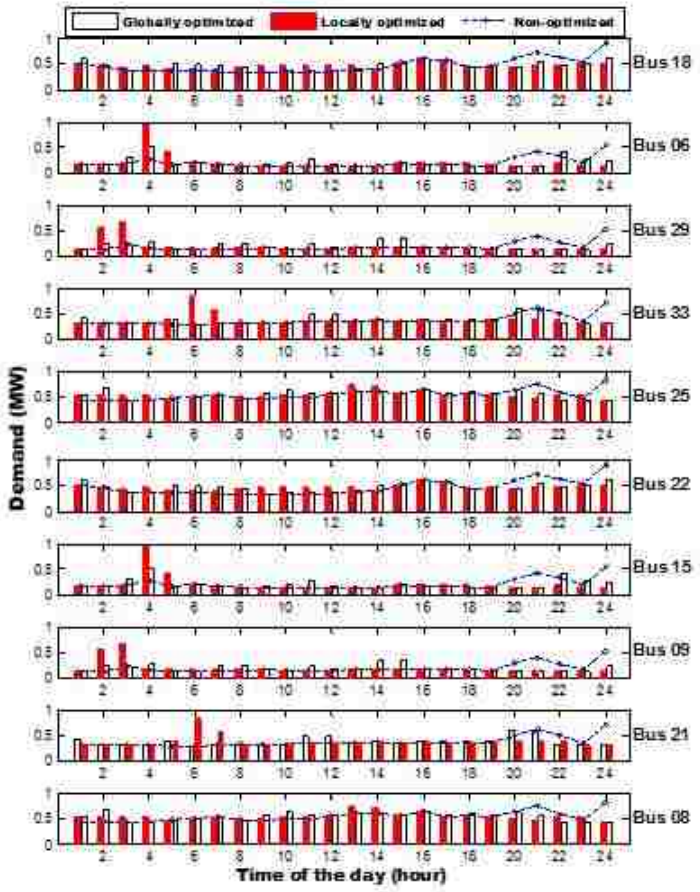


Figure 3.3: Demand Profile comparison

Fig.3.3 shows the load profiles at each bus where there are schedulable loads for each scenario. In Scenario 1, there are very limited amount of deferrable load at each bus, which makes it difficult to smooth out the profiles. The scheduling ends up in some instances, e.g. buses 06, 33, 21 and 15, result in a worst load profile. Fig.3.4 compares the demand profiles obtained for each of the

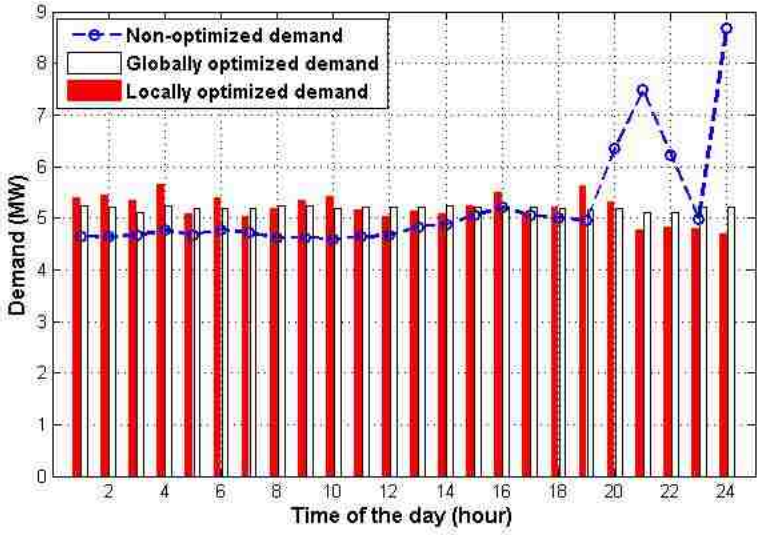


Figure 3.4: Total aggregate demand profile comparison

3 scenarios. Compared to Scenario 0, the globally optimized option (Scenario 2) yields a flatter load profile than the bus-by-bus optimized profile (Scenario 1). The reason behind this fact is that in Scenario 2, we have more flexibility in scheduling due to the larger amount of deferrable load available to choose from.

To compare the impact of the two aggregation solutions proposed in scenarios 1 and 2, we define four performance metrics, namely $(i)$ the peak power reduction, $(ii)$ the accumulated absolute voltage magnitude deviation (AAVMD) $\triangle_V$, $(iii)$ the consumer bill reduction and $(iv)$ the generation cost reduction. The AAVMD is defined by (3.22).

$$\triangle_V = \sum_{t,k} (v^{k,t} - v^k_{\max}) u^{k,t}_+ + (v^k_{\min} - v^{k,t}) u^{k,t}_- \tag{3.22}$$

with $u^{k,t}_+$ and $u^{k,t}_-$ equals 1 if the voltage magnitude at bus $k$ in time $t$, $v^{k,t}$ is greater than $v^{k,t}_{\max}$ and less than $v^{k,t}$min respectively; and 0 otherwise.

The results obtained in the aggregation scenarios 1 and 2 are compared with the base case scenario 0 in Table 3.1. Our results indicate that consumers enjoy an overall daily bill reduction of 3% in Scenario 1 and 6% in Scenario 2. In the same time the DSO experiences a generation cost reduction of 10% in Scenario 1 and 13% in Scenario 2. It is clear that the more flexible load, the more savings both DSO and consumer groups can achieve. From a technical standpoint, both power and voltage profiles are improved. As Fig.3.4 supports, the DSO obtains 35% peak power reduction in Scenario 1 and 40% in Scenario 2. This is equivalent to a load factor of 99% in

Table 3.1: Performance evaluation

| | Scenario 0 (Non-opt.) | Scenario 1 (Locally opt.) | Scenario 2 (Globally opt.) |
|---|---|---|---|
| Peak demand (MW) | 8.664 | 5.646 (-35%) | 5.239 (-40%) |
| Voltage deviation (p.u) | 0.209 | 0.020 | 0 |
| Consumer bill ($) | 6,667 | 6,488 (-3%) | 6,236 (-6%) |
| Generation cost ($) | 5,972 | 5,367 (-10%) | 5,217 (-13%) |

Scenario 2, 92% in Scenario 1 against 60% in Scenario 0. Fig.3.5, 3.6 and 3.7 plot the bus voltage magnitude profile across all 33 buses and throughout the 24 hours horizon for scenarios 0, 1 and 2 respectively. One can easily see that there are more voltage violations in Scenario 0, e.g. in hour 24 for buses 15 through 23, than in Scenario 1. Scenario 2 does not violate any voltage constraint as confirms the AAVMD value $\triangle_V$ in Table 3.1. Note that the voltage references considered in the IEEE 33-bus system are 0.94 and 1.06. From a theoretical point of view, the implication of voltage violation may simply be an unfeasible problem (see the DSo's problem in equations (3.17) through (3.21)). In practice, this is perceived as voltage drop or voltage spike which can be damaging for appliances. The DSO would have to deploy other (likely costly) solutions to hedge these violations.

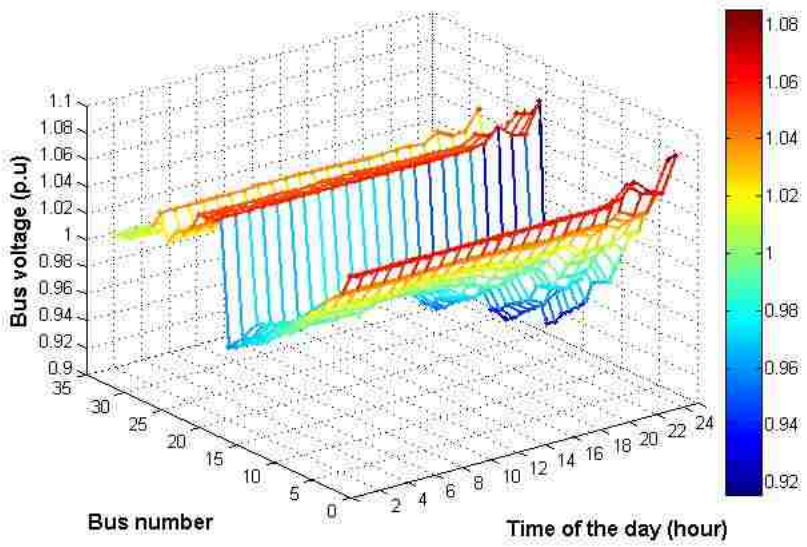


Figure 3.5: Voltage Profile - Scenario 0

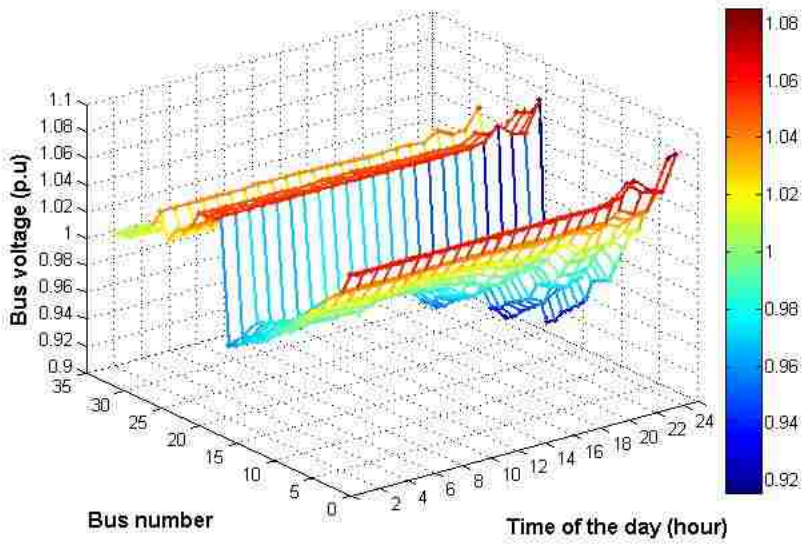


Figure 3.6: Voltage Profile - Scenario 1

## 3.7 Conclusion

This chapter gives the evidence that consumers can significantly impact the electric grid's operations both economically and technically for good if they pool their DR resources under an appropriate retail pricing scheme such as Minimax. Economically, both DSOs and consumer groups can see significant reduction in their costs. In this particular study on the IEEE 33-bus system with 40-home energy usage along with deferrable loads, end-users achieved 3% bill reduction when they optimized their profile on a bus-by-bus basis (Scenario 1) and 6% in case of globally optimized profile (Scenario 2). The DSO's savings amounted 10% in Scenario 1 and 13% in Scenario 2. From a technical standpoint, we observed 35% peak power reduction in Scenario 1 against 40% in Scenario 2. In addition, the base case scenario (Scenario 0) incurred 0.209 p.u voltage magnitude violation against 0.020 p.u for scenario 1. With a more regular voltage profile, Scenario 2 showed no voltage violation. Clearly, under Minimax, massive load aggregation is a win-win game. This is also another evidence that Minimax pricing scheme has much potential for electricity peak demand management.

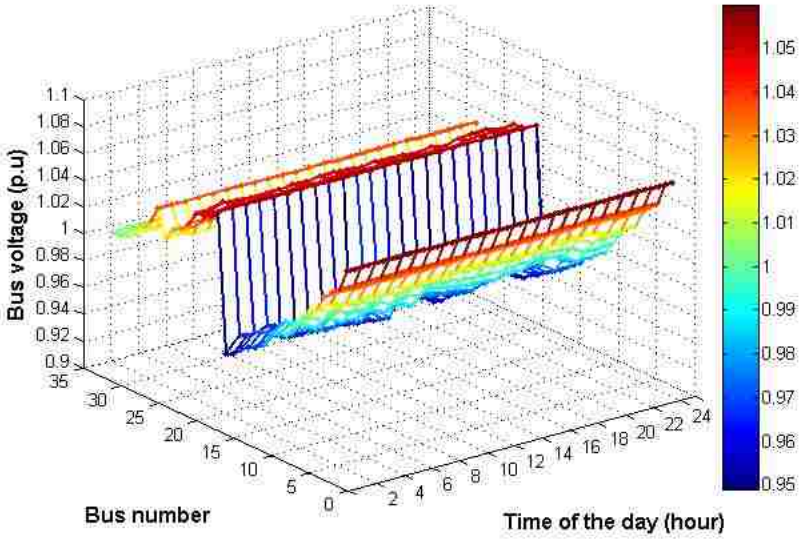


Figure 3.7: Voltage Profile - Scenario 2

# Chapter 4

# GenMinimax Pricing, a Market Tool For Reliable Electric Grids

## 4.1 Introduction

High peak power demand can threaten grid reliability as it drives the power system to its operational limits. Even though, these peak events occur only a few hours a year as shown in Fig.4.1, they significantly affect the electric grid's capital and operational expenses. Thus, increasing demand responsiveness at end-user level in order to reduce peak demands is a key asset for efficient grid operations. Options to achieve responsive demands range from reducing or curtailing loads against payment to dynamic pricing.

The main contribution of this chapter is the introduction of a new retail pricing scheme that uses a combined threshold-penalty/reward approach to provide end-users with the opportunity to affect the price they pay for their energy usage at any time by reducing or increasing their demand. While in other schemes, consumers are charged a given rate at a given time, GenMinimax charges consumers at any given time according to how close or far their consumption is to their threshold of that time. In a sense, the energy price is a function of end-users' "consumption performance" with respect to a predetermined threshold profile. This provides a performance differentiated scheme that incentivizes consumers to adjust their demand on the identified reference profile and therefore enables them to become more active participants. This way, efficient users are charged less than inefficient users.

The remainder of the chapter is organized as follows. Section 4.2 presents the GenMinimax

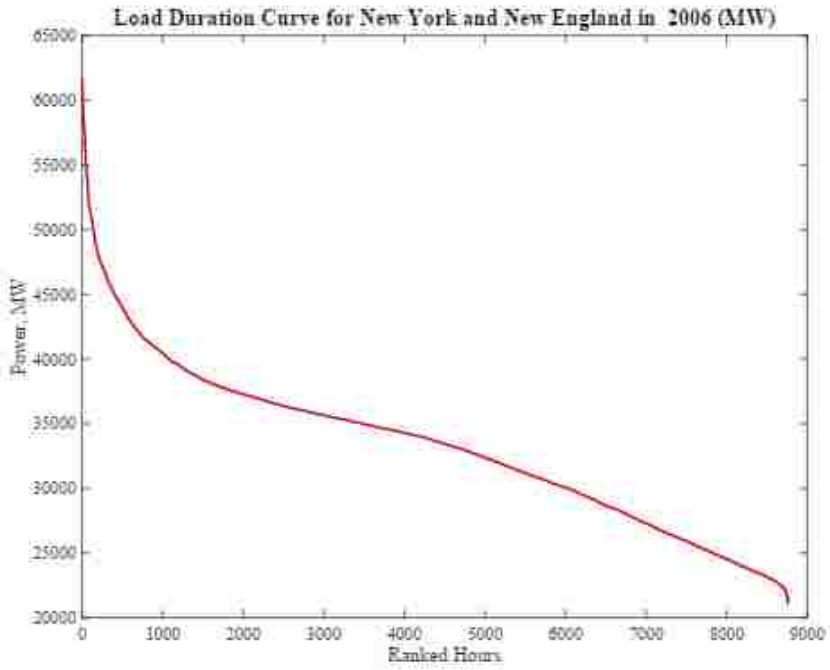


Figure 4.1: Load Duration Curve for New York & New England,2006

pricing scheme, Section 4.3 describes how aggregator and consumer groups would potentially react to GenMinimax. To evaluate the impacts of the proposed novel scheme on grid reliability and consumer bills, we conduct a case study in Section 4.4. The results are presented and discussed in the same section. Section 4.5 presents the concluding remarks of the chapter.

## 4.2 The proposed scheme

The generalized Minimax maintains the concept we previously described in [24], assuming that at any time there is a desirable demand level that ensures efficient generation dispatch, transmission and distribution. In [24] we assumed this demand level to be constant throughout the day. Therefore, customers are charged a higher rate once their aggregate demand exceeds a certain threshold, and they are charged a lower rate when their demand drops under the threshold. In the event their demand equals the threshold, they are charged the lowest rate. We extend this by relaxing the assumption that the desirable demand level (reference profile) is constant. The objective here is to incentivize the consumer group to follow the aggregator's reference profile as closely as possible while allowing consumers to curtail some of their loads, if necessary. The rate $C^t$ at any time $t$ depends on the amount of the power request $p^t$. The pricing schedule is (see Fig.4.2)

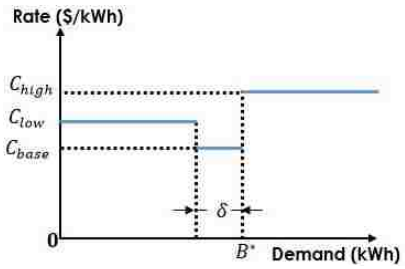


Figure 4.2: Generalized Minimax Rate Structure

$$C^t = \begin{cases} C_{\text{low}} = k_1 C_{\text{base}} & if\ p^t < B^{t*} - \delta, \\ C_{\text{high}} = k_2 C_{\text{base}} & if\ p^t > B^{t*}, \\ C_{\text{base}} & \text{otherwise}, \end{cases} \tag{4.1}$$

where $\delta$ defines the width of the tolerance band below the threshold $B^{t*}$ as shown in Fig. 4.2. $C_{\text{low}}$, $C_{\text{base}}$ and $C_{\text{high}}$ are the rates charged if the realized demand is below, within, or above the threshold band, defined by $B^{t*}$ and $B^{t*} - \delta$, respectively. The parameter $\delta$ can be expressed either as a percentage of $B^{t*}$ or as a constant value. It determines how much deviation below the reference $B^{t*}$ the aggregator is willing to tolerate without charging extra premium.[1] The consumer group can negotiate the value of $\delta$ based on his load granularity and his response history. However, $\delta$ has to be bounded. Note that in GenMinimax, the threshold $B^{t*}$ is not necessarily a constant as opposed to $B$ in [24]. $B^{t*}$ is the solution of the aggregator's optimization problem. $k_1$ and $k_2$ are rate differentiating parameters defined by (4.2) [24].

$$1 < k_1 < k_2. \tag{4.2}$$

## 4.3 Players' response models

To evaluate the performance of GenMinimax, we devise in this subsection optimization models to mimic both aggregator and consumer group's response to market signals.

[1] This constitutes an additional incentive for the consumer group who is no longer forced to exactly attain the threshold to qualify for the lowest rate $C_{\text{base}}$.

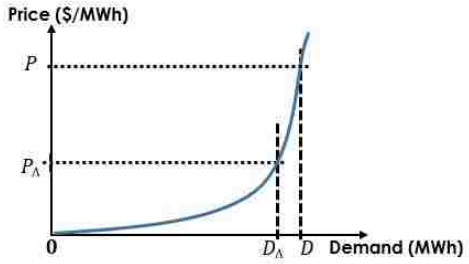


Figure 4.3: Typical supply-demand curve and aggregators' impact

### 4.3.1 The Leader's Problem

To understand the Aggregator's problem, we refer to the typical supply-demand curve, presented in Fig. 4.3.

The mission of the aggregator is twofold: to provide demand response services to the system operator, and to furnish bill reduction opportunities to users [16]. The aggregator is rewarded by the operator for helping shape the consumption in order to meet all technical constraints (e.g., capacity limits) and/or achieve optimal operation costs. Fig. 4.3 illustrates a representative aggregator's impact on supply costs. Here, we assume an initial demand $D$ with corresponding supply cost $P$. By reducing the demand by an amount $\Delta$, the aggregator helps the system operator to reduce the supply cost, to $P_\Delta$. The aggregator is then rewarded with a portion of the cost savings $P - P_\Delta$ for every unit of demand. To maximize her reward from the operator, the aggregator develops a strategy around the expected price signal received from the operator for each time slot in the 24-hour time horizon. [103] shows that the aggregator's optimal strategy would be to determine for each time slot a threshold price $P_{\text{thres}}$ above which not to buy.[2]

On the other hand, in the aggregator's attempt to shape the users' demands, some power requests may be delayed or even curtailed. End-users are rewarded for the changes experienced in those cases. Additionally, the aggregator pays a distribution charge $c_{\text{d}}$ for the energy that flows through the distribution system toward her customers. The aggregator's objective function is therefore given by.

$$\text{Total-Cost} = TEC - DRR + TDC + TCC, \tag{4.3}$$

where *(i)* TEC is the total energy purchase cost, *(ii)* DRR is the total reward earned by participating in demand reduction upon system operator's call, *(iii)* TDC is the total distribution

[2]The consumer group can also buy only the minimum required.

charges paid to the system operator (or the entity in charge of the distribution system), and *(iv)* TCC (Total Curtailment Cost) is the total reward paid by the aggregator to consumers because of delays and curtailments. In this work, we only consider curtailment rewards. Equations (4.4), (4.6), (4.7) and (4.9) define these components.

$$TEC = \sum_t b(t) * c(b^0(t)), \tag{4.4}$$

where $b^0(t)$ is the *ex-ante* (starting) demand the aggregator requests a day ahead, $b(t)$ is the actual demand requests due to the aggregator's participation in Demand Response (DR) or to the consumer group's unwillingness to cooperate, and $c(b^0(t))$ is the rate that the aggregator has to pay based on her initial bid. The procurement cost is assumed to be a piecewise discrete function of $b^o(t)$ as shown in Fig. 4.4. We adopt a three-rate model to represent $c(b^0(t))$.

$$c(b^0(t)) = \begin{cases} rate_1(t) & if\ b^0(t) < b^0_{\text{ref1}}(t), \\ rate_3(t) & if\ b^0(t) > b^0_{\text{ref2}}(t), \\ rate_2(t) & \text{otherwise.} \end{cases} \tag{4.5}$$

We assume this discretization is based on historical data. The cost $c(b^0(t))$ is completely defined by 2 thresholds, $b^0_{\text{ref1}}$ and $b^0_{\text{ref2}}$, and three rates, $rate_1$, $rate_2$ and $rate_3$. The aggregator may request a $b^0(t)$ higher than her expected $b(t)$. But if $b^0(t)$ falls in a higher rate zone, the aggregator would end up paying more than necessary. The fact that the aggregator is paying $c(b^0(t))$ instead of $c(b(t))$ would prevent him to request a higher quantity than what her consumers really need (and potentially trade the difference in the DR market). It is in both the SO and aggregator's interest that $b(t)$ and $b^0(t)$ are kept in the same rate zone. In fact, if aggregators are allowed to choose $b(t)$ and $b^0(t)$ in different rate zones, the supplier may adjust its rates such that they end up paying more. In addition the system operator's next planning period may be drastically affected by the present gap between the expected and the actual demand level; this gap could be very large if all aggregators have anticipated a call for DR participation which does not happen. The demand response reward $DRR$ is given by

$$DRR = \sum_t \alpha(t) * \Delta c(t) * (b^0(t) - b(t)), \tag{4.6}$$

where $\Delta c(t)$ is the anticipated total cost savings yielded by the DR program at time $t$ and $\alpha(t)$

denotes a coefficient which is inversely proportional to the amount of anticipated demand reduction that would yield the above savings. Equation (4.6) suggests that the aggregator is penalized if her actual demand $b(t)$ goes beyond her ex-ante bids.

The total curtailment cost $TCC$ is given by

$$TCC = [l - \sum_t b(t)] * c_{\mathrm{c}}, \tag{4.7}$$

with:

$$l = \sum_t BL^t + \sum_i SL^i * \mathrm{Dur}^i, \tag{4.8}$$

where $l$ is the total daily demand from the consumer group defined by (4.8), $\sum_t b(t)$ the actual energy provided by the aggregator and $c_{\mathrm{c}}$ the contractual curtailment reward.

The total distribution cost $TDC$ is the "rent" paid by the aggregator to the owner of the distribution infrastructure.

$$TDC = \sum_t b(t) * c_{\mathrm{d}}, \tag{4.9}$$

where $c_d$ is the fixed distribution cost per kWh.

We adopt the same load model as in [24]. $BL^t$ stands for the non-deferrable demand in time slot $t$ and $SL^i$ and $\mathrm{Dur}^i$ the rated power and duration of deferrable load $i$ respectively.

Based on the above problem definition, the aggregator's problem can be formulated as follows:

$$\min : \mathrm{Aggregator\_Cost} = TEC - DRR + TDC + TCC \tag{4.10}$$

Subject to:

$$\textstyle\sum_t b(t) \geq \mu * (\sum_t BL^t + \sum_i SL^i * \mathrm{Dur}^i) \tag{4.11}$$

$$b_{max} \geq b(t) \geq BL^t, \quad \forall t \in T \tag{4.12}$$

$$0 < \alpha(t) \leq 1, \quad \forall t \in T \tag{4.13}$$

$$\alpha(t) * (b^0(t) - b(t)) \leq \gamma, \quad \forall t \in T \tag{4.14}$$

$$b^0(t) \leq b_{max}, \quad \forall t \in T \tag{4.15}$$

$$0 \leq \gamma \leq 1, \quad \forall t \in T, \tag{4.16}$$

where besides the variables and parameters already defined, $\gamma$ represents the portion of DR market shared by the aggregator, i.e., the maximum portion of the DR resource that the aggregator is allowed to provide.

Constraint (4.12) ensures that the consumer group's non-deferrable demand is serviced regardless of the market conditions. Constraints (4.14) and (4.16) limit the supplied energy to at most 100% of the required DR resource. The aggregator agrees to serve at least $\mu$ fraction of the total demand (constraint (4.11)).

The formulation in (4.10) through (4.16) has a non-linearity introduced by the definition of TEC, equation (4.4). In fact, the energy rate $c(b^0(t))$ paid at any time $t$ depends on the aggregator's original demand $b^0(t)$ which is a decision variable. Hence, the energy cost $b(t) * c(b^0(t)$ in (4.4) is non-linear. (4.5) is non-convex because $c(b^0(t))$ is not continuous. To make the aggregator's problem solvable, we reformulate equation (4.4) by decoupling rates and demands. This requires additional constraints and binary variables. Equations (4.17) through (4.33) present the constraints to replace (4.4) in the formulation.

$$TEC = \textstyle\sum_t TEC_1(t) + TEC_2(t) + TEC_3(t) \tag{4.17}$$

with, $\forall t \in T$:

$$TEC_1(t) = rate_1(t) * (r_1(t) * b^0_{ref1}(t) - b_1^-(t)) \tag{4.18}$$

$$TEC_2(t) = rate_2(t) * (r_2(t) * b^0_{\text{ref2}}(t) - b_2'^-(t)) \tag{4.19}$$

$$TEC_3(t) = rate_3(t) * (r_3(t) * b^0_{\text{ref2}}(t) + b_2^+(t)) \tag{4.20}$$

$$b_j^+(t) - b_{\mathrm{j}}^-(t) = b(t) - b_{\mathrm{refj}}^0(t), \forall j = 1, 2 \tag{4.21}$$

$$b_1'^+(t) = b_1^+(t) - (r_3(t) * (b_{\mathrm{ref2}}^0(t) - b_{\mathrm{ref1}}^0(t)) + b_2^+(t)) \tag{4.22}$$

$$b_2'^-(t) = b_2^-(t) - (r_1(t) * (b_{\mathrm{ref2}}^0(t) - b_{\mathrm{ref1}}^0(t)) + b_2^-(t)) \tag{4.23}$$

$$M * r_1(t) + b(t) + \varepsilon \geq b_{\mathrm{ref1}}^0(t) \tag{4.24}$$

$$M * (1 - r_1(t)) + b_{\mathrm{ref1}}^0(t) \geq b(t) + \varepsilon \tag{4.25}$$

$$M * r_3(t) + b_{\mathrm{ref2}}^0(t) \geq b(t) + \varepsilon \tag{4.26}$$

$$M * (1 - r_3(t)) + b(t) + \varepsilon \geq b_{\mathrm{ref2}}^0(t) \tag{4.27}$$

$$M * r_1^0(t) + b^0(t) + \varepsilon \geq b_{\mathrm{ref1}}^0(t) \tag{4.28}$$

$$M * (1 - r_1^0(t)) + b_{\mathrm{ref1}}^0(t) \geq b^0(t) + \varepsilon \tag{4.29}$$

$$M * r_3^0(t) + b_{\mathrm{ref2}}^0(t) \geq b^0(t) + \varepsilon \tag{4.30}$$

$$M * (1 - r_3^0(t)) + b^0(t) + \varepsilon \geq b_{\mathrm{ref2}}^0(t) \tag{4.31}$$

$$r_k^0(t) = r_k(t), \quad \forall k = 1, 2, 3 \tag{4.32}$$

$$\sum_{k=1}^{3} r_k(t) = 1 \tag{4.33}$$

$$b_{\mathrm{j}}^{s}(t) \geq 0, \forall j = 1, 2, \forall s \in \{-, +\} \tag{4.34}$$

$$b_{\mathrm{ref2}}^{0}(t) \geq b_{\mathrm{ref1}}^{0}(t) \geq 0 \tag{4.35}$$

$$rate_3(t) \geq rate_2(t) \geq rate_1(t) \geq 0 \tag{4.36}$$

$$r_k(t) \in \{0, 1\}, \forall k = 1, 2, 3, \tag{4.37}$$

where $r_1(t), r_2(t), r_3(t)$ are binary variables, equal to 1 if the original demand $b^0(t)$ is less than $b^0_{ref1}(t)$, between $b^0_{ref1}(t)$ and $b^0_{ref2}(t)$, or greater than $b^0_{ref2}(t)$ respectively. $b_1^-(t)$ and $b_1^+(t)$ are the absolute values of the negative and positive deviations of the actual demand $b(t)$ from the lower reference $b^0_{ref1}(t)$; analogously, $b_2^-(t)$ and $b_2^+(t)$ are the absolute values of the negative and positive deviations of the actual demand $b(t)$ from the upper reference $b^0_{ref2}(t)$. Because $b_1^-(t)$ in zone C and $b_2^-(t)$ in zone A are non-zero, we introduce $b_1'^+(t)$ and $b_2'^-(t)$ such that $b_1'^+(t)$ is equal to $b_1^+(t)$ within the threshold band and 0 outside, (4.22), and $b_2'^-(t)$ is equal to $b_2^-(t)$ within the threshold band and 0 outside, (4.23). For each relevant constraint, $M$ is chosen according to the principles of the so-called "big M" method [104]. $\varepsilon$ is a small real number that helps enforce strict inequality. Given our formulation, the following can be shown.

**Theorem 1.** *Assuming that* $b^0(t)$ *and* $b(t)$ *need to be in the same rate zone as required by constraint* (4.31)*, equation* (4.4) *is exactly the same as* (4.17) *given that* (4.18) *through* (4.37) *hold.*

*Proof:* For clarity, refer to Fig. 4.4, which illustrates the expected supply cost structure along with key variable values for each demand zone. All the relations shown in Fig. 4.4 are trivial, except for $b_2'^-(t)$ in Zone A, and $b_1'^+(t)$ in Zone C, which are explained by constraints (4.22) and (4.23). By replacing the variable values of Fig. 4.4 in (4.18), (4.19) and (4.20) for each demand zone, one can see that:

For demands $b^0(t)$ and $b(t)$ in Zone A.

(1): $TEC_1(t) = rate_1(t) * (b^0_{ref1}(t) - b_1^-(t)) = c(b^0(t)) * b(t)$,

(2): $TEC_2(t) = 0$,

(3): $TEC_3(t) = 0$.

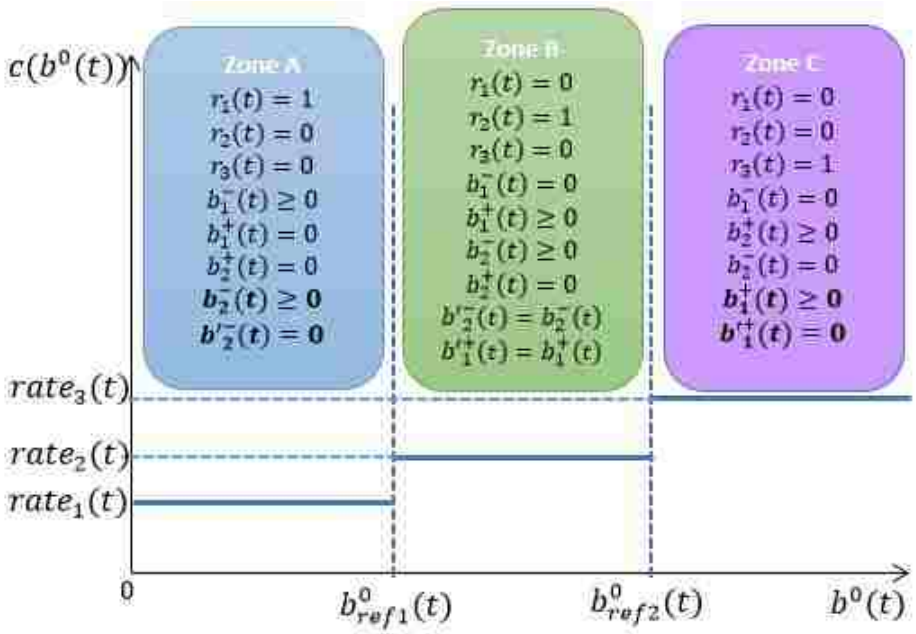


Figure 4.4: Expected Supply cost structure as viewed by the aggregator

For demands $b^0(t)$ and $b(t)$ in Zone B

(4): $TEC_1(t) = 0$,

(5): $TEC_2(t) = rate_2(t) * (b^0_{ref2}(t) - b'^-_2(t)) = c(b^0(t)) * b(t)$,

(6): $TEC_3(t) = 0$.

For demands $b^0(t)$ and $b(t)$ in Zone C

(7): $TEC_1(t) = 0$,

(8): $TEC_2(t) = 0$,

(9): $TEC_3(t) = rate_3(t) * (b^0_{ref2}(t) + b^+_2(t)) = c(b^0(t)) * b(t)$.

In all cases, (4.4) *is exactly the same as* (4.17). Therefore, the leader's problem can be linearized by replacing (4.4) with constraints (4.17) through (4.37).

### 4.3.2 The Follower's Problem

The consumer group's problem is to find an optimal schedule for all deferrable loads with the objective to minimize the group's daily cost. The follower's decision is based on $(i)$ the optimal reference demand profile $B^*$ given by the aggregator, and $(ii)$ the pricing scheme presented in section 4.2. We use similar techniques as in the leader's problem to formulate the follower's

problem presented in equations (4.38) through (4.71). The consumer group's total cost is made of $(i)$ the daily energy bill denoted by *Bill*, $(ii)$ the total cost of utility cost $CU$ which represents the dissatisfaction experienced due to load curtailment, and $(iii)$ the curtailment reward $CR$.

$$\min : \text{Consumer-Cost} = Bill + CU - CR \tag{4.38}$$

Subject to:

$$Bill = \sum_t Bill_1(t) + Bill_2(t) + Bill_3(t) \tag{4.39}$$

$$CU = \sum_i SL^i u^i ucost^i \tag{4.40}$$

$$CR = (\sum_t BL^t + \sum_i SL^i * \text{Dur}^i - \sum_t p^t) * c_{\text{c}} \tag{4.41}$$

$$p^t = BL^t + \sum_i z^{it} SL^i, \ \forall t \in T \tag{4.42}$$

$$Bill_1(t) = C_{\text{low}} * (X_-^t (B^{t*} - \delta) - p_{1-}^t), \ \forall t \in T \tag{4.43}$$

$$Bill_2(t) = C_{\text{base}} * (X_{\text{base}}^t B^{t*}(t) - p_{2-}^t), \ \forall t \in T \tag{4.44}$$

$$Bill_3(t) = C_{\text{high}}^t (X_+^t * B^{t*} + p_{2+}^t), \ \forall t \in T \tag{4.45}$$

$$p_{1+}^t - p_{1-}^t = p^t - (B^{t*} - \delta), \ \forall t \in T \tag{4.46}$$

$$p_{2+}^t - p_{2-}^t = p^t - B^{t*}, \ \forall t \in T \tag{4.47}$$

$$p_{1+}'^t = p_{1+}^t - (\delta X_+^t + p_{2+}^t), \ \forall t \in T \tag{4.48}$$

$$p'^{t}_{2-} = p^{t}_{2-} - (\delta X^{t}_{-} + p^{t}_{1-}),\ \forall t \in T \tag{4.49}$$

$$MX^{t}_{-} + p^{t} + \varepsilon \geq (B^{t*} - \delta),\ \forall t \in T \tag{4.50}$$

$$M(1 - X^{t}_{-}) + (B^{t*} - \delta) \geq p^{t} + \varepsilon,\ \forall t \in T \tag{4.51}$$

$$MX^{t}_{+} + B^{t*} \geq p^{t} + \varepsilon,\ \forall t \in T \tag{4.52}$$

$$M(1 - X^{t}_{)} + p^{t} + \varepsilon \geq B^{t*}),\ \forall t \in T \tag{4.53}$$

$$X^{t}_{-} + X^{t}_{\text{base}} + X^{t}_{+} = 1,\ \forall t \in T \tag{4.54}$$

$$p^{t}_{\text{sj}} \geq 0, \quad \forall s = -, + \quad \forall j = 1, 2 \quad \forall t \in T \tag{4.55}$$

$$B^{t*} \geq \delta \geq 0,\ \forall t \in T \tag{4.56}$$

$$C_{\text{high}} \geq C_{\text{low}} \geq C_{\text{base}} \geq 0 \tag{4.57}$$

$$X^{t}_{-}, X^{t}_{\text{base}}, X^{t}_{+} \in \{0, 1\},\ \forall t \in T \tag{4.58}$$

$$\textstyle\sum_t z^{it} = \text{Dur}^{i} * \sum_t y^{it}, \quad \forall i \in I \tag{4.59}$$

$$u^{i} = \text{Dur}^{i} - \textstyle\sum_t z^{it}, \quad \forall i \in I \tag{4.60}$$

$$z^{i0} = 0, \quad \forall i \in I \tag{4.61}$$

$$M * (1 - y^{it}) + z^{it} \geq z^{i(t-1)} + \varepsilon, \quad \forall i \in I \quad \forall t \in T \tag{4.62}$$

$$M * y^{it} + z^{i(t-1)} \geq z^{i}(t) - \varepsilon, \quad \forall i \in I \quad \forall t \in T \tag{4.63}$$

$$\textstyle\sum_t y^{it} \leq 1, \quad \forall i \in I \tag{4.64}$$

$$es^i \geq 1 \quad \forall i \in I \tag{4.65}$$

$$lc^i \leq |T| \quad \forall i \in I \tag{4.66}$$

$$\mathrm{Dur}^i \leq lc^i - es^i + 1 \leq |T|, \quad \forall i \in I \tag{4.67}$$

$$z^{it} = 0, \quad \forall t \geq lc^i + \varepsilon, or \quad \forall t \leq es^i - \varepsilon, \quad \forall i \in I \tag{4.68}$$

$$y^{it} \in \{0, 1\}, \quad \forall i \in I \quad \forall t \in T \tag{4.69}$$

$$z^{it} \in \{0, 1\}, \quad \forall i \in I \quad \forall t \in T \tag{4.70}$$

$$B^{t*} = \mathrm{argmin}_{\{b(t)\}}\{\text{Aggregator-Cost}\}, \ \forall t \in T, \tag{4.71}$$

where, besides the previously defined variables and parameters: $z^{it}$ is a binary decision variable, 1 if deferrable load $i$ of the set $I$ is scheduled to be powered at time $t$ of the horizon $T$; $BL^t$ the aggregate base load or non-deferrable demand from the consumer group; $SL^i$ the rated power of the deferrable load $i$; $p^t$ the total scheduled demand (including deferrable load and base load) to be serviced in time slot $t$. $\delta$ is the width of the threshold band; $X^t_-$, $X^t_{\text{base}}$ and $X^t_+$ are binary variables indicating that the demand $p^t$ falls respectively under, within, or above the threshold band in the time slot $t$; $p^t_{1-}$ and $p^t_{1+}$ are the absolute values of the negative and positive deviations

of $p^t$ from the lower threshold limit $(B^{t*} - \delta)$ respectively; $p^t_{2-}$ and $p^t_{2+}$ are the absolute values of the negative and positive deviations of $p^t$ from the upper threshold limit $B^{t*}$ respectively. $u^i$ is the inventory of the amount of time during which the deferrable load $i$ is not serviced (equation (4.60)); and $y^{it}$ is a binary variable, equal to 1 if load $i$ comes online in time $t$ after being offline in time $(t-1)$.

Constraints (4.39) through (4.45) define the objective function (4.38). Constraints (4.46) through (4.47) decouple demand and energy price and are key in linearizing the objective function. Constraints (4.50) through (4.58) define variables and cost components associated with the linearized form of the objective function [104]. Constraint (4.59) states that the load $i$ should not be scheduled for more than its duration $\text{Dur}^i$, and ensures that the load $i$ is not interrupted in its operation. Hence, once a load comes online it has to be powered for its entire operation cycle. Constraint (4.68) prevents load $i$ to be scheduled outside certain boundaries defined by $es^i$ (earliest starting time) and $lc^i$ (latest completion time).

## 4.4 Case Study

This section presents simulation results of aggregator and consumer strategies. We also compare the optimal consumer demand profiles under GenMinimax, ToU and RTP. In our simulation, we use an energy utilization dataset released by researchers at the University of Massachusetts Amherst (UMass) [4,98]. We select 40 homes from this dataset and then add additional deferrable loads such as 40 space heaters, 20 large and 10 small electric vehicles (EVs). We assume each space heater is rated 10 kW and an average usage time of four hours or one hour according to scenarios. The large fast-charging EV can be charged in two hours at a charging rate of 12.50 kW while the small EV can be charged at a rate of 3.50 kW for four hours [101]. The base load demand ranges from 151.28 kWh to 212.03 kWh with an average and standard deviation of 167.35 kWh and 17.25 kWh respectively. We set fundamental model parameters as presented in table 4.1 to explore key possible scenarios. $\alpha$ is given in $kWh^{-1}$, $\triangle c$ in \$, $b^0_{\text{ref1}}$ and $b^0_{\text{ref1}}$ in $kWh$ and the rates in \$. Besides the parameter of table 4.1, we set the curtailment cost $c_{\text{c}}$ to \$0.12/kWh, the distribution charge $c_{\text{d}}$ to \$0.02/kWh, the share factor $\gamma$ to 20%, the minimum load service factor $\mu$ to 90%, and the threshold bandwidth $\delta$ to 3 kW. The maximum allowable demand $b_{\max}$ is set to 350 kW. The consumer group modifies their deferrable loads' consumption patterns to reduce their daily energy

Table 4.1: Aggregator's model input parameters

| Time | 1 | 2 | 3 | 4 | 5 | 6 | 7 | 8 | 9 | 10 | 11 | 12 | 13 | 14 | 15 | 16 | 17 | 18 | 19 | 20 | 21 | 22 | 23 | 24 |
|---|---|---|---|---|---|---|---|---|---|---|---|---|---|---|---|---|---|---|---|---|---|---|---|---|
| $\alpha(t) \times 1000$ | 1 | 1 | 1 | 2 | 1 | 2 | 1 | 1.5 | .8 | 1 | 1 | 5 | 1 | 1.5 | 1.5 | .9 | 1 | 1 | 1 | 1 | 2 | 1 | 2 | 1 |
| $\triangle c(t)/100$ | .02 | .01 | .02 | .05 | .12 | 0.6 | 1.2 | .8 | 1.5 | 1.2 | 4 | 7 | 5 | 8 | 5 | 7 | 4 | 9 | 10 | 5 | 4 | 1 | .5 | .02 |
| $b^0_{\text{ref1}}(t)/10$ | 20 | 19 | 19 | 18 | 19 | 19 | 19 | 18 | 20 | 17 | 18 | 17 | 18 | 18 | 17 | 15 | 17 | 19 | 19 | 17 | 17 | 17 | 19 | 20 |
| $b^0_{\text{ref2}}(t)/10$ | 26 | 24 | 22 | 23 | 23 | 22 | 21 | 20 | 22 | 25 | 23 | 24 | 22 | 24 | 21 | 20 | 26 | 22 | 21 | 20 | 20 | 23 | 25 | 26 |
| $rate_1(t) \times 100$ | 4 | 4 | 4 | 4 | 4 | 4 | 4 | 4 | 4 | 4 | 4 | 4 | 4 | 4 | 5 | 5 | 5 | 4 | 4 | 4 | 4 | 4 | 4 | 4 |
| $rate_2(t) \times 100$ | 6 | 6 | 6 | 6 | 6 | 6 | 6 | 6 | 6 | 6 | 6 | 6 | 6 | 6 | 6 | 6 | 6 | 6 | 6 | 6 | 6 | 6 | 6 | 6 |
| $rate_3(t) \times 100$ | 8 | 8 | 8 | 8 | 8 | 8 | 9 | 9 | 9 | 9 | 9 | 9 | 9 | 9 | 9 | 9 | 9 | 9 | 9 | 9 | 9 | 9 | 9 | 9 |

Table 4.2: Simulation setup

| | SCENARIO 1 : The reference profile covers 90% of the total load | SCENARIO 2 : The reference profile covers 100% of the total load |
|---|---|---|
| Case 1 | $c_c$ = \$0.12, $ucost <$ \$0.22; SH duration: 4 hrs. | $c_c = 0$, $ucost$ = \$0.1 for SH and \$0.07 for the rest; SH duration: 1 hr. |
| Case 2 | $c_c$ = \$0.12, $ucost$ = \$0.22; SH duration: 4 hrs. | $c_c = 0$, $ucost$ = \$0.1 for all deferrable loads; SH duration: 1 hr. |
| Case 3 | $c_c$ = \$0.12, $ucost >$ \$0.22 ; SH operating time: 4 hrs. | - |

cost. Note that the bi-level GenMinimax problem is one in which the objective and constraints of the inner problem do not depend on the outer's problem decision variables. Therefore, the GenMinimax problem can be solved sequentially, that is, the inner problem is solved first, and the optimal values of the inner problem are used to define $B^*(t)$ $\forall t$ in the outer problem, which is then solved as a single-level optimization problem. Thus, we solve the Mixed Integer Linear Program (MILP) problems formulated in Section 4.3 using AMPL and CPLEX.

We consider two scenarios to evaluate the impacts of Generalized Minimax with different chosen pricing parameter values so that we can confirm their proper settings.

1. In scenario 1, the aggregator provides only 90% of consumers' total demand. Consumers react to the aggregator's signal based on their own deferrable loads' utility costs and the proposed curtailment reward. Under this scenario, three cases corresponding to three different utility cost settings are explored.

2. In scenario 2, the aggregator provides 100% of the total load. No curtailment reward is proposed. Two cases corresponding to two utility cost settings are considered.

Table 4.2 shows the details of these scenarios and cases.

### 4.4.1 Aggregator's strategy

We obtain the *ex-ante* demand $b^0(t)$ and actual demand $b(t)$ curves shown in Fig. 4.5 for scenario 1, using the UMass data to simulate the aggregator's response. It is noteworthy that in hours 1, 2, 3, 4, 5 and 24, $b^0(t)$ and $b(t)$ are exactly the same. There is no "gaming" on the aggregator's side. This is consistent with her perception of the market. In fact, the aggregator

perceives a very low potential DR reward for these hours and consequently does not bid for any extra demand to trade in the DR market, a strategy which is fairly intuitive. On the other hand, for the rest of the time, she bids beyond the actual demand because of substantial DR reward anticipated. The aggregator bids the least of her maximum market share imposed by $\gamma$ in constraint (4.14) and the maximum of the pricing zone in which the actual demand falls. Note that the actual planned demand $b(t)$ and related aggregator profit are realized only if the consumer group follows exactly the consumption signal $b(t)$, which is not trivial since consumers have their own profits to maximize. In the event of a different demand profile, the aggregator would have to update her profit. The only tools the aggregator has at hand are the contract parameters. Given that for the sake of privacy, the aggregator only knows the base load profile and the gross deferrable demand, we can not expect the consumer group to exactly match the reference profile. However, if all parameters are appropriately chosen, the reference profile should envelop the scheduled profile or set a trend for it. The next subsection discusses the consumers's strategy.

### 4.4.2 Consumer group's strategy

The consumer group's response to the aggregator's demand signal depends not only on the pricing parameters but also on the utility cost and the curtailment reward offered. In fact, looking at only one time unit, for the consumer group to schedule an additional deferrable load $i$ on top of the current demand $p^t$, the energy bill growth $[(p^t + SL^i) * C(p^t + SL^i) - p^t * C(p^t)]$ has to be less than the cost of keeping load $i$ offline which is $SL^i * (ucost^i - c_{\mathrm{c}})$. We assume a case where the demand is initially under the threshold band i.e., $C(p^t) = C_{\mathrm{low}}$. With the added deferrable load $i$, the demand $(p^t + SL^i)$ can $(i)$ still stay under the threshold band (in which case $C(p^t + SL^i) = C_{\mathrm{low}}$), $(ii)$ fall within the band (in which case $C(p^t + SL^i) = C_{\mathrm{base}}$) or $(iii)$ go above it (in which case $C(p^t + SL^i) = C_{\mathrm{high}}$). These cases are respectively expressed by (4.72) through (4.74).

$$C_{\mathrm{low}} \leq ucost^i - c_{\mathrm{c}}, \tag{4.72}$$

$$C_{\mathrm{base}} \left[1 + \tfrac{p^t}{SL^i}(1 - k_1)\right] \leq ucost^i - c_{\mathrm{c}}, \tag{4.73}$$

$$C_{\mathrm{high}} \left[1 + \tfrac{p^t}{SL^i}(1 - \tfrac{k_1}{k_2})\right] \leq ucost^i - c_{\mathrm{c}}. \tag{4.74}$$

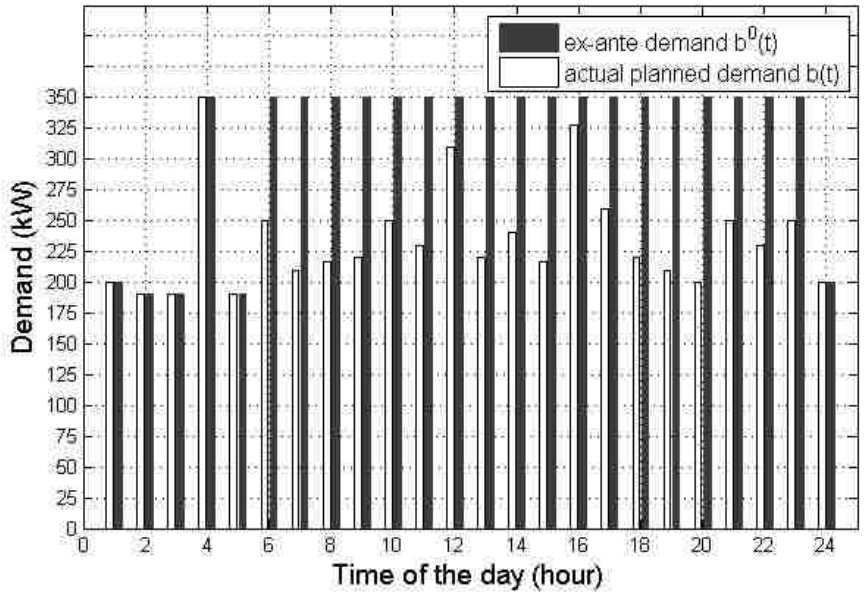


Figure 4.5: Aggregator's optimal strategy - scenario 1

For the load aggregator, the desirable situations are the first two (see (4.72) and (4.73)). Given that $k_1 \geq 1$, the second case (equation (4.73)) is always realized as long as $ucost^i \geq c_c$. However, the situation depicted by (4.74) is detrimental to the load aggregator since she would like to discourage the consumer group's aggregate demand to exceed the threshold band. Hence the aggregator has to set the prices so as to reverse the inequality in (4.74). Without lost of generality, we suggest the contractual constraint (equation (4.75)) to bind all pricing parameters. In practice, the actual values of $k_1$ and $k_2$ must be obtained from price elasticity based consumer behavioral studies [105, 106].

$$C_{\text{low}} \leq (ucost^i - c_c) \leq C_{\text{high}}, \quad \forall i \in I. \tag{4.75}$$

Fig. 4.6 shows how critical the utility cost is in the consumers' reaction. We recall that the utility cost $ucost^i$ of deferrable load $i$ is the measure of the "*harm*" caused to end-users if load $i$ is not served. Thus, we understand that in the current load model, the base load has a utility cost of $+\infty$. It is intuitive to foresee that if the curtailment reward $c_c$ is greater than the utility cost *ucost*, consumers would rather have all their flexible loads curtailed. The profile obtained in scenario 1, case 1 of Fig. 4.6 represents the consumer group's optimal demand profile under the assumption that the curtailment reward is greater than the utility cost. This profile is exactly the same as the base load profile which the aggregator has to serve under any circumstance.

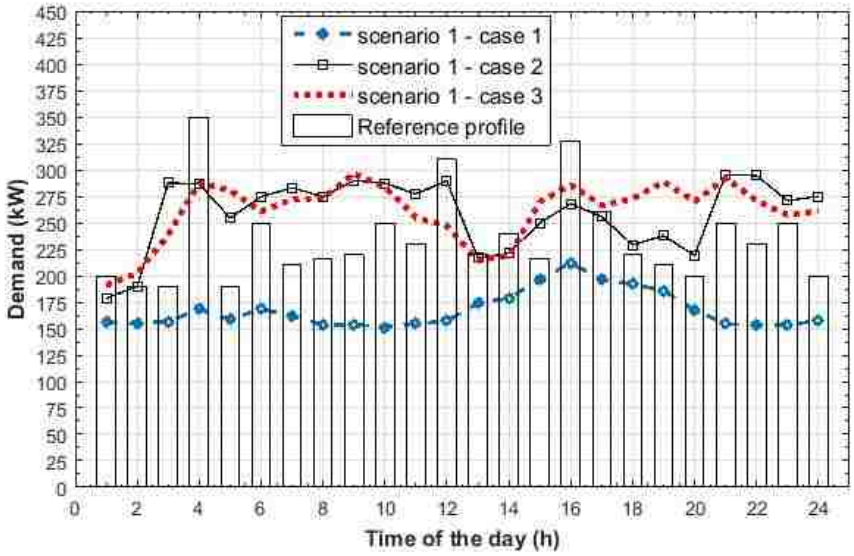


Figure 4.6: Consumer group's optimal strategy in scenario 1 for cases 1, 2 and 3

However, we observe a change in the profile only at a utility cost of \$0.22 for all $i$. Recall that we use a curtailment reward $c_c$ of \$0.12 in this simulation. Note that the reference profile in this scenario covers only 90% of the total load, i.e., $\mu$ in equation (4.11) is set to 0.9. Fig. 4.6 underlines the fact that the utility cost is key in the consumers' decision. If the utility costs are very high compared to the curtailment reward and pricing penalties expressed by $k_2$ in (4.1), the threshold band is violated to prevent high $CU$. This is shown by both scheduled profiles which are not confined within or under the threshold band. These outcomes confirm the discussion around equations (4.72) through (4.75).

In addition, Fig. 4.6 reveals a certain inertia in the scheduled profiles. Recall that we set space heaters' operating time to 4 hours, that of large EVs to 2 hours and small EVs to 4 hours. Constraints (4.59), (4.62), (4.63) and (4.64) ensure that load $i$, if served, is not interrupted before its completion time. No such requirement is accounted for in the aggregator's model. This means that the longer the non-stop operation times, the more inertia we see in the scheduled profile and the less likely the latter is to match a reference profile. To illustrate this analysis, we set the space heaters' duration to *1 hour* for all cases in Scenario 2. For simplicity, we assume there is no curtailment reward ($c_c = 0$) meaning that consumers have no profit based incentive to withhold some of their flexible loads. After all, the difference ($ucost^i - c_c$) compared to the consumer's rate

is what matters.

Fig. 4.7 presents the consumer group's strategy for 2 types of utility cost. The resulting profile in scenario 2, case 1 corresponds to the optimal demand profile when the cost of utility of the space heaters is \$0.10/kWh and the EVs are worth \$0.07/kWh based on their relative criticality. We chose \$0.09/ kWh as $C_{\text{base}}$, $k_1$ and $k_2$ are respectively 1.1 and 1.3 as in Scenario 1. Hence, $C_{\text{low}}$ is slightly lower than the cost of utility of the heaters. In this case, only the heaters came online in the optimal scheduling. All EVs are curtailed because serving them would lead to a higher total cost.

In the second case (Scenario 2, Case 2), we set the cost of utility for all deferrable loads to \$0.10/kWh to keep the difference ($ucost^i - c_{\text{c}}$) at \$0.10/kWh as in Scenario 1, Case 2. This time, 5 heaters and 1 large EV are curtailed and the scheduled profile matches *almost* perfectly the reference profile in Fig. 4.7. The effect of short-term loads can be seen in hours 17, 21 and 23 where relatively sharp transitions are obtained without violating the threshold band. For more flexibility in matching the reference profile under *Generalized Minimax*, we suggest that the continuity constraints embodied by equations (4.59) and (4.64) can be relaxed by removing the term $\sum_t y^{it}$ and replacing the *equality* by *less or equal* in (4.59), and simply changing (4.64) into $\sum_t y^{it} \geq 0$. Even if this cannot realistically be done for all types of loads, one can create a subset of loads for which this relaxation is possible and thus contribute to a better demand responsiveness.

To evaluate how well (or tight) the scheduled consumption of the consumer group matches the reference profile, we define a performance index (relative error) $\epsilon^t$ given by (4.76). The lower $\epsilon^t$, the better the performance.

$$\epsilon^t = \frac{B^{t*} - p^{t*}}{B^{t*}}. \tag{4.76}$$

The daily performance can be assessed by either averaging the absolute value of $\epsilon^t$ or taking its maximum absolute value. Fig.4.8 shows the performance index for the different cases and scenarios investigated. in Scenario 1, the average and maximum absolute deviations are 27% and 52% for Case 1, 18% and 51% for Case 2, and 19% and 48% for Case 3 respectively. The large deviation is caused by the fact that the aggregator had planned ahead of time to curtail 10% of the loads while the consumer group simply reacts to the pricing signal given the costs of utility. In Scenario

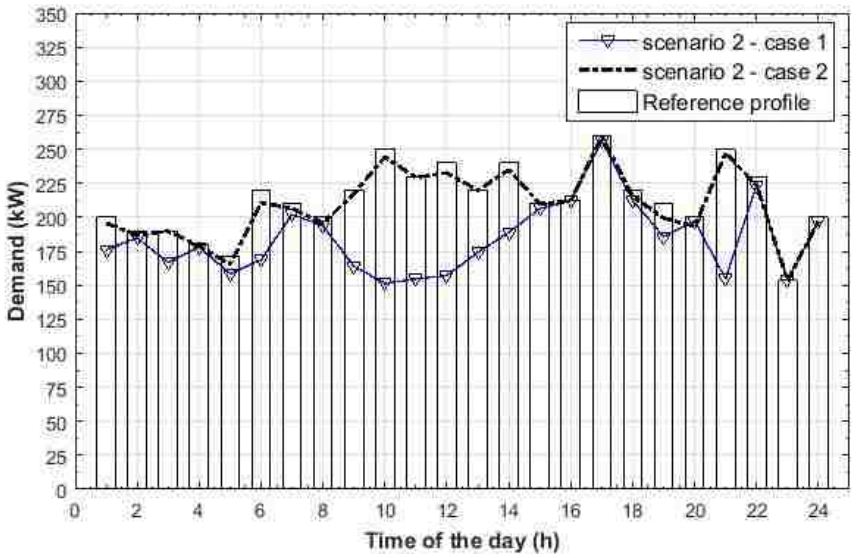


Figure 4.7: Consumer group's optimal strategy in scenario 2 (cases 1 and 2)

2, the average and maximum absolute deviations are 13% and 39% for Case 1, 2% and 5% for Case 2 respectively. The relatively large deviation in Case 1 is due to the fact that according to the consumer group, the EVs are not worth paying \$0.09/kWh to serve them, their cost of utility being only \$0.07/kWh in this case, while the aggregator has planned to serve them. One can easily see that the right profiling signal is the one made of concordant price settings satisfying constraint (4.75) for Scenario 2 case 2, our best performance instance. Additionally, both aggregator and consumer group should be in harmony with regard to how much load is to be covered.

### 4.4.3 Comparison of GenMinimax, TOU and RTP

Under TOU and RTP, the rate applied at any time $t$ does not depend on the demand while in GenMinimax the rate is a discrete function of the demand, a function that varies according to the desired demand profile.

To evaluate GenMinimax with regard to TOU and RTP, we simulate the consumer group's optimal profiles in response to the above pricing scheme and compute the relative error given by equation (4.76). Consumers respond to GenMinimax according to the strategy presented in subsection 4.4.2. We briefly discuss in this subsection the consumer group's response model. In TOU pricing, consumers are bound to 2 or 3 rates corresponding each to predefined off-peak, mid-peak and/or peak periods. On the other hand, the energy rate paid by consumers in RTP is subject to change every hour. Consumers are given a day-ahead RTP signal to which they

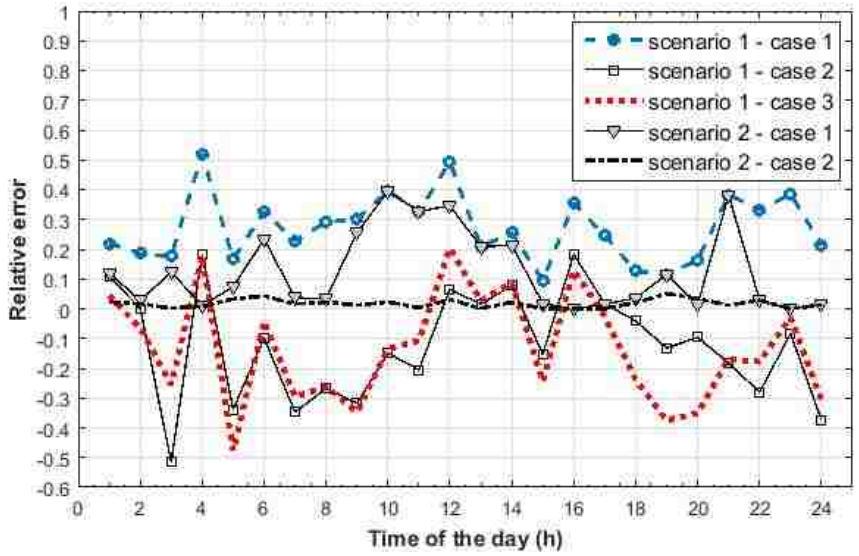


Figure 4.8: Performance evaluation in all scenarios and cases

react by scheduling their daily demand profile. Fig.4.9 shows the TOU signal adapted from the 2012 Ontario rates [107] and the RTP signal is obtained as inversely proportional to the reference or desirable demand profile such that it has the same average daily rate as the TOU rate, for comparison purposes.

The consumer group's objective has not changed: minimize the group's total energy cost. Given that the energy rates are independent on the demand in RTP and TOU pricing, the consumer model can be expressed by equations (4.77) through (4.80).

$$\min : Bill = \sum_{t=1}^{|T|} C^t * p^t \tag{4.77}$$

Subject to: constraints (4.42), (4.61) - (4.63), (4.65) - (4.70)

$$p^t \leq Pmax, \ \forall t \in T \tag{4.78}$$

$$\sum_t z^{it} = \text{Dur}^i, \ \forall i \in I \tag{4.79}$$

$$\sum_t y^{it} = 1, \ \forall i \in I \tag{4.80}$$

The only new parameter in this formulation is $Pmax$ which is the maximum demand possible.

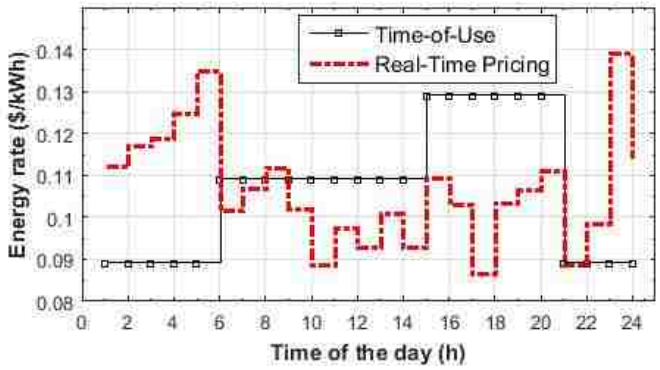


Figure 4.9: TOU and RTP pricing signals

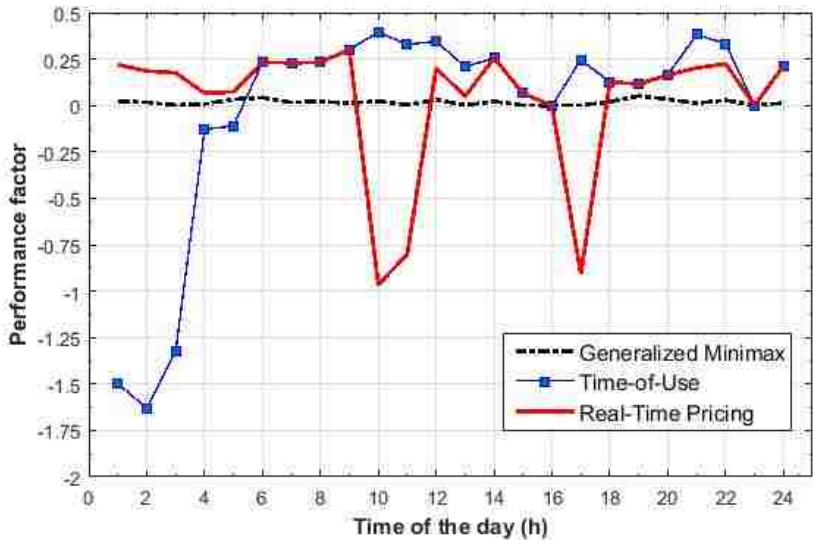


Figure 4.10: Comparison of response performance factor for TOU, RTP and GenMinimax

$z^{it}$, the decision variable is the same as defined in previous models in this part. $C$ is the rate vector whether we are in TOU or RTP.

We use the GenMinimax parameters used in scenario 2 case 2 and compare the resulting demand profile with those obtained under TOU and RTP as described above. We base the comparison on the performance factor $\epsilon$ defined by equation (4.76). Fig.4.10 plots $\epsilon$ for TOU, RTP and GenMinimax. One can see that with GenMinimax, the resulting profile is closer to the reference. The maximum relative gap between the reference supply profile and the scheduled one is 163% for TOU, 97% for RTP and 5% for GenMinimax. The average relative gaps are 37%, 25% and 1.7% for TOU, RTP and GenMinimax respectively. The performance of GenMinimax is justified by its time and demand dependency.

## 4.5 Conclusion

Price responsiveness of demand is key under the future smart grid paradigm where higher renewable penetrations are expected. Major dynamic pricing mechanisms such as TOU and RTP do not provide incentives to match the available resources with the demand due to behavioral and strategic considerations amongst others. In this work, we generalize the concept of *Minimax pricing* first introduced in [24], seeking to nudge end-users to match their demand to any type of supply reference either variable or flat provided that they have sufficient deferrable loads. The results also show that selfish gaming on aggregator's and/or consumers' side is likely to lead to an unstable power system. For a proper response from consumers, aggregator should consider the average cost of utility of the deferrable loads. Results indicate that it is crucial to set cost of utility higher than the curtailment reward for a consumer to schedule the corresponding loads. Additionally, the second highest rate ($C_{\text{low}}$) should not be higher than the difference between cost of utility and the curtailment reward. With appropriately chosen pricing parameters, *Generalized Minimax* can incentivize the customer group to follow closely the reference supply profile sent by a single aggregator as a solution to her own profit maximization problem given anticipated market conditions, and the consumer group is able to fit the reference profile with 5% maximum error and less than 2% average error. The consumers, under GenMinimax, have the opportunity or the power to reduce their energy rate by reducing or increasing their demand. In fact, the demand is time-dependent and GenMinimax rates are demand-dependent with respect to the optimal demand signal. In contrary, TOU and RTP are solely time-dependent. Consumers cannot change their energy rate at any time if they reduce or increase their consumption. Consequently, TOU and RTP lead to higher maximum and average errors: 163% and 37% for TOU, and 97% and 25% for RTP. The problem setup structure in this part supports further research in models with increased user cooperation, most importantly by modeling the strategic interactions between several aggregators.

# Chapter 5

# Reliabilty-aware Renewable Integration: Introduction of a Short-term Reserve Market

## 5.1 Introduction

With the expected increase of intermittent renewable energy resources on the electric power grid, short-term reserve markets can prove to be a critical reliability asset. This chapter considers a hypothetical market structure that includes a short-term reserve market where the realized energy is drawn within the bounds of the hourly capacity offered. The study presents a risk-aware stochastic solution process that determines, based on the day-ahead offer derived using a classic newsvendor formula, the best intra-day offers for a wave energy farm. Uncertainties related to energy production and market prices are accounted for. To demonstrate the effectiveness of the proposed formulation, we study the case of a wave farm. The introduction of the short-term reserve market results in a wider risk range but induces 5% profit increase and a lower profit reduction across the risk range.

The remainder of this chapter is structured as follows. Section 5.2 describes the market model and energy management framework under consideration in this work. Section 5.3 introduces the analysis of the day-ahead energy bidding as a newsvendor problem and evaluates the implications of such a bidding strategy. Section 5.4 formulates the resulting second stage offering problem in

Table 5.1: Nomenclature (Part A)

| Symbol | Description |
|---|---|
| $\alpha$ | confidence level. |
| $\beta$ | loss of profit risk sensitivity factor. |
| $c_{\mathrm{d}}$ | storage unit depletion cost incurred when the state of charge *soc* violates healthy operation thresholds. |
| $C_{\mathrm{o}}^{t}$ | overage cost in time $t$, $\forall t \in \mathcal{T}$. |
| $C_{\mathrm{u}}^{t}$ | underage cost of time slot $t$, $\forall t \in \mathcal{T}$. |
| $CVaR_{\alpha}$ | conditional value at risk, at the confidence level $\alpha$. |
| $DA^{t}$ | day-ahead energy offer for the time $t$, $\forall t \in \mathcal{T}$. |
| $\delta_{\mathrm{C}}^{ts\omega}, \delta_{\mathrm{D}}^{ts\omega}$ | charge, discharge energy for scenario $\omega$ in time $t$ and time-slot $s$, $\forall\ t \in \mathcal{T},\ s \in \mathcal{S},\ \omega \in \Omega$. |
| $\Delta_{\mathrm{s}}$ | duration in hour of one time-slot unit ($\Delta_{\mathrm{s}} = 0.0833\ h$ (5 min)). |
| $\Delta_{\mathrm{t}}$ | duration in hour of one time unit ($\Delta_{\mathrm{t}} = 1\ h$). |
| $E_{\mathrm{G}}^{ts\omega}$ | energy output of the renewable converter in scenario $\omega$, time $t$ and time-slot $s$, $\forall t \in \mathcal{T},\ s \in \mathcal{S},\ \omega \in \Omega$. |
| $E_{\mathrm{net}}^{t\omega}$ | net energy output of the renewable farm after reserve energy in scenario $\omega$ and time $t$, $\forall\ t \in \mathcal{T},\ \omega \in \Omega$. |
| $E_{\mathrm{out}}^{ts\omega}$ | energy output of the renewable farm in scenario $\omega$, time $t$ and time-slot $s$, $\forall t \in \mathcal{T},\ s \in \mathcal{S},\ \omega \in \Omega$. |
| $\eta_{\mathrm{C}}, \eta_{\mathrm{D}}$ | charge and discharge efficiency. |
| $F^{t}(.)$ | cumulative distribution function of all possible realizations in time $t$, $\forall\ t \in \mathcal{T}$. |
| $\gamma^{t}$ | price fractile in time $t$, $\forall t \in \mathcal{T}$. |
| $\lambda^{t\omega}$ | positive imbalance charge for scenario $\omega$ in time $t$, $\forall\ t \in \mathcal{T},\ \omega \in \Omega$. |
| $\Omega$ | set of scenarios. |
| $P_{\mathrm{cap}}$ | storage power capacity. |
| $P_{\mathrm{max}}$ | interconnection feeder capacity. |
| $p^{t}$ | day-ahead market clearing price in time $t$, $\forall t \in \mathcal{T}$. |
| $p_{\mathrm{r}}^{\omega}$ | probability of scenario $\omega$, $\forall \omega \in \Omega$. |
| $\pi^{t\omega}$ | farm profit for scenario $\omega$ in time $t$, $\forall\ t \in \mathcal{T},\ \omega \in \Omega$. |
| $q^{t\omega}$ | negative imbalance charge in scenario $\omega$ and time $t$, $\forall\ t \in \mathcal{T}, \omega \in \Omega$. |
| $r^{ts\omega}$ | reserve market energy price (\$/kW) for scenario $\omega$ in time $t$, $\forall\ t \in \mathcal{T},\ \omega \in \Omega$. |
| $R_{\mathrm{g}}^{ts\omega}$ | energy output in the reserve market for scenario $\omega$ in time $t$ and time-slot $s$, $\forall t \in \mathcal{T},\ s \in \mathcal{S},\ \omega \in \Omega$. |
| $RT^{t}$ | real-time market bid in time $t$, $\forall t \in \mathcal{T}$. |
| $RV^{t}$ | reserve market bid in time $t$, $\forall t \in \mathcal{T}$. |
| $\rho^{t\omega}$ | real-time market price for scenario $\omega$ in time $t$, $\forall\ t \in \mathcal{T},\ \omega \in \Omega$. |
| $\mathcal{S}$ | set of time-slots. |
| $S_{-}$ | minimum healthy storage state of charge threshold. |
| $S_{+}$ | maximum healthy storage state of charge threshold. |
| $S_{\mathrm{cap}}$ | storage energy capacity. |
| $soc^{ts\omega}$ | state of charge for scenario $\omega$ in time $t$ and time-slot $s$, $\forall t \in \mathcal{T},\ s \in \mathcal{S},\ \omega \in \Omega$. |
| $\sigma$ | storage efficiency. |
| $\mathcal{T}$ | set of times. |
| $VaR_{\alpha}$ | value at risk. |
| $v^{t\omega}$ | reserve market capacity price (\$/kWh) for scenario $\omega$ in time $t$, $\forall\ t \in \mathcal{T},\ \omega \in \Omega$. |

the presence of an ESS as a risk-aware two-stage stochastic model. In Section 5.5, we conduct a case study to evaluate the impacts of the short-term market on farm profitability. Section 5.6 concludes the chapter.

Table 5.2: Nomenclature (Part B)

| Symbol | Description |
|---|---|
| $x_{\mathrm{z}}^{t\omega}$ | output energy deviation binary variables of zone z ($\mathrm{z} \in \{1,2,3\}$) for scenario $\omega$ in time $t$, $\forall\ t \in \mathcal{T},\ \omega \in \Omega$. |
| $\hat{y}$ | expected value of the stochastic parameter $y$. |
| $Y^{\omega}$ | CVaR's slack variable for scenario $\omega$, $\omega \in \Omega$. |
| $z_{\mathrm{DA}}^{t\omega}$ | day-ahead energy shortage for scenario $\omega$ in time $t$, $\forall\ t \in \mathcal{T},\ \omega \in \Omega$. |
| $z_{\mathrm{ES}+}^{ts\omega}$ | deviation above the healthy storage operation upper threshold for scenario $\omega$ in time $t$ and time-slot $s$, $\forall t \in \mathcal{T},\ s \in \mathcal{S},\ \omega \in \Omega$. |
| $z_{\mathrm{ES}-}^{ts\omega}$ | deviation below the healthy storage operation lower threshold for scenario $\omega$ in time $t$ and time-slot $s$, $\forall t \in \mathcal{T},\ s \in \mathcal{S},\ \omega \in \Omega$. |
| $z_{\mathrm{ES}}^{ts\omega}$ | Total state of charge deviation in scenario $\omega$, time $t$ and time-slot $s$, $\forall t \in \mathcal{T}$, $s \in \mathcal{S},\ \omega \in \Omega$. |
| $z_{\mathrm{out}}^{t\omega}$ | market energy excess for scenario $\omega$ in time $t$, $\forall\ t \in \mathcal{T},\ \omega \in \Omega$. |
| $z_{\mathrm{RT}}^{t\omega}$ | real-time energy shortage for scenario $\omega$ in time $t$, $\forall\ t \in \mathcal{T},\ \omega \in \Omega$. |
| $\zeta^{ts\omega}$ | reserve energy signal for scenario $\omega$ in time $t$ and time-slot $s$, $\forall t \in \mathcal{T},\ s \in \mathcal{S}$, $\omega \in \Omega$. |

## 5.2 System Framework

Environmental concerns raised about predominant conventional energy fuels such as oil and coal, position renewable energy resources as a must-have in any electricity fleet worldwide. Calls for an increased renewable share in the energy portfolio are persistent. The increasing levels of intermittent energy are adding to the inherent uncertain variability of electricity grids. System operators will have to deal with a decreasing inertia grid. On the other hand, renewable producers would have to face high imbalance penalties or frequent curtailments. To hedge against these alarming future challenges for both system operators and sustainable energy producers, it is important that renewable generation units are operated in a reliability-centered fashion. This calls for establishing a standard operation framework that showcases a composite reliability assets such as accurate recurrent forecasts, energy storage, multi-step and multi-period control techniques, and multi-market opportunities. We present in Fig. 5.1 a typical renewable market integration framework. The framework comprises a renewable farm (e.g., wave, wind, or solar) coupled with an energy system. The farm has the opportunity to bid in day-ahead, real-time and short-term reserve markets. The day-ahead market clears daily, the real-time market clears hourly and 15 minutes before realization hour. We introduce a short-term reserve market made of capacity offers and energy outputs. The energy output is imposed by the system operator (via an energy signal) within the limits of the cleared reserve capacity. In all these markets, the renewable producer is a price-taker. The framework boasts a forecasting engine that predicts price and energy information needed by the decision making modules. The farm controller executes the optimal schedules. Fig.

5.1 presents the operating environment of the wave energy farm considered in this chapter.

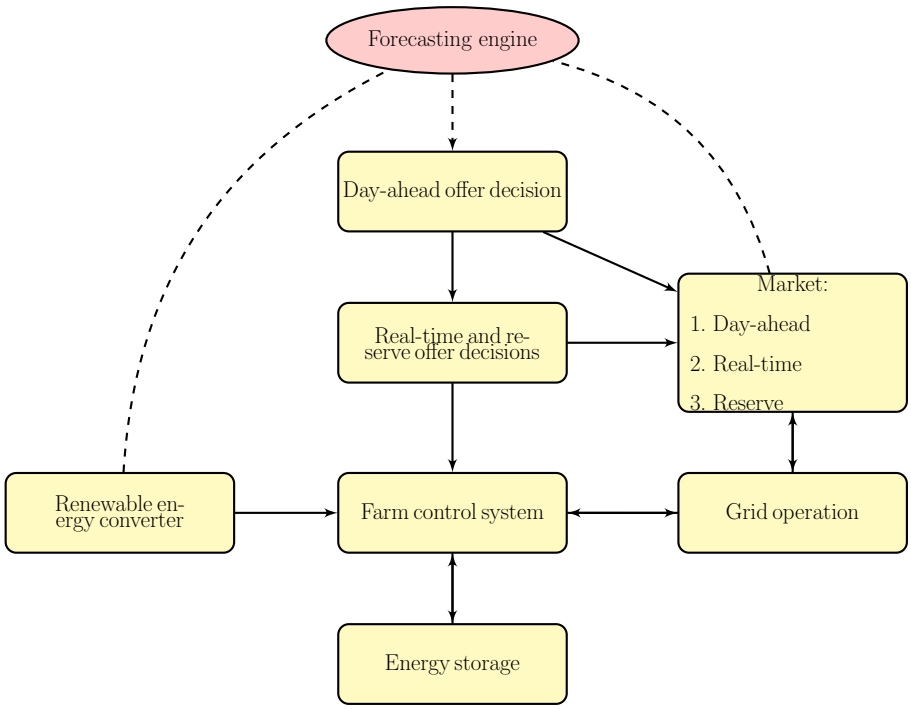


Figure 5.1: Renewable integration framework

## 5.3 Day-ahead Bidding as a Newsvendor Problem

We pose the day-ahead optimal bidding problem as a newsvendor problem [59]. The market considered is of the traditional two-settlement structure. Under this model, energy supplier $i$ places his offer made of the amount of energy $DA^{it}$ he plans to output and the price $p^{it}$ he will sell it, for any time slot $t \in \mathcal{T}$ the next day. The system operator (SO) clears the market at a price $p^t$ and all suppliers with $p^{it}$ less than or equal to $p^t$ are selected and get $p^t$ for each unit of energy output the next day at time $t$, for all $t \in \mathcal{T}$. At the time of realization, depending on the grid balancing needs (with the use of emergency generators) in any time $t$, the SO charges for any unit of negative deviation the price $q^t$. For any extra unit of energy above $DA^{it}$, the supplier $i$ is charged $\lambda^t$. For the sake of simplicity and clarity we will consider only one renewable farm and get rid of the subscript $i$. According to the formulae established by Bitar et al. [59], the optimal

day-ahead bid at time $t$, $DA^{t*}$, is given by (5.1)

$$DA^{t*} = \begin{cases} 0, & \hat{p}^t < -\hat{\lambda}^t \\ {F^t}^{-1}(\gamma^t), & -\hat{\lambda}^t \leq \hat{p}^t \leq \hat{q}^t \\ E^t_{\mathrm{Gmax}}, & \hat{p}^t > \hat{q}^t \end{cases} \tag{5.1}$$

with the price fractile $\gamma^t$:

$$\gamma^t = \frac{\hat{p}^t + \hat{\lambda}^t}{\hat{q}^t + \hat{\lambda}^t} \tag{5.2}$$

where $F^t$ is the CDF of the REC's output energy distribution in time-slot $t$; $\hat{q}^t$ and $\hat{\lambda}^t$ the expected negative and positive imbalance prices at time $t$.

The classical way of proving (5.1) in inventory theory is to determine the underage (or shortfall) and overage (or holding) costs associated with the farm's participation in the DA market. In fact, if the actual output ends up being ${E_{\mathrm{G}}}^t = DA^t + 1$, the expected revenue becomes the sum of the opportunity revenue $(DA^t + 1).p^t$ and the *positive imbalance* charge $\hat{\lambda}^t$ instead of $DA^t.p^t$ initially expected. The financial impact of the extra unit generated, known as the overage cost is:

$$C^t_{\mathrm{o}} = p^t + \hat{\lambda}^t \tag{5.3}$$

Analogously, the expected revenue, when the realized output is one unit short, becomes the sum of the opportunity revenue $(DA^t - 1).p^t$ and the *negative imbalance* charge $\hat{q}^t$ instead of $DA^t.p^t$ initially expected. The underage cost is given by (5.4)

$$C^t_{\mathrm{u}} = -p^t + \hat{q}^t \tag{5.4}$$

Randomizing over all possible realizations, (5.5) defines the optimality condition.

$$C^t_{\mathrm{u}}.Prob({E_{\mathrm{G}}}^t \leq DA^{t*}) = C^t_{\mathrm{o}}.Prob({E_{\mathrm{G}}}^t > DA^{t*}) \tag{5.5}$$

(5.5) leads to the results presented by Snyder and Shen in [108]

$$DA^{t*} = {F^t}^{-1}\left(\frac{C^t_{\mathrm{u}}}{C^t_{\mathrm{u}} + C^t_{\mathrm{o}}}\right) \tag{5.6}$$

$\frac{C^t_{\mathrm{u}}}{C^t_{\mathrm{u}}+C^t_{\mathrm{o}}}$ being the price fractile $\gamma^t$ defined in (5.2).

According to (5.1), once $p^t < -\hat{\lambda}^t$, the renewable farm should bid its maximum expected or forecast energy output $E^t_{\text{Gmax}}$ in the real-time market even though realistically it is uncertain whether the foreseen output will be achieved. The opposite happens whenever the negative deviation charge is believed to be less than the expected DA market clearing price. In both cases, there is little incentive for the renewable farm to be reliability minded. We can draw an important observation from (5.1): *To provide enough incentive for renewable farm to be concerned about grid reliability,* $\hat{q}^t$*,* $\hat{\lambda}^t$ *and* $\hat{p}^t$ *should satisfy* (5.7):

$$-\hat{\lambda}^t \leq \hat{p}^t \leq \hat{q}^t \tag{5.7}$$

Consequently, for the remainder of this work we assume condition (5.7) satisfied and the DA optimal bid given by (5.8).

$$DA^{t*} = F^{t-1}\left(\frac{\hat{p}^t + \hat{\lambda}^t}{\hat{q}^t + \hat{\lambda}^t}\right) \tag{5.8}$$

Given that the distribution is involved in the determination of the DA bidding solution, the offer $DA^{t*}$ obtained is the best across the entire spectrum of all possible realizations. However, in each instance only one element in the spectrum can be realized at the time. This leaves room for improvement. To enable the renewable farm to actively participate in the real-time market, assume that the REC is coupled with an energy storage system (ESS). The purpose of the intra-day participation is to mitigate deviations and reduce the balancing needs. Section 5.4 presents a strategic offering solution model for an active real-time and reserve market participation.

## 5.4 Intra-day market strategy

Because the REC's output $E_{\text{G}}$ is prone to uncertainty, an intra-day offer optimization model is needed to maximize the renewable farm's profit while contributing to enhance grid reliability. The first stage solution, the DA offer, is given by equation (5.8). Due to intermittent output, one should expect discrepancies between $DA^{t*}$ and the actual realization $E^t_{\text{G}}$, for all $t \in \mathcal{T}$. Instead of "polluting the grid" with or spilling the difference $(E^t_{\text{G}} - DA^{t*})$, it can be traded in the real-time market and/or in the reserve market. We consider the following post day-ahead market structure: for every hour $t$, at the beginning of the hour, the farm is allowed to submit an energy offer $RT^t$ to the real-time market and a capacity offer $RV^t$ to the reserve market. The RT energy offer is

binding, but the reserve capacity offer is not. However, the system operator sends a reserve energy signal $\zeta^{ts}$ every time slot $s$, say every *five minutes*, of the corresponding hour $t$ that the farm has to follow. The reserve energy output $R_{\mathrm{g}}^{ts}$ is determined by $\zeta^{ts}$ and the "committed" reserve capacity $RV^t$ as shown in (5.22). In terms of compensation, the farm is paid $v^t$ for every capacity unit of $RV^t$, $r^{ts}$ for each unit of reserve energy $R_{\mathrm{g}}^{ts}$ provided, and $\rho^t$ for any fulfilled unit of its real-time energy offer $RT^t$. Day-ahead and real-time deviations with respect to offers are subject to positive and negative imbalance penalties $\lambda^t$ and $q^t$ respectively. We assume that the farm is a zero marginal cost producer, and thus, is a price taker. As such, it is always cleared.

To account for the uncertainties related to these parameters, we formulate the intra-day market problem as a two-stage stochastic optimization model.

### 5.4.1 The Profit Function

At the outset of the intra-day bidding process, the farm manager knows the values of $p^t, \forall t \in \mathcal{T}$, but only has a belief about the parameters $\rho^t$, $q^t$, $\lambda^t$, $v^t$, $r^t$, $R_{\mathrm{g}}^{ts}$ and the generation output $E_{\mathrm{G}}^{ts}$, for all $t \in \mathcal{T}$, $s \in \mathcal{S}$. In the rest of this chapter, we denote by $\hat{y}$, the expected or believed value of the parameter $y$. In general, this belief comes from a trusted forecasting package. We express the objective function in terms of the expected revenue and a penalty value that accounts for all possible realizations of the above uncertain parameters. We define a scenario set $\Omega$ to represent these realizations. All uncertain parameters and second-stage variables bear the superscript $\omega$, $\omega$ being the scenario index. Equation (5.9) presents the profit function for all hour $t \in \mathcal{T}$ and scenario $\omega \in \Omega$.

$$\pi^{t\omega} = \mathrm{Rev}^{t\omega} - \mathrm{Cost}^{t\omega} \tag{5.9}$$

with:

$$\mathrm{Rev}^{t\omega} = p^t DA^{t^*} + \rho^{t\omega} RT^t + v^{t\omega} RV^t + \sum_{s=1}^{|\mathcal{S}|} r^{ts\omega} R_{\mathrm{g}}^{ts\omega} \tag{5.10}$$

$$\mathrm{Cost}^{t\omega} = q^{t\omega}(z_{\mathrm{DA}}^{t\omega} + z_{\mathrm{RT}}^{t\omega}) + \lambda^{t\omega} z_{\mathrm{out}}^{t\omega} + c_{\mathrm{d}} z_{\mathrm{ES}}^{t\omega} \tag{5.11}$$

where $z_{\mathrm{DA}}^{t\omega}$ and $z_{\mathrm{RT}}^{t\omega}$ are day-ahead and real-time shortages respectively; $z_{\mathrm{out}}^{t\omega}$ represents the real-time excess at hour $t \in \mathcal{T}$ and scenario $\omega \in \Omega$. $z_{\mathrm{ES}}^{t\omega}$ defines the total state of charge deviations, and $c_{\mathrm{d}}$, the fixed storage deviation cost.

### 5.4.2 The Operational Constraints

Storage management is key in the second-stage of the stochastic model. The energy storage system (ESS) control is designed to adapt to all scenarios $\omega \in \Omega$. An ESS of capacity $S_{cap}$ operates efficiently in the range $S_-$ - $S_+$ given by (5.12). Typical healthy operating thresholds are $\gamma_- = 10\%$ and $\gamma_+ = 90\%$. Once these thresholds are violated, the ESS is said depleted or overcharged. This can speed up its aging process and shorten its lifespan. To account for this in the objective function, we assign a depletion/overcharge penalty unit cost $c_{\mathrm{d}}$ incurred each time the healthy operation bounds are violated. Constraints (5.13) - (5.14) track the state of charge, *soc*.

$$\begin{aligned} S_- &= \gamma_- S_{\mathrm{cap}} \\ S_+ &= \gamma_+ S_{\mathrm{cap}} \\ 0 &< \gamma_- < \gamma_+ < 1 \end{aligned} \tag{5.12}$$

$$0 \leq soc^{ts\omega} \leq S_{\mathrm{cap}}, \forall t \in \mathcal{T},\ s \in \mathcal{S},\ \omega \in \Omega \tag{5.13}$$

$$\begin{aligned} S_- - z^{ts\omega}_{\mathrm{ES}-} \leq soc^{ts\omega} \leq S_+ + z^{ts\omega}_{\mathrm{ES}+} \\ z^{ts\omega}_{\mathrm{ES}+} \geq 0, \forall t \in \mathcal{T},\ s \in \mathcal{S},\ \omega \in \Omega \\ z^{ts\omega}_{\mathrm{ES}-} \geq 0, \forall t \in \mathcal{T},\ s \in \mathcal{S},\ \omega \in \Omega \end{aligned} \tag{5.14}$$

$$z^{ts\omega}_{\mathrm{ES}} = z^{ts\omega}_{\mathrm{ES}-} + z^{ts\omega}_{\mathrm{ES}+}, \forall t \in \mathcal{T},\ s \in \mathcal{S},\ \omega \in \Omega \tag{5.15}$$

$$z^{t\omega}_{\mathrm{ES}} = \sum_{s=1}^{|\mathcal{S}|} z^{ts\omega}_{\mathrm{ES}},\ \forall t \in \mathcal{T},\ \omega \in \Omega \tag{5.16}$$

Because ESSs do not retain 100% of the charge stored on them, we introduce the storage efficiency factor $\sigma$ to represent the portion of charge available in time slot $s$, hour $t$ and scenario $\omega$, that is still available at the beginning of time period $s+1$ in scenario $\omega$, hour $t$. Taking into account the charge and discharge efficiencies $\eta_{\mathrm{C}}$ and $\eta_{\mathrm{D}}$, the storage inter-temporal equilibrium constraint is given by (5.17).

$$soc^{t(s+1)\omega} = \sigma soc^{ts\omega} + \eta_{\mathrm{C}} \delta^{ts\omega}_{\mathrm{C}} - \frac{\delta^{ts\omega}_{\mathrm{D}}}{\eta_{\mathrm{D}}}, \forall t \in T,\ s \in \mathcal{S},\ \omega \in \Omega \tag{5.17}$$

where $\delta_{\mathrm{C}}^{ts\omega}$ and $\delta_{\mathrm{D}}^{ts\omega}$ are respectively the charge and discharge amounts. They must satisfy the ramping constraints (5.18).

$$\begin{aligned} 0 \leq \delta_{\mathrm{C}}^{ts\omega} \leq P_{\mathrm{cap}}\Delta_{\mathrm{s}}, \forall t \in T,\ s \in \mathcal{S},\ \omega \in \Omega \\ 0 \leq \delta_{\mathrm{D}}^{ts\omega} \leq P_{\mathrm{cap}}\Delta_{\mathrm{s}}, \forall t \in T,\ s \in \mathcal{S},\ \omega \in \Omega \end{aligned} \tag{5.18}$$

The system's balance constraints are given by (5.19).

$$E_{\mathrm{G}}^{ts\omega} + \delta_{\mathrm{D}}^{ts\omega} = E_{\mathrm{out}}^{ts\omega} + \delta_{\mathrm{C}}^{ts\omega}, \forall t \in T,\ s \in \mathcal{S},\ \omega \in \Omega \tag{5.19}$$

with the farm output $E_{\mathrm{out}}^{ts\omega}$ satisfying (5.20).

$$0 \leq E_{\mathrm{out}}^{ts\omega} \leq P_{\mathrm{max}}\Delta_{\mathrm{s}}, \forall t \in T,\ s \in \mathcal{S},\ \omega \in \Omega \tag{5.20}$$

### 5.4.3 Market Constraints

In the assumed market model, a supplier makes a portfolio of offers and fulfill those offers in one package at a single point of interconnection. The main challenge would be how to determine what is considered as shortage or excess with regard to a specific offer (DA or RT for example). To clarify, let us consider a farm which offers in DA 2 kWh and 1 kWh in RT. If at the time of realization, the farm ends up with an output of 1 kWh, how do we determine the mismatches? Would we say we have 1 kWh unfulfilled in DA and 1kWh unfulfilled in RT, or 2kWh unfulfilled in DA? Since the mismatch charges can differ from one market to the other, there is a potential for conflict. A conservative way of avoiding such conflict is to clearly define a market hierarchy. In this chapter, we assume the following order of priority: reserve offers have to be fulfilled first, followed by DA offers, then RT offers.

Given the high priority of the reserve energy output $R_{\mathrm{g}}^{ts\omega}$, the renewable farm would make sure that the reserve market offer $RV^t$ is available to be deployed whenever necessary. Constraints (5.21) and (5.22) bind the reserve capacity and energy offers.

$$0 \leq RV^t \leq P_{\mathrm{cap}}, \forall t \in T \tag{5.21}$$

$$\begin{aligned} R_{\mathrm{g}}^{ts\omega} = \zeta^{ts\omega} RV^t \Delta_{\mathrm{s}},\ \forall t \in T,\ s \in \mathcal{S},\ \omega \in \Omega \\ 0 \leq \zeta^{ts\omega} \leq 1,\ \forall t \in T,\ s \in \mathcal{S},\ \omega \in \Omega \end{aligned} \tag{5.22}$$

Due to uncertain production, market offers are may not be exactly supplied. The net energy output, $E_{\text{net}}^{t\omega}$ (see (5.23)), can fall in any of the three zones described by (5.24). We introduce in (5.25) slack binary variables $x_1^{t\omega},\ x_2^{t\omega},\ x_3^{t\omega}$ to indicate the deviation zone in which lies the farm output for all hour $t \in \mathcal{T}$, and scenario $\omega \in \Omega$. Constraints (5.27) through (5.30) define energy shortage and excess in day-ahead and real-time realizations.

$$E_{\text{net}}^{t\omega} = \sum_{s=1}^{|\mathcal{S}|} E_{\text{out}}^{ts\omega} - R_{\text{g}}^{ts\omega} \tag{5.23}$$

$$\begin{cases} (\text{zone}_1) : 0 \leq E_{\text{net}}^{t\omega} \leq DA^{t^*} \\ (\text{zone}_2) : DA^{t^*} \leq E_{\text{net}}^{t\omega} \leq RT^t + DA^{t^*} \\ (\text{zone}_3) : E_{\text{net}}^{t\omega} \geq RT^t + DA^{t^*} \end{cases} \tag{5.24}$$

$$\begin{aligned} & E_{\max} x_1^{t\omega} + E_{\text{net}}^{t\omega} + \epsilon \geq DA^{t^*} \\ & E_{\max}(1 - x_1^{t\omega}) + DA^{t^*} \geq E_{\text{net}}^{t\omega} + \epsilon \\ & E_{\max}(1 - x_3^{t\omega}) + E_{\text{net}}^{t\omega} + \epsilon \geq DA^{t^*} + RT^t \\ & E_{\max} x_3^{t\omega} + DA^{t^*} + RT^t \geq E_{\text{net}}^{t\omega} + \epsilon \\ & x_1^{t\omega} + x_2^{t\omega} + x_3^{t\omega} = 1,\ \forall t \in T,\ \omega \in \Omega \end{aligned} \tag{5.25}$$

with:

$$E_{\max} = P_{\max} \Delta_{\text{t}} \tag{5.26}$$

where $P_{\max}$ is the interconnection feeder capacity, and $\Delta_{\text{t}}$, the duration in hour of one time unit.

Any day-ahead shortage $z_{\text{DA}}$ ($\text{zone}_1$) is given by:

$$\begin{aligned} & z_{DA}^{t\omega} \leq DA^{t^*} - E_{\text{net}}^{t\omega} + (1 - x_1^{t\omega}) DA^{t^*} \\ & z_{DA}^{t\omega} \geq DA^{t^*} - E_{\text{net}}^{t\omega} - (1 - x_1^{t\omega}) DA^{t^*} \\ & 0 \leq z_{DA}^{t\omega} \leq x_1^{t\omega} DA^{t^*},\ \forall t \in T,\ \omega \in \Omega \end{aligned} \tag{5.27}$$

Real-time shortage can happen in both $\text{zone}_1$ ($z_{RT1}^{t\omega}$) and $\text{zone}_2$ ($z_{RT2}^{t\omega}$) as expressed respectively by (5.28) and (5.29).

$$\begin{aligned} & z_{RT1}^{t\omega} \leq RT^t + (1 - x_1^{t\omega}) E_{\max} \\ & z_{RT1}^{t\omega} \geq RT^t - (1 - x_1^{t\omega}) E_{\max} \\ & 0 \leq z_{RT1}^{t\omega} \leq x_1^{t\omega} E_{\max},\ \forall t \in T,\ \omega \in \Omega \end{aligned} \tag{5.28}$$

$$
\begin{aligned}
& z_{RT2}^{t\omega} \leq DA^{t^*} + RT^t - E_{\text{net}}^{t\omega} + (1 - x_2^{t\omega})E_{\max} \\
& z_{RT2}^{t\omega} \geq DA^{t^*} + RT^t - E_{\text{net}}^{t\omega} - (1 - x_2^{t\omega})E_{\max} \\
& 0 \leq z_{RT2}^{t\omega} \leq x_2^{t\omega} E_{\max},\ \forall t \in T,\ \omega \in \Omega
\end{aligned} \tag{5.29}
$$

At any hour $t \in \mathcal{T}$, and for any scenario $\omega \in \Omega$, the overall real-time market shortage is:

$$
z_{RT}^{t\omega} = z_{RT1}^{t\omega} + z_{RT2}^{t\omega},\ \forall t \in T,\ \omega \in \Omega. \tag{5.30}
$$

When it comes to market excess $z_{\text{out}}$ ($\text{zone}_3$), we have:

$$
\begin{aligned}
& z_{\text{out}}^{t\omega} \leq E_{\text{net}}^{t\omega} - DA^{t^*} - RT^t + (1 - x_3^{t\omega})E_{\max} \\
& z_{\text{out}}^{ts\omega} \geq E_{\text{net}}^{t\omega} - DA^{t^*} - RT^t - (1 - x_3^{t\omega})E_{\max} \\
& 0 \leq z_{\text{out}}^{t\omega} \leq x_3^{t\omega} E_{\max},\ \forall t \in T,\ \omega \in \Omega.
\end{aligned} \tag{5.31}
$$

### 5.4.4 The Model

We propose two modeling approaches in connection with this problem. The farm can choose to optimize its intra-day portfolio as often as every hour while looking ahead up to the end of the bidding horizon, which is hour $t = 24$, or to the end a given rolling horizon. This approach offers the advantage of updating the scenario set $\Omega$ with shorter term forecasting outputs that are expected to be more accurate. In this case, the objective at the beginning of any time $t_0$ is given by:

$$
\max : \hat{\pi} = \sum_{\omega \in \Omega} p_{\text{r}}^{\omega} \pi^{\omega} \tag{5.32}
$$

with:

$$
\pi^{\omega} = \sum_{t=t_0}^{|\mathcal{T}|} \pi^{t\omega} \tag{5.33}
$$

where $t_0$ is the starting time (we will use $t_0 = 1$) The objective in (5.32) provides a very conservative solution approach in the sense that it maximizes the expected profit.

The second modeling approach takes into account risk through a conditional value-at-risk (CVaR) formulation. It minimizes the risk of losses for the intra-day portfolio $\{RT, RV\}$, at a confidence level $\alpha$. Equation (5.34) gives the corresponding objective function.

$$
\max : CVaR_{\alpha} \tag{5.34}
$$

with:

$$CVaR_\alpha = VaR - \frac{1}{1-\alpha}\sum_{\omega\in\Omega} p_r^\omega Y^\omega \tag{5.35}$$

$$\begin{aligned} Y^\omega &\geq VaR - \pi^\omega \\ Y^\omega &\geq 0,\ \forall\omega \in \Omega \end{aligned} \tag{5.36}$$

We adopt a more general objective by combining the above approaches. Equation (5.37) expresses the weighted hybrid objective function of our proposed model, with $\beta$, a trade-off parameter.

$$\max : \hat{\pi} + \beta CVaR_\alpha \tag{5.37}$$

where $\hat{\pi}$ is the expected farm profit (see, (5.32)). The trade-off parameter $\beta$ indicates how risk-averse the farm intends to be. Thus, a high $\beta$ means low risk tolerance. Conversely a low $\beta$ is indicative of a high risk allowance. The extreme risk tolerance, also known as risk neutrality, is achieved when $\beta = 0$. The extreme risk aversion is obtained when $\beta = +\infty$.

**Proposition**

The expected profit $\hat{\pi}$ as a function of the risk measure $CVaR_\alpha(\beta)$, $\beta \in [0, +\infty[$, is concave.

**Proof**

Consider the objective function $\theta$:

$$\theta = \hat{\pi} + \beta CVaR_\alpha$$

Assuming $\theta$ is continuous in both $\hat{\pi}$ and $CVaR_\alpha$, we can write the optimality condition:

$$\mathrm{d}\theta(\beta) = \frac{\partial\theta}{\partial\hat{\pi}}\mathrm{d}\hat{\pi} + \frac{\partial\theta}{\partial CVaR_\alpha}\mathrm{d}CVaR_\alpha = 0$$

i.e.:

$$\frac{\mathrm{d}\hat{\pi}(\beta)}{\mathrm{d}CVaR_\alpha(\beta)} = -\beta \tag{5.38}$$

Let's consider a set of risk aversion parameters $\beta^{i-1}$, $\beta^i$ and $\beta^{i+1}$ such that $0 \leq \beta^{i-1} \leq \beta^i \leq \beta^{i+1}$ and $CVaR_\alpha(\beta^{i-1}) \leq CVaR_\alpha(\beta^i) \leq CVaR_\alpha(\beta^{i+1})$. The following approximation holds:

$$\frac{\hat{\pi}(\beta^{i+1}) - \hat{\pi}(\beta^{i-1})}{CVaR_\alpha(\beta^{i+1}) - CVaR_\alpha(\beta^{i-1})} = -\beta^i \tag{5.39}$$

There exists $\mu \in [0, 1]$ such that:

$$CVaR_\alpha(\beta^i) = \mu CVaR_\alpha(\beta^{i+1}) + (1-\mu)CVaR_\alpha(\beta^{i-1})$$

i.e.:

$$\mu = \frac{CVaR_\alpha(\beta^i) - CVaR_\alpha(\beta^{i-1})}{CVaR_\alpha(\beta^{i+1}) - CVaR_\alpha(\beta^{i-1})} \tag{5.40}$$

From (5.39), (5.41) gives $\hat{\pi}(\beta^{i+1})$:

$$\hat{\pi}(\beta^{i+1}) = \hat{\pi}(\beta^{i-1}) - \beta^i \left[CVaR_\alpha(\beta^{i+1}) - CVaR_\alpha(\beta^{i-1})\right] \tag{5.41}$$

Using (5.40) and (5.41), we have:

$$\mu\hat{\pi}(\beta^{i+1}) + (1-\mu)\hat{\pi}(\beta^{i-1}) = \hat{\pi}(\beta^{i-1}) - \beta^i \left[CVaR_\alpha(\beta^i) - CVaR_\alpha(\beta^{i-1})\right] \tag{5.42}$$

Hence,

$$\hat{\pi}(\beta^i) - \left[\mu\hat{\pi}(\beta^{i+1}) + (1-\mu)\hat{\pi}(\beta^{i-1})\right] = \hat{\pi}(\beta^i) - \hat{\pi}(\beta^{i-1}) + \beta^i(CVaR_\alpha(\beta^i) - CVaR_\alpha(\beta^{i-1})) \tag{5.43}$$

There exists $\beta^{i'}$ such that $\beta^{i-1} \leq \beta^{i'} \leq \beta^i$ for which the optimality condition (5.39) holds, that is:

$$\frac{\hat{\pi}(\beta^i) - \hat{\pi}(\beta^{i-1})}{CVaR_\alpha(\beta^i) - CVaR_\alpha(\beta^{i-1})} = -\beta^{i'} \tag{5.44}$$

Thus, (5.43) is equivalent to:

$$\hat{\pi}(\beta^i) - \left[\mu\hat{\pi}(\beta^{i+1}) + (1-\mu)\hat{\pi}(\beta^{i-1})\right] = (\beta^i - \beta^{i'})(CVaR_\alpha(\beta^i) - CVaR_\alpha(\beta^{i-1})) \tag{5.45}$$

It follows that:

$$\hat{\pi}(\beta^i) \geq \mu\hat{\pi}(\beta^{i+1}) + (1-\mu)\hat{\pi}(\beta^{i-1}) \tag{5.46}$$

Given that it is logical to rewrite $\hat{\pi}(\beta^k)$ as $\hat{\pi}(CVaR_\alpha(\beta^k))$, the concavity of the expected profit as a function of the risk measure $CVaR_\alpha$ is proven by (5.47):

$$\hat{\pi}(\mu CVaR_\alpha(\beta^{i+1}) + (1-\mu)CVaR_\alpha(\beta^{i-1})) \geq \mu\hat{\pi}(CVaR_\alpha(\beta^{i+1})) + (1-\mu)\hat{\pi}(CVaR_\alpha(\beta^{i-1})) \tag{5.47}$$

## 5.5 Case Studies

### 5.5.1 The Data

To evaluate the proposed market integration model, we consider a hypothetical 750 kW wave energy farm placed in the same sea state conditions as `Station 32012` [109]. We use 2007 through 2015 sea state data and assume a `Pelamis` wave energy converter. We use the real-time and day-ahead historical price data from PJM to generate market imbalance charges, and reserve capacity and energy prices. The price and imbalance charge expectations, prior to the day-ahead market offer, are presented in Fig. 5.2. The imbalances charges are simulated using the day ahead and

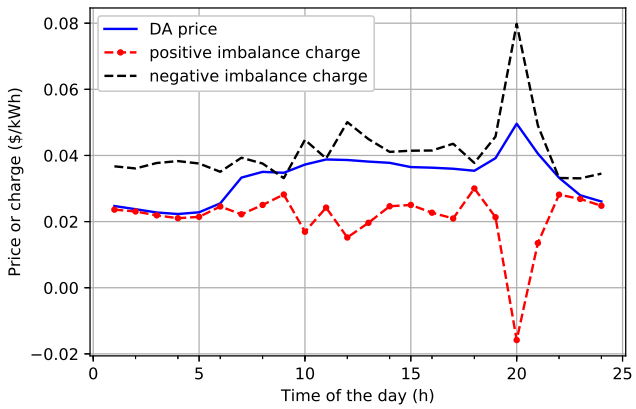


Figure 5.2: Day-ahead model price input

real-time price scenarios in such a way that:

$$\lambda^t \leq p^t \leq q^t \tag{5.48}$$

Following the DA market clearing, the assumed realized DA price is represented in Fig. 5.3.

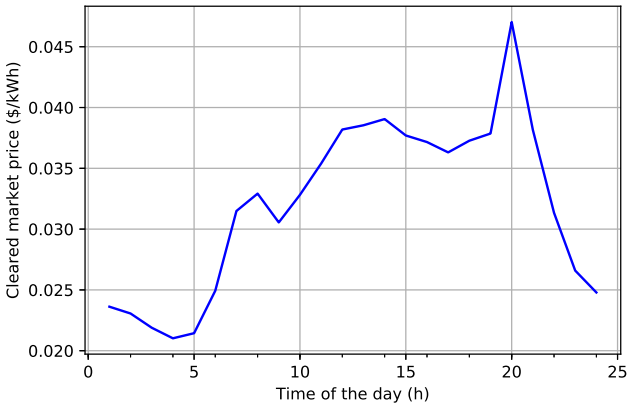


Figure 5.3: Cleared DA market prices

### 5.5.2 Day-ahead model results

As shown in (5.8), the day-ahead (DA) model produces day-ahead market offers. Fig. 5.4 presents the wave farm's resulting DA bids. The obtained DA offers constitute an input for the

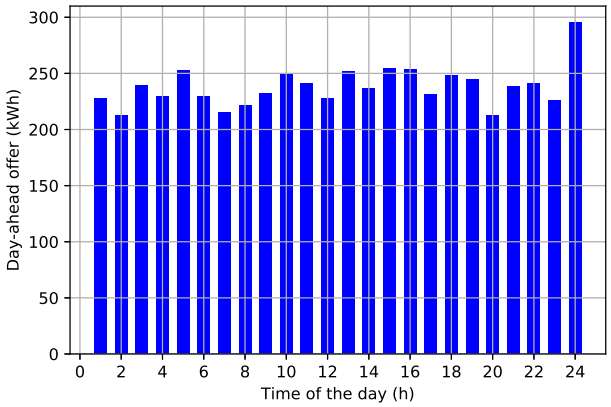


Figure 5.4: Day-ahead energy offers

intra-day market portfolio model described in Section 5.4.

### 5.5.3 Intra-day model results

Using a confidence level $\alpha = 95\%$ and a risk factor range 0 through $\infty$, the sensitivity study reveals the efficient frontier shown in Fig. 5.5. Fig. 5.5(a) shows, for $\beta \in [0, 10^9]$, how the expected profit varies as a function of the risk measure $CVaR_\alpha(\beta)$. When the short-term reserve market is introduced the efficient frontier obtained is shown in Fig. 5.5(b). The sensitivity curves are annotated with the risk aversion factor values. Overall, from $\beta = 0$ to $\beta = 1$, we have a small drop in expected profit compared to a relatively large increase in CVaR. We observe the opposite

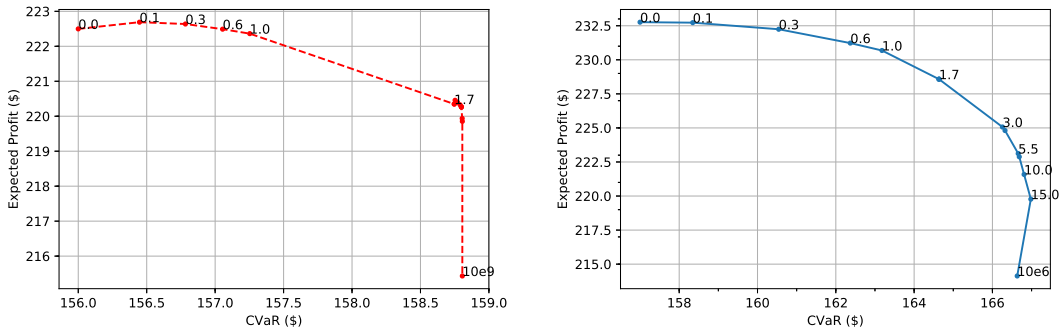


(a) Profit - no reserve

(b) Profit - with reserve

Figure 5.5: Farm profit risk sensitivity

variation when $\beta \in \left[3, 10^6\right]$ for the market with reserve, and $\beta \in \left[1.7, 10^9\right]$ when no reserve market is considered. The expected profit decrease quicker than CVaR increases. The risk of profit loss is not uniformly distributed. Depending on how risk-averse a farm owner or operator is, the farm can experience a significant profit reduction. Fig. 5.5 shows the corresponding variation of the real-time energy offer for both no-reserve intra-day market (cf., Fig. 5.6(a)) and a market with the proposed short-term reserve structure (see, Fig. 5.6(b)). To evaluate the impact of the introduced short-term reserve market, we define a risk metric called *risk range* (RR) and a profit metric designated by *risk impact* (RI) defined as:

$$RR = CVaR_\alpha(\beta = +\infty) - CVaR_\alpha(\beta = 0) \tag{5.49}$$

$$RI = \frac{\hat{\pi}(\beta = 0) - \hat{\pi}(\beta = +\infty)}{\hat{\pi}(\beta = 0)} \tag{5.50}$$

With the introduction of the short-term reserve, comes more price and energy signal uncertainty. This justifies the wider risk range observed, nearly 3.5 times the RR when no reserve market is considered. However, the risk impact in case of reserve market is lower compared to the no-reserve case, 24% against 29%. The RI expresses the maximum profit reduction due to risk consideration. That said, the farm experiences more profit reduction in a market without reserve than in a market with reserve. What is more, the overall profit increases by 5% in a market with short-term reserve opportunity compared to a real-time only intra-day market, for the same expected energy generation. The concavity proven in 5.4.4 is confirmed by Fig.5.5

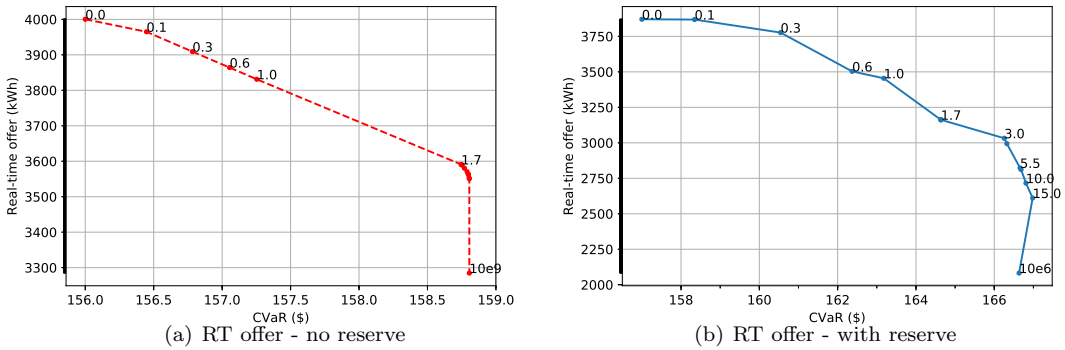


(a) RT offer - no reserve

(b) RT offer - with reserve

Figure 5.6: Risk sensitivity of the RT offer

## 5.6 Conclusion

There is a value in introducing the proposed short-term reserve market for both the system operator and the wave energy farm considered. The system operator gains in securing additional generation capacity, even from renewable farms, to pull from whenever necessary for balancing purposes. The simulation case study shows that there is a financial incentive for renewable energy farms to participate in the short-term reserve market. In the particular case studied in this chapter, even though the risk range is multiplied by 3.4, participating in the reserve market results in 5% profit increase and lower profit reduction for the same expected energy generation. As we witness more renewable grid penetration, in addition to long-term capacity contracts, short-term reserve markets would be critical for a reliable system operation. In this work, we considered a simplistic reserve market structure. In future work, we expect more insights from studies that allow for more detailed market structures with access to more accurate market and system data.

# Chapter 6

# Post-disaster Grid Recovery Through Optimal Microgrid Formation

## 6.1 Introduction

Microgrid formation is a potential solution in post-disaster electric grid recovery efforts. Recent works propose a distribution level microgrid formation model that applies to radial distribution systems characterized by directed power flows. However, with high renewable penetration levels in future power systems, the flows are expected to be undirected even in distribution grids. In this work, we develop a model to deal with the restoration process of future power systems, embedding some of the characteristics these systems are likely to have. More specifically, our formulation can deal with radial and meshed topologies, and it requires little pre-processing of the input data. Additionally, we extend the model to allow for possible mobile and fixed distributed generation technologies and distributed energy resources, and explicitly include demand responsive loads with a minimum satisfiability constraint. Thus, this extended formulation can be used as an operation and a short term planning tool for the DG scenario-based location problem. We compare our extended formulation results to those obtained for the radial cases found in the literature. Also, we apply the proposed approach to other instances of the problem based on the IEEE 37-bus, 30-bus and 118-bus systems.

The socio-economic losses due to power outages during the last decades are evidence that enhancing the ability to rapidly restore the functionality of the power system is a fundamental concern for operators and planners. According to the Executive Office of the President, weather-related outages are estimated to have cost the U.S. economy an inflation-adjusted annual average of $18 to $33 billion over the period from 2008 to 2012 [1]. Campbell estimates that weather-related outages cost the U.S. between $20 and $55 billion annually [60], and superstorm Sandy, the second most costly storm in US history, left 8.5 million customers without electricity across 15 U.S. states [61]. The National Centers for Environmental Information (NCEI) [62] reports 196 weather and climate disasters from 1980 to 2016 in the U.S., with related costs of approximately $1 billion, adjusted by the consumer price index (CPI). Further, according to NERC, all of the top-10 most severe power outages (ranked based on the severity risk index - SRI) in 2014 were initiated or aggravated by weather events [63].

Even though operational reliability and the effects of events with low impact but medium to high probability of occurrence have long been in the realm of system operators [64], the capacity to restore the functionality of the system after a low probability, high impact event, what we define as *grid resilience*, is garnering increasing attention. The severe impact of natural disasters on the electric power system and the increasing trend of power outages has been considered in [1]. The criticality of resiliency in grid modernization efforts has been considered in [65]. Descriptive studies, such as [66], examine the resiliency of the power network by developing spatial and non-spatial econometric models to estimate factors affecting the restoration time, including the restoration priority, infrastructure characteristics and weather related variables. Generally, strategies to deal with extreme event disruptions can be grouped into two broad categories: preventive and corrective actions. The objective of preventive pre-disaster strategies is to find the most potentially vulnerable components in order to replace or upgrade them before any potential disturbance. Preventive actions include but are not limited to installing power lines underground, reinforcement of poles, management of vegetation and stockpiling of power lines [67]. However, strategies such as installing lines underground cost two to ten times as much as overhead lines [68], and create issues with restoration [69]. Other works, such as Ma et al. [70], approach the grid resilience enhancement problem from a preventive viewpoint by proposing an optimal hardening strategy that finds critical components (lines, poles, etc.). This is done through a greedy search that minimizes the hardening investment cost.

Corrective strategies are scenario-based backup plans designed to reduce the impact of a dis-

aster, if any, and recover from disruptions as quickly as possible. In a corrective approach, Sarkar et al. [71] propose an adaptive distribution grid restoration method based on tie-line switching that is formulated as a non-linear mixed-integer program (MIP) that is solved by a greedy search algorithm to reduce the combinatorial search space. Choobineh and Mohagheghi [72] propose a non-linear MIP to optimally dispatch energy resources within a microgrid subject to capacity and fuel availability constraints, in the aftermath of a natural disaster. However, [72] does not address how the post-disaster microgrids are formed.

Several system restoration models have been proposed in the literature to circumvent either reliability or resiliency disrupting events (see, e.g., [73]). Ren et al. [74] develop a multi-agent system with a dynamic agent team forming mechanism for interconnected power systems restoration. Nagata et al. [75] propose a multi-agent framework for power system restoration in which bus agents are coordinated by a facilitator agent in order to reach a suboptimal system configuration after fault events, ten years before the work in [74]. Kirschen and Volkmann [76] introduce a hierarchically structured expert system that separates strategic and tactical reasonings in order to minimize the restoration time. The same grid resiliency is the subject of Z. Wang and J. Wang [77], formulating a stochastic self-healing model, that accounts for intermittent energy resources. Farzin et al. [78] devise a two-stage hierarchical outage management scheme to enhance the resilience of a multi-microgrid distribution system as a mixed-integer linear program (MILP) using the total energy curtailment as a resiliency index. In [78] the authors assume that the distribution grid is designed as a collection of microgrids with a known structure prior to the events. In fact, microgrids are considered as key assets in improving grid resilience and studies to validate them as a viable grid hardening solution are being conducted by New York, Connecticut and California as well as the U.S. Department of Energy. One of the most attractive features of microgrids is their ability to operate in island and grid-connected modes [79]. Tan et al. [80] propose a grid recovery scheme based on a black-start sequence algorithm and spanning tree search, assuming that a fixed distributed generator (DG) with black-start capability is available after the disaster. Microgrids are first formed around the DG units without including any load. Loads belonging to microgrids are picked up according to Kirchhoff's laws and other critical isolated loads are connected through a spanning tree search. Gao et al. [81] introduce a critical load restoration method using microgrids and considering generation resource availability as well as uncertainties associated to intermittent energy sources and loads in a continuous operation time mode. Guidelines on microgrid operation and system restoration dynamics can be found in [82, 83].

Most of the existing methods based on topological control seek to isolate the faulted line or area by reconfiguring the feeder to allow as much load as possible to be served. A general assumption when these strategies are applied to the distribution grid is that the substation (the interface between the transmission and distribution systems) is healthy after the fault. Recent work by Chen et. al [84] relaxes this assumption in the context of *chaotic* weather events where the only supply solutions available following the disaster might be DG units arbitrarily positioned. The problem then transitioned from a topological structure alteration to a network partitioning problem where each partition, called a *microgrid*, is supplied by a DG. However, the MILP model proposed applies only to radial distribution grids, in which there is only one generation bus. In [84], the DG units are prepositioned, possibly precluding to reach maximum load pick-up. In [85], the authors address this DG location constraint by dynamically allocating DG units to candidate nodes. They assumed DG units to be mobile emergency generators (e.g., truck-mounted), a conjecture consistent with overall restoration efforts. In fact, amongst the lessons learned after the severe ice storm that affected eastern Canada and the northeastern US from 20 to 23 December 2013, the use of large-scale portable Diesel generators comes out as recommended in the preparedness process [86]. These emergency generators can be placed in any location where there may be a need to support the microgrid formation. However, the distribution system model considered in [85] is still one with a single microgrid root.

In this chapter, we extend the previous work, particularly [84] to account for a future grid, where the direction of flows on a given branch is not necessarily known beforehand. We focus on resiliency events assuming reliability as a prerequisite [87–89]. Our main contributions are (1) we do not assume a radial network, allowing distribution systems where consumers may have energy sources on their premises, in which case the direction of the flow on a given branch is not predetermined, that is, the relationship parent-child nodes is reversible because there are potentially multiple root nodes; (2) we account for both fixed and mobile DG units that can be optimally placed in the system, and evaluate the benefits that this optimal location has on the objective function, a proxy for social welfare.

Throughout this chapter, it is assumed that the state of the network (after a possible disruption) is known before designing the microgrids. For articles in which the state of the network is not known in advance, but a much simpler microgrid design problem is required to be solved, we direct the reader to Eskandarpour et al. [90] and the references therein.

The remainder of this chapter structured as follows. Section 6.2 describes the microgrid forma-

Table 6.1: Nomenclature

| Symbol | Description |
|---|---|
| $\alpha$ | real positive number scaling factor |
| $b^{ij}$ | switch state variable: 1 if line $(i,j)$ is closed, 0 otherwise |
| $c^{ijk}$ | line-to-microgrid assignment variable: 1 if line $(i,j)$ is assigned to microgrid $k$, 0 otherwise |
| $d^i$ | load dispatchability indicator: 1 if the load at node $i$ is dispatchable, 0 otherwise |
| $\delta^{ij}$ | voltage slack variable for line $(i,j)$ |
| $K$ | set of microgrids |
| $K_f$ | subset of fixed distributed generator (DG) units |
| $K_m$ | subset of mobile or truck-mounted DG units |
| $L$ | set of lines |
| $L_c$ | subset of lines with faulted closed line switches |
| $L_o$ | subset of faulted open lines |
| $N$ | set of nodes |
| $N_c$ | subset of nodes with faulted closed switches |
| $n^k$ | location index of fixed DG $k$ |
| $N_o$ | subset of nodes with faulted open switches |
| $p_d^i$ | dispatched active load at node $i$ |
| $Pg^i$ | dispatched active power generation at node $i$ |
| $p^i$ | total active load at node $i$ |
| $P^{ij}$ | active power flow from node $i$ to node $j$ |
| $p^i_{\text{lb}}$ | minimum demand to serve if the dispatchable load at node $i$ is picked up |
| $P^k_{\max}$ | active power generation capacity of DG $k$ |
| $P^k_{\min}$ | minimum active power of DG $k$ |
| $p_s^i$ | served active load at node $i$ |
| $Qg^i$ | dispatched reactive power generation at node $i$ |
| $q^i$ | total reactive load at node $i$ |
| $Q^{ij}$ | reactive power flow from node $i$ to node $j$ |
| $Q^k_{\max}$ | reactive power generation capacity of DG $k$ |
| $Q^k_{\min}$ | minimum reactive power of DG $k$ |
| $s^i$ | load-to-node switch state binary variable: 1 if load at node $i$ is picked up, 0 otherwise |
| $T_P^{ij}$ | active transmission capacity of line $(i,j)$ |
| $T_Q^{ij}$ | reactive transmission capacity of line $(i,j)$ |
| $V^i$ | Voltage magnitude of node $i$ |
| $v^{ik}$ | node-to-microgrid assignment binary variable: 1 if node $i$ is assigned to microgrid $k$, 0 otherwise |
| $V_o$ | nominal voltage magnitude |
| $V_R$ | rated voltage |
| $w^i$ | criticality weight of the load at node $i$ |
| $z^{ki}$ | DG-to-node assignment variable: 1 if DG $k$ is physically connected at node $i$, 0 otherwise |

tion problem and elaborates on the assumptions made. Section 6.3 presents the proposed MILP formulation and discusses its application to the pre-located DG units and mobile DG units problems. Section 6.4 evaluates the proposed formulation on different cases and discusses the results obtained. Section 6.5 concludes the article.

## 6.2 Problem Statement

Let us consider a power system defined by its graph-theoretical notation $G(N, L)$, where $N$ and $L$ stand for the sets of nodes (vertices) and lines (edges) respectively. After an extreme weather or disturbance event, the system can experience the loss of individual elements, e.g., lines, poles, substations, or loads. It can also end up with non-controllable elements, e.g., faultily hardened lines and node-load switches. The resulting post-disaster graph can be specified by the distinct subsets of faulty closed and open node-load switches, $N_c$ and $N_o$ respectively, and the distinct subsets of faulty closed and open line switches, $L_c$ and $L_o$ respectively, such that $(N_c \cup N_o) \subseteq N$ and $(L_c \cup L_o) \subseteq L$. We assume that the aftermath graph $G'$ is observable and fully observed i.e., the sets and subsets $N$, $N_c$, $N_o$, $L$, $L_c$, $L_o$ are known. We consider undirected graphs.

We additionally assume that DG units with black-start capability are available. We designate the set of DG units by $K$. Given that DG units can be fixed (unchangeable location) [84] or mobile (e.g., truck-mounted) [85, 86], we account for both cases by defining subsets $K_f, K_m \subseteq K$ (with $K_f \cap K_m = \emptyset$ and $K_f \cup K_m = K$) to represent the sets of fixed and mobile DG units respectively. Around each DG $k \in K$, we aim to form a self-sustaining microgrid that we denote using the same index $k \in K$.

The problem we have is to (*i*) locate mobile DG units, (*ii*) form microgrids with a DG for each one, (*iii*) dispatch the DG units in order to serve the maximum criticality-weighted total load possible, and (*iv*) dispatch responsive loads from a contractual minimum satisfiability threshold, while taking into account the post-disaster grid conditions. Post-disaster conditions include line capacities and voltage constraints within the limits of the aforementioned assumptions. Section 6.3 presents the corresponding MILP formulation of this problem for any network topology.

## 6.3 Problem Formulation

Equations (6.1) through (6.19) present the MILP formulation of the post-disaster microgrid formation problem. The objective is to maximize the total load pickup given the criticality factor vector $w \in \mathbb{R}_+^{\mathrm{N}}$ as expressed in (6.1). To solve the problem described in Section 6.2, the following set of constraints need to be satisfied. First, to achieve the grid partitioning objective, a key constraint is that line $(i, j)$ can be assigned to a microgrid $k$ only if its end-nodes $i$ and $j$ belong to microgrid $k$. In other words, the line switch $b^{ij}$ is forced to open (i.e., $b^{ij} = 0$), whenever possible, if node $i$ and node $j$ are not assigned to the same microgrid. The set of constraints (6.5) take care

of this. In addition, since our objective is to serve as much load as possible, every node must be assigned to a microgrid. Constraints (6.2) ensure that each node is part of exactly one microgrid. Constraints (6.3) guarantee that each DG node is automatically assigned to the microgrid formed around the corresponding DG, with a single DG per microgrid as enforced by (6.4).

When it comes to load pickup conditions, it is not necessary to keep track of which load is picked up in which microgrid, because a load is served only through the node at which it is located. Thus, the load belongs to the same microgrid as its host-node. Therefore, given that each node $i$ belongs to exactly one microgrid, the load pick-up variable is the load-node switch state binary variable $s^i$ for all $i \in N$. This observation, among others, is key in obtaining a model that is much simpler to solve than simply extending in a naive way the model proposed in [84] for radial networks and fixed DG units. This fact is discussed in more detail in the Appendix. Another direct consequence of this observation is that faulty closed load-node switches impose their loads as priority. As a corollary, the only ways to avoid locating DG units at isolated nodes $i \in N$ are to (1) set their load $(p^i, q^i)$ to zero, or to (2) remove them from the graph during a preprocessing stage.

The post-disaster system constraints are expressed by (6.17) for lines and (6.18) for load-node switches. An outaged substation can be modeled by opening all lines connected to it.

Kirchhoff laws (KCL and KVL) are satisfied by all microgrids, as well as acceptable operational boundary limits, as established by (6.7) through (6.16). The constraints (6.7) and (6.8) maintain the nodal balance (KCL). The line flow limits are enforced by constraints (6.9) and (6.10). The operational dispatch bounds of the DG units are enforced by constraints (6.11) and (6.12). The voltage drop is one of the most important factors in how the nodes are clustered into microgrids. The voltage drop from node $i$ to node $j$ is a function of parameters $r^{ij}$ (resistance) and $x^{ij}$ (reactance) of the line $(i, j)$ and the corresponding flows. This drop must fit into an allowable gap generally expressed as a percentage of the nominal voltage $V_o$ of the system. Equation (6.13) calculates the voltage at node $i$ as a function of the voltage at node $j$ and the potential drop for all $(i, j) \in L$. The slack variable $\delta^{ij}$ bounded in (6.15) takes care of the cases where node $i$ and node $j$ are no longer connected. Equation (6.16) sets the voltage bounds given the voltage drop tolerance factor $\epsilon \geq 0$, whereas constraint (6.14) sets the DG nodes' voltage to $V_o$.

For each pre-located DG $k$, i.e., $k \in K_f$, there exists exactly one node $n^k$ where the DG is located. For this node, the DG location variable $z^{kn^k} = 1$, meaning DG $k$ is located at node $n^k$, as enforced by (6.19).

$$\max : \sum_{i \in N} w^i s^i p^i \tag{6.1}$$

subject to:

$$\sum_{k\in K} v^{ik} = 1, \forall i \in N \tag{6.2}$$

$$v^{ik} \geq z^{ki}, \quad \forall i \in N, \quad k \in K \tag{6.3}$$

$$\sum_{k\in K} z^{ki} \leq 1, \forall i \in N \tag{6.4}$$

$$\begin{aligned} c^{ijk} &\leq v^{ik}, && \forall k \in K, \quad (i,j) \in L \\ c^{ijk} &\leq v^{jk}, && \forall k \in K, \quad (i,j) \in L \\ c^{ijk} &\geq v^{ik} + v^{jk} - 1, && \forall k \in K, \quad (i,j) \in L \end{aligned} \tag{6.5}$$

$$b^{ij} = \sum_{k\in K} c^{ijk}, \forall (i,j) \in L \tag{6.6}$$

$$\sum_{j:(j,i)\in L} P^{ji} - \sum_{j:(i,j)\in L} P^{ij} + Pg^i - s^i p^i = 0, \forall i \in N \tag{6.7}$$

$$\sum_{j:(j,i)\in L} Q^{ji} - \sum_{j:(i,j)\in L} Q^{ij} + Qg^i - s^i q^i = 0, \forall i \in N \tag{6.8}$$

$$-T_P^{ij} b^{ij} \leq P^{ij} \leq T_P^{ij} b^{ij}, \forall (i,j) \in L \tag{6.9}$$

$$-T_Q^{ij} b^{ij} \leq Q^{ij} \leq T_Q^{ij} b^{ij}, \forall (i,j) \in L \tag{6.10}$$

$$\sum_{k\in K} z^{ki} P^k_{\min} \leq Pg_i \leq \sum_{k\in K} z^{ki} P^k_{\max}, \forall i \in N \tag{6.11}$$

$$\sum_{k\in K} z^{ki} Q^k_{\min} \leq Qg_i \leq \sum_{k\in K} z^{ki} Q^k_{\max}, \forall i \in N \tag{6.12}$$

$$V^i = V^j + \frac{r^{ij}P^{ij} + x^{ij}Q^{ij}}{V_o} + \delta^{ij}, \quad \forall (i,j) \in L \tag{6.13}$$

$$V_o \sum_{k\in K} z^{ki} \leq V^i \leq V_o, \forall i \in N \tag{6.14}$$

$$(-1 + b^{ij})V_o \leq \delta^{ij} \leq (1 - b^{ij})V_o, \forall (i,j) \in L \tag{6.15}$$

$$(1-\epsilon)V_R \leq V^i \leq (1+\epsilon)V_R, \quad \forall i \in N \tag{6.16}$$

$$\begin{aligned} b^{ij} &= 1, \quad \forall (i,j) \in L_c \\ b^{ij} &= 0, \quad \forall (i,j) \in L_o \end{aligned} \tag{6.17}$$

$$\begin{aligned} s^i &= 1, \quad \forall i \in N_c \\ s^i &= 0, \quad \forall i \in N_o \end{aligned} \tag{6.18}$$

$$z^{ki} = 1, \forall i = n^k, k \in K_f. \tag{6.19}$$

It is important to note that the exclusive use of discrete loads might not guarantee an efficient use of the available black-start resource. In fact, if a discrete load is picked up, its total value must be served. If the available generation capacity cannot serve its total value, then the load is not picked up at all. This can leave fractions of unused generation capacity or cause more critical loads to be left out to avoid voltage bound violations. We introduce a scenario with hybrid loading to increase the resource allocation efficiency. This setup is made of dispatchable and non-dispatchable loads, with dispatchable loads participating in a demand response (DR) program that allows utility operators to do partial or total curtailment. The objective function then changes from (6.1), to $\sum_{i \in N} w^i s^i p_d^i$ where the dispatched load $p_d^i$ is bounded by constraints (6.20). The binary parameter $d^i$ indicates whether the load at node $i$ is dispatchable ($d^i = 1$) or not ($d^i = 0$). The parameter $p_{\text{lb}}^i \leq p^i$ denotes a minimum load amount that must be served, as specified in the DR contract, if the load at node $i$ is picked up.

$$d^i p_{\text{lb}}^i + (1 - d^i) p^i \leq p_d^i \leq p^i, \forall i \in N. \tag{6.20}$$

Given that $p_d^i$ and $s^i$ are variables, the new objective function $\sum_{i \in N} w^i s^i p_d^i$ is nonlinear. We introduce an additional variable called served demand $p_s^i$, defined by the linearization constraints (6.21).

$$\begin{aligned} & p_s^i \leq s^i p^i, && \forall i \in N \\ & 0 \leq p_s^i \leq p_d^i, && \forall i \in N \\ & p_s^i \geq p_d^i - (1 - s^i) p^i, && \forall i \in N. \end{aligned} \tag{6.21}$$

Analogously, we define a served reactive load $q_s^i$ at node $i$ orthogonal to $p_s^i$ as defined by (6.22).

$$q_s^i = \frac{q^i}{p^i} p_s^i, \forall i \in N : p^i \neq 0. \tag{6.22}$$

In this context, the nodal balance constraints (6.7) and (6.8) become (6.23) and (6.24) respectively.

$$\sum_{j:(j,i) \in L} P^{ji} - \sum_{j:(i,j) \in L} P^{ij} + Pg^i - p_s^i = 0, \forall i \in N \tag{6.23}$$

$$\sum_{j:(j,i) \in L} Q^{ji} - \sum_{j:(i,j) \in L} Q^{ij} + Qg^i - q_s^i = 0, \forall i \in N. \tag{6.24}$$

The resulting DR-enabled model is given by:

$$\max : \sum_{i \in N} w^i p_s^i \tag{6.25}$$

subject to: Equations (6.2) - (6.6), (6.9) - (6.19) and (6.20) - (6.24).

## 6.4 Case Studies

In order to evaluate the effectiveness of our proposed model, we present a series of case studies in this section. We consider instances with both fixed and mobile DG units. The location of the fixed DG units in the network is assumed to be known in advance; that is, their location is an initial condition of the problem, while the location of the mobile DG units is optimally chosen for each network instance using the mixed integer linear problem described in Section 6.3.

### 6.4.1 Experiment Setup

The instances considered in our case studies are defined by five main features. Each instance is unique depending on (1) whether the network topology is radial or not, (2) whether the inputs used correspond to a reduced post-disaster network by eliminating isolated nodes or not, (3) whether fixed generators are used, (4) whether mobile DG units are used, and (5) whether dispatchable (or DR) loads are considered. In order to compare the proposed model with the one in [84] for the radial network cases, we define an instance $S_0$ corresponding to the results in [84] (see equations (20-26) in [84]). Instances $S_1$ - $S_4$ are based on the formulation given by (6.1) through (6.19) with the following differences in the setup. In $S_1$, $K_f \equiv K$, i.e., the subset of mobile DG units $K_m$ is empty. In instance $S_2$ $K_m \equiv K$, making the subset of fixed DG units $K_f$ empty. Instance $S_3$ extends $S_2$ to the non-preprocessed network. Instance $S_4$ is a "reconciliation" of $S_1$ and $S_2$, applied to the whole network (i.e., without any reduction), where $K_m$ and $K_f$ are non-empty. Instance $S_5$ integrates dispatchable loads by using the DR-enabled model formulated in (6.2) - (6.6), (6.9) - (6.24) and (6.25). Table 6.2 presents all instances $S_0$ through $S_5$ as defined across the above-mentioned five features. In the next subsection, we consider three network cases. In Case 1, the network studied is the post-disaster IEEE 37-bus system as presented by Chen et al. in [84] and shown in Fig. 6.1(a). In this case, we study instances $S_0$ through $S_5$. Instances $S_0$ and $S_1$ assume $DG_1$, $DG_2$ and $DG_3$ are located at buses 702, 728 and 710 respectively, as in [84], for comparison and benchmarking purposes. In instances $S_4$ and $S_5$, $DG_3$ is fixed and located at bus 710. In

Table 6.2: Scenario Description

| Instances | Network Topology | Reduced Network? | Fixed DG units? | Mobile DG units? | DR Loads? |
|---|---|---|---|---|---|
| $S_0$ [84] | Radial | Yes | Yes | No | No |
| $S_1$ | Any | Yes | Yes | No | No |
| $S_2$ | Any | Yes | No | Yes | No |
| $S_3$ | Any | No | No | Yes | No |
| $S_4$ | Any | No | Yes | Yes | No |
| $S_5$ | Any | No | Yes | Yes | Yes |

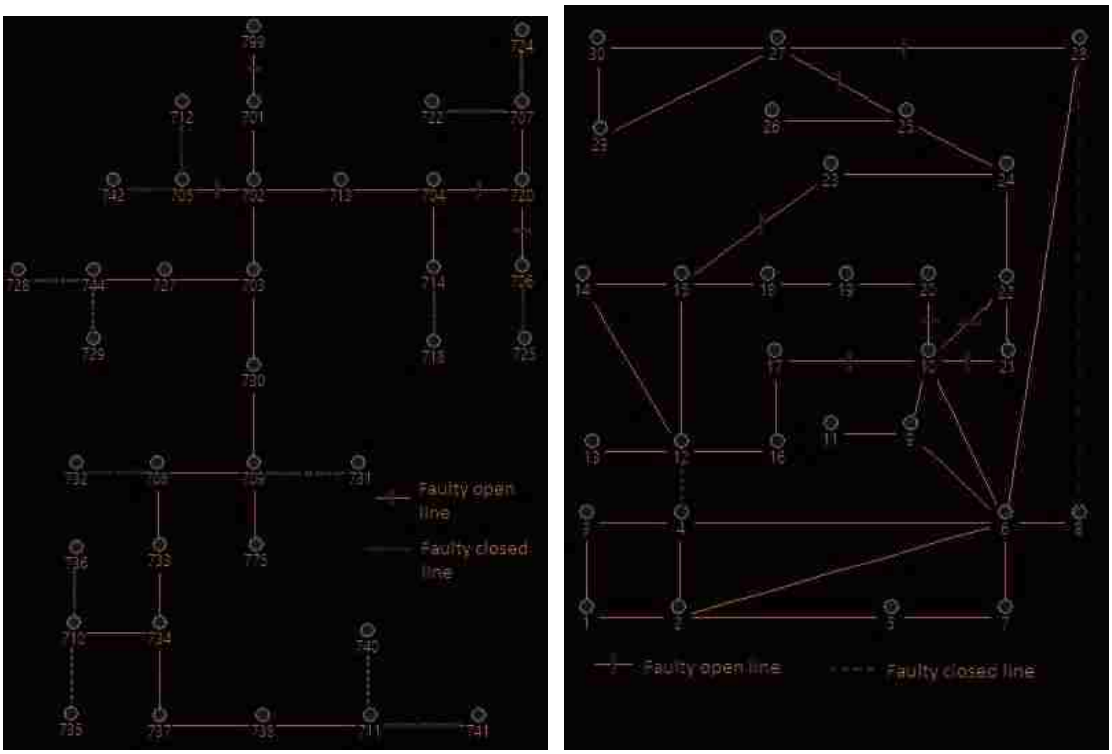


(a) IEEE 37-bus

(b) IEEE 30-bus

Figure 6.1: Modified post-disaster systems

Case 2, we investigate instances $S_1$ through $S_5$ for a meshed network of average node degree 2: the IEEE 30-bus system in its post-disaster state as shown in Fig. 6.1(b). In instance $S_1$ we assume, after a random draw, that $DG_1$, $DG_2$ and $DG_3$ are located at buses 1, 23 and 28 respectively. In instances $S_4$ and $S_5$, after a random draw, $DG_2$ is fixed and located at bus 10.

In Case 3, we present the IEEE 118-bus system (with average node degree 3) under instances $S_1$, $S_3$ and $S_5$. The aftermath status of the IEEE 118-bus test system is presented in Fig. 6.2. In instance $S_1$ we assume, after a random draw, that $DG_1$ is located at bus 12, $DG_2$ at bus 32, $DG_3$ at bus 112 and $DG_4$ at bus 118. Instance $S_3$ considers all DG units mobile.

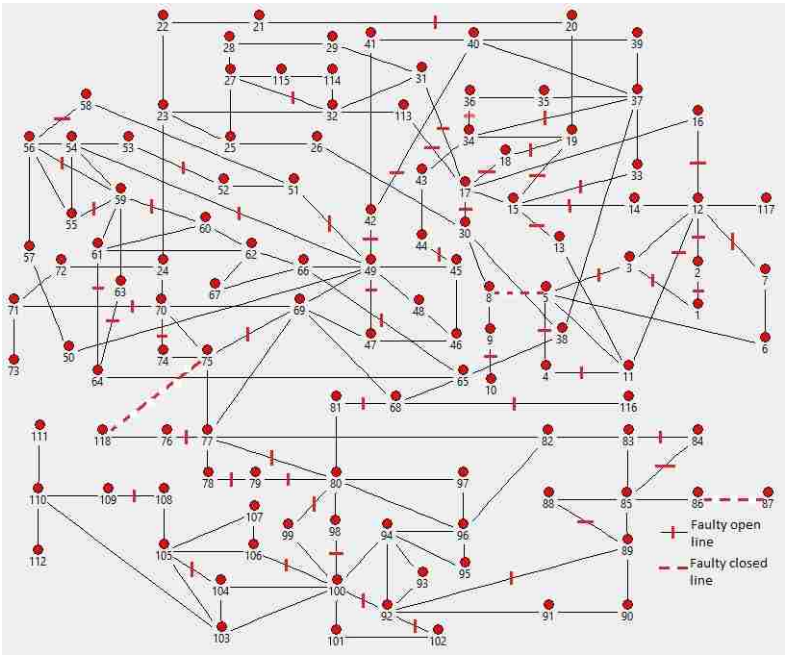


Figure 6.2: The modified post-disaster IEEE 118-bus system

In instance $S_5$, after a random draw, $DG_1$ and $DG_2$ are fixed and located at buses 12 and 32 respectively while $DG_3$ and $DG_4$ are mobile.

In all cases, the minimum served demand $p^i_{\text{lb}}$ of dispatchable loads is set to 10% their total load $p^i$ for all $i \in N$. The dispatchable loads (DR loads) are marked in the figures related to instance $S_5$, see e.g., Figs. 6.4(b), 6.5(c) and 6.7. The generation characteristics of the DG units are summarized in Table 6.3, and further details about load and criticality weight data used are shown in Table 6.5 for Cases 1 and 2 and Table 6.6 for Case 3.

Changing the location of the fixed DG units in the network would result in a different optimal location for the mobile DG units. However, running the proposed approach in problem instances with different locations of the fixed DG units would lead to similar results as the ones presented in the article in terms of solution time and benefits (in terms of served load) with respect to assuming that all DG units must be initially set to a fixed location.

The models are implemented in AMPL, solved using CPLEX 12.6 and tested on an AMD Opteron 2.0 GHz machine with 32GB memory and 16 cores (each core is a 2.0 GHz. 64 bit architecture), from the COR@L laboratory.

Table 6.3: Parameters of the DG units

| | IEEE 37-bus | IEEE 30-bus | IEEE 118-bus |
|---|---|---|---|
| DG | ($P_{\max}$, $Q_{\max}$) | ($P_{\max}$, $Q_{\max}$) | ($P_{\max}$, $Q_{\max}$) |
| $DG_1$ | (252.53 , 46.30) | (60 , 40) | (100 , 80) |
| $DG_2$ | (120.42 , 171.72) | (50 , 35) | (250 , 160) |
| $DG_3$ | (202.99 , 197.48) | (40 , 25) | (400 , 240) |
| $DG_4$ | - | - | (500 , 100) |

### 6.4.2 Results and Discussion

Table 6.4 presents the post-disaster resource allocation solutions after applying the models described in Section 6.3 to the scenarios and cases presented in Section 6.4.1.

For the IEEE 37-bus radial system, Figs. 6.3(a) and 6.3(b) show consistency between the results of our proposed model and those in [84], leading to the same microgrid formation. The fact that the objective functions are different in Table 6.4 for $S_0$ (Chen's) and $S_1$ (ours) is explained by the decision of our model to serve the load at bus 701 instead of the one at 703 as found by Chen et al. Our model's decision is justified by the discrepancy between the products $w^{701}p^{701}$ and $w^{703}p^{703}$, respectively 100.928 and 41.559. This results in the difference of about 59 observed in the objective functions of instances $S_0$ and $S_1$.

Comparing instances $S_1$ and $S_2$, we notice that the achievable total criticality-weighted load pickup depends on DG location. In fact, by optimally locating the available DG units, the objective function value increases from $2,892$ in $S_1$ to $3,384$ in $S_2$. Instances $S_3$ and $S_4$ yield the same objective value as $S_2$ due to two reasons: (1) in the full network approach, the load at bus 725 can be served through the post-disaster hardened line $706 - 725$; and (2) the hardened load-node switch $s^{725}$ has been set to 0 to avoid locating a DG at either 706 or 725, as recommended in Section 6.3. This contrasts with the initial condition $s^{725} = 1$ in $S_0$, as shown in Table 6.5. Otherwise, the objective value functions in $S_3$ and $S_4$ would be less than that of $S_2$. It is also important to note that the choice of the fixed DG location set $K_f$ is critical for instance $S_4$. Here we choose a subset of the location set $K$ obtained in previous instances. In general, instances $S_2$, $S_3$ and $S_4$ lead to the same microgrids even though the DG locations may vary from one instance to the other. Fig. 6.4 (a) shows the microgrid formation solution obtained in instance $S_3$ for the IEEE 37-bus system. Instance $S_5$ outperforms the others, by allowing certain loads to be dispatchable. Fig. 6.4(b) showcases the strategic mobile DG placement and the optimal topology control. This highlights once again the value of demand-responsive loads in grid resiliency.[1] The results in non-

[1] In normal operation, responsive loads also support the reliability of the system (see, e.g., [110]).

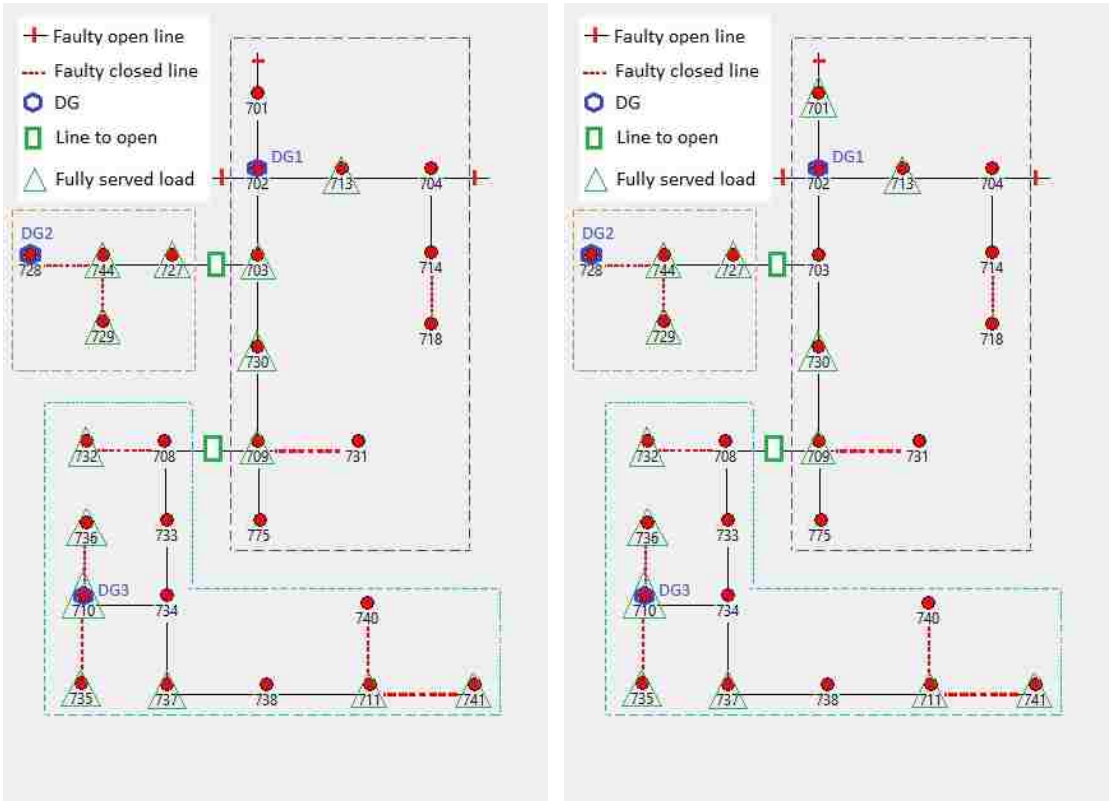


(a) Chen's result ($S_0$)

(b) Proposed model ($S_1$)

Figure 6.3: Microgrid formation on the IEEE 37-bus

radial network cases 2 and 3 are consistent. Figs. 6.5(a), 6.5(b) and 6.5(c) show the microgrid formation solutions $S_1$, $S_3$ and $S_5$ respectively for the IEEE 30-bus system (case 2). Because $S_2$ and $S_4$ are similar to $S_3$, we do not explicitly represent them.

The most common practical action to take in any instance is to open line and load-node switches in order to form the suggested microgrids.

It is important to point out that in non-radial network cases, instance $S_5$ tends to suggest greater number of lines to open (e.g., see Fig. 6.7). However, in the practice of power systems operations, taking a line out of service involves more than merely opening a switch. The time, logistical effort, and resources required to restore the system is increasing in the number of lines taken out. Additionally time is critical in grid restoration. It would be practical to take this fact into consideration by adding to our objective functions in (6.1) and (6.25) the term $\alpha \sum_{(i,j)\in L} b^{ij}$, with $\alpha > 0$, denoting a real number small enough so that it minimally affects the overall solution. Specifically, (6.1) and (6.25) become (6.26) and (6.27) respectively. We suggest choosing $\alpha$ such that $0 < \alpha \ll \min\{w^i, i \in N\}$, since the objective of keeping as many existing lines as possible is

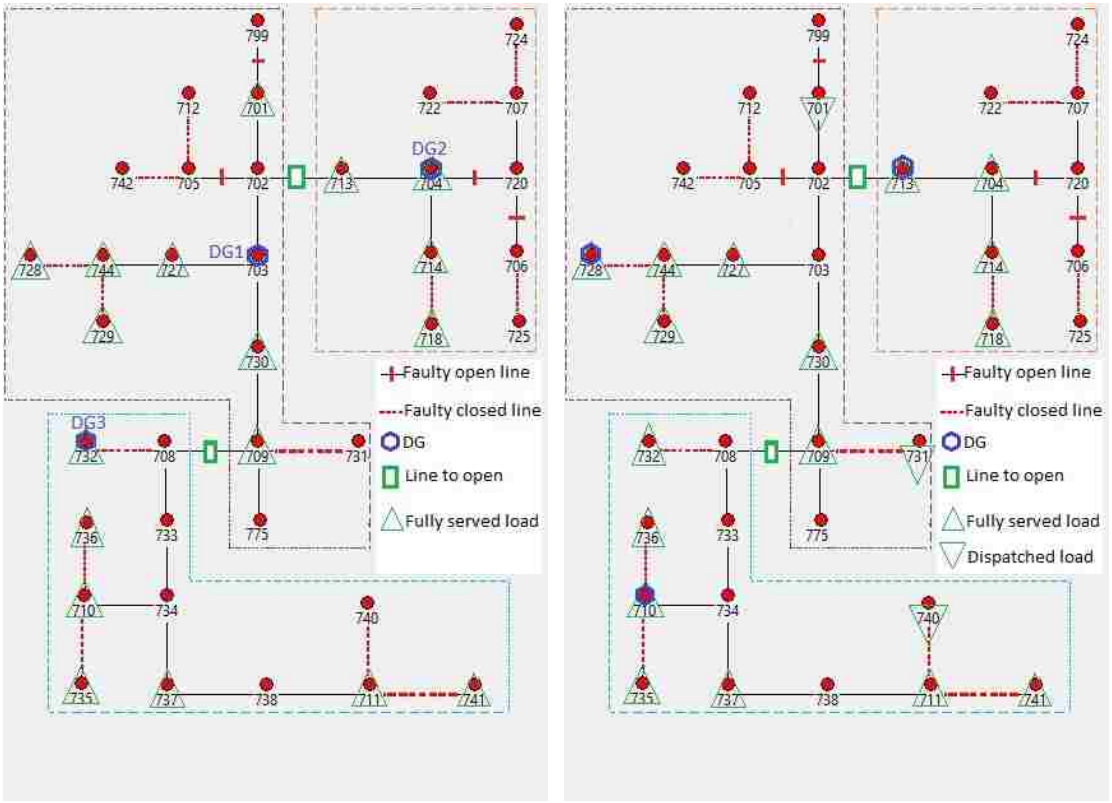


(a) Instance $S_3$ (b) Instance $S_5$

Figure 6.4: Microgrid formation results on the IEEE 37-bus

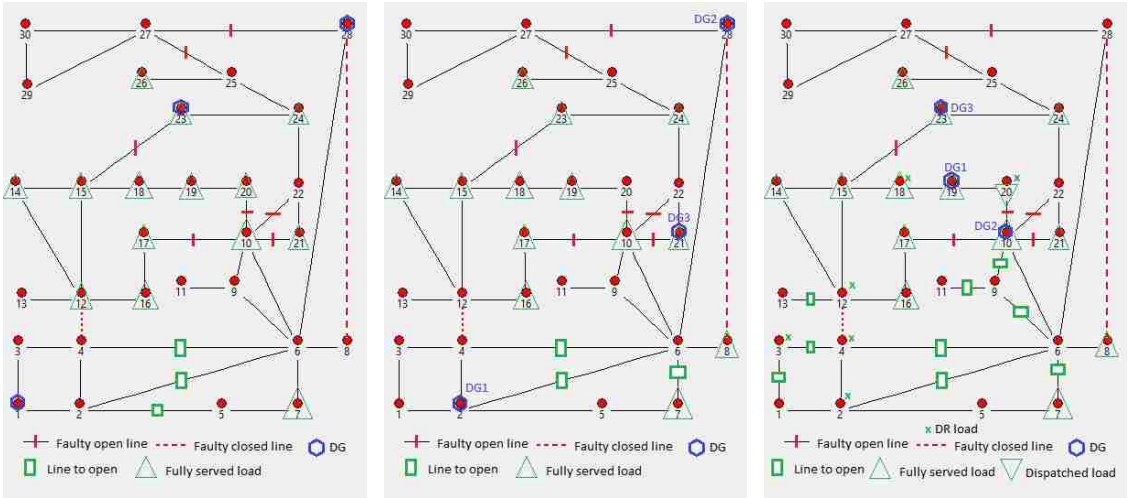


(a) Instance $S_1$ (b) Instance $S_3$ (c) Instance $S_5$

Figure 6.5: Microgrid formation results on the IEEE 30-bus

secondary. The new objectives ensures that lines are not opened unnecessarily.

$$\max : \sum_{i \in N} w^i s^i p^i + \alpha \sum_{(i,j) \in L} b^{ij} \tag{6.26}$$

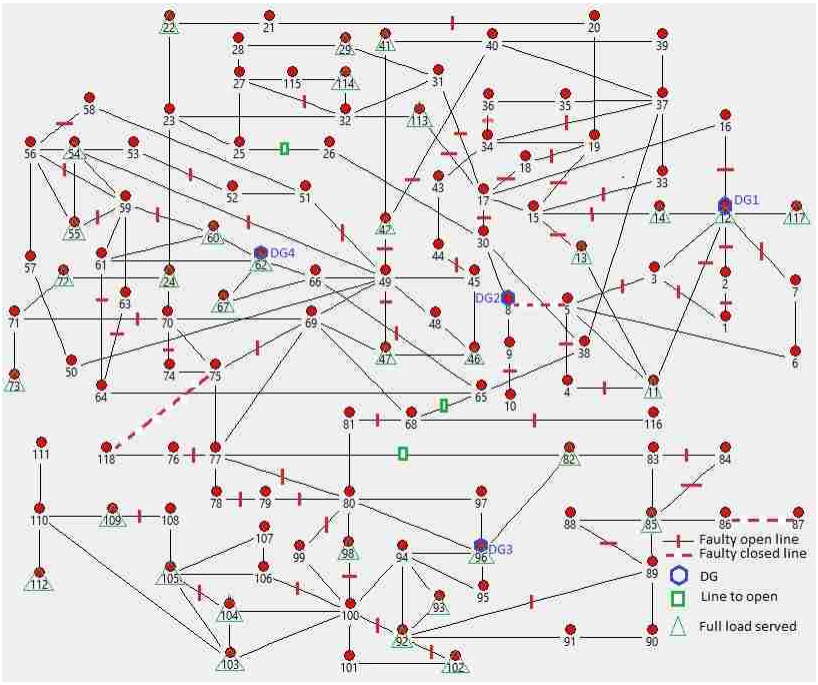


Figure 6.6: Microgrid formation results for IEEE 118-bus, Instance $S_3$

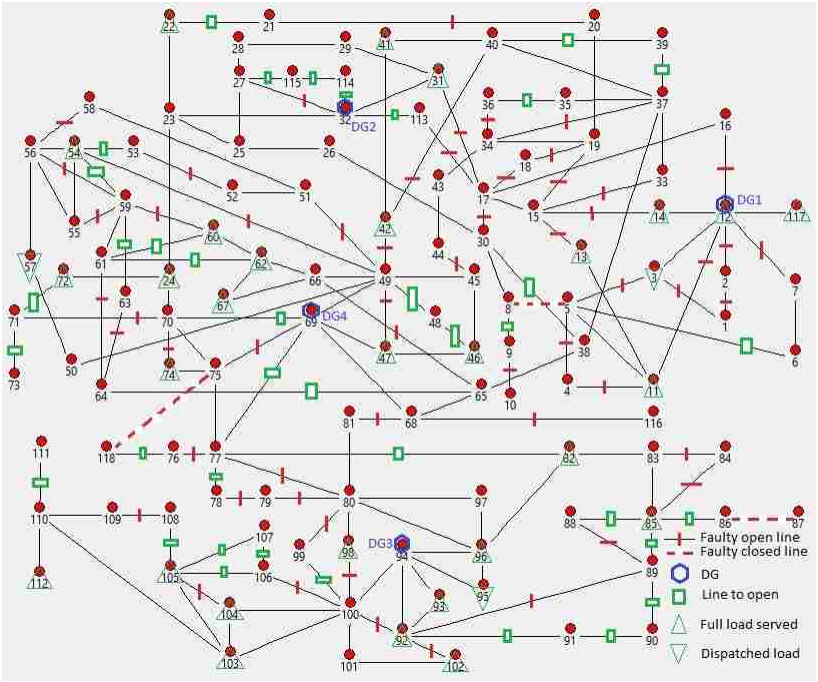


Figure 6.7: Microgrid formation results for the IEEE 118-bus, instance $S_5$

$$\max : \sum_{i \in N} w^i p_s^i + \alpha \sum_{(i,j) \in L} b^{ij} \tag{6.27}$$

Here we choose $\alpha = 10^{-4}$. However, changing this parameter by an order of magnitude does not

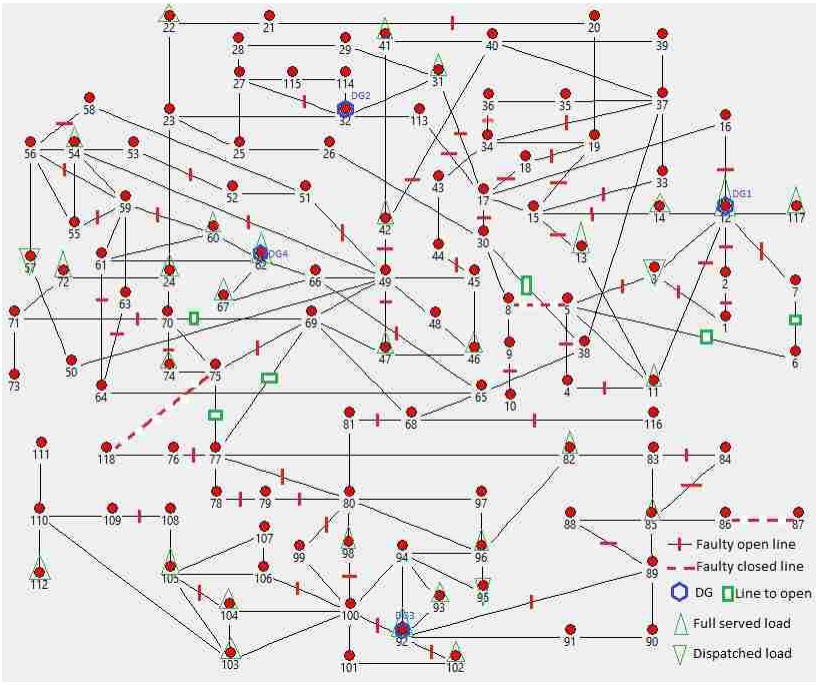


Figure 6.8: Microgrid formation results for the IEEE 118-bus, instance $S_5$ with reduced recovery actions

alter the optimal solutions. Using the modified objective on instance $S_5$ in the IEEE 118-bus case, we obtain an objective value that is numerically close to the one shown in Table 6.4 (the slight difference comes from the added term), with reduced number of open lines. In fact, the number of lines taken out of service drops from 37 (see, Fig. 6.7) to only 6 (see, Fig. 6.8). Note that the mobile DG units 3 and 4 are now located at buses 92 and 62 respectively. For $S_5$ in the IEEE 30-bus case, the number of lines to open drops from 9 in Fig. 6.5(c) to 3 (i.e., lines $2-6$, $4-6$ and $6-7$) and the mobile (e.g., truck-mounted) DG units 1 and 3 are located respectively at buses 7 and 24. In all cases, the amount of load pickup is the same as in instance $S_5$, 30-bus and 118-bus systems of Table 6.4. In terms of computational time, the case IEEE 118-bus takes 774.27 seconds to solve, the 30-bus case takes 19.98 seconds to solve, and the 37-bus case takes 9.50 seconds to solve.

## 6.5 Conclusion

In this chapter, we present a methodology to form microgrids based on an optimization model whose objective is to restore critical loads after a large external disturbance, while satisfying post-disaster and operational constraints within each microgrid. Our proposed model applies to general power network topologies, including radial and meshed configurations and integrates demand re-

Table 6.4: Case study Results

| Cases | Inst. | Obj. | $DG_1$ | | | $DG_2$ | | | $DG_3$ | | | $DG_4$ | | |
|---|---|---|---|---|---|---|---|---|---|---|---|---|---|---|
| | | | $n_1$ | $Pg_1$ (kW) | $Qg_1$ (kVar) | $n_2$ | $Pg_2$ (kW) | $Qg_2$ (kVar) | $n_3$ | $Pg_3$ (kW) | $Qg_3$ (kVar) | $n_4$ $n_4$ | $Pg_4$ (kW) | $Qg_4$ (kVar) |
| 37-bus | $S_0$ | 2833 | 702 | 163.51 | 45.13 | 728 | 98.65 | 26.03 | 710 | 199.76 | 96.42 | - | - | - |
| | $S_1$ | 2892 | 702 | 155.07 | 44.46 | 728 | 98.65 | 26.03 | 710 | 199.76 | 96.42 | - | - | - |
| | $S_2$ | 3384 | 703 | 238.25 | 43.75 | 704 | 114.4 | 85.37 | 732 | 199.76 | 96.42 | - | - | - |
| | $S_3$ | 3384 | 703 | 238.25 | 43.75 | 704 | 114.4 | 85.37 | 732 | 199.76 | 96.42 | - | - | - |
| | $S_4$ | 3384 | 701 | 238.25 | 43.75 | 713 | 114.4 | 85.37 | 710 | 199.76 | 96.42 | - | - | - |
| | $S_5$ | 3421 | 728 | 241.94 | 46.31 | 713 | 114.39 | 85.36 | 710 | 203 | 103.21 | - | - | - |
| 30-bus | $S_1$ | 558 | 1 | 53 | 24.2 | 23 | 32.9 | 21.8 | 28 | 28.6 | 12.9 | - | - | - |
| | $S_2$ | 666 | 13 | 59.2 | 26 | 11 | 35.8 | 32 | 21 | 32.9 | 21.8 | - | - | - |
| | $S_3$ | 666 | 2 | 59.2 | 26 | 28 | 35.8 | 32 | 21 | 32.9 | 21.8 | - | - | - |
| | $S_4$ | 666 | 15 | 59.2 | 26 | 10 | 35.8 | 32 | 22 | 32.9 | 21.8 | - | - | - |
| | $S_5$ | 671 | 19 | 60 | 40 | 10 | 35.8 | 35 | 23 | 32.9 | 21.8 | - | - | - |
| 118-bus | $S_1$ | 7349 | 12 | 98 | 19 | 32 | 197 | 81 | 112 | 268 | 116 | 118 | 400 | 92 |
| | $S_3$ | 8177 | 12 | 81 | 19 | 8 | 237 | 72 | 96 | 400 | 168.9 | 62 | 500 | 100 |
| | $S_5$ | 8325 | 12 | 100 | 23.87 | 32 | 250 | 160 | 94 | 400 | 170.9 | 69 | 495 | 100 |

Table 6.5: Load data for the IEEE 37 & 30-bus test network

| IEEE 37-bus | | | | | IEEE 30-bus | | | | |
|---|---|---|---|---|---|---|---|---|---|
| $i$ | $p^i$ | $q^i$ | $w^i$ | $s^i$ | $i$ | $p^i$ | $q^i$ | $w^i$ | $s^i$ |
| 701 | 30.4 | 5.09 | 3.32 | 0/1 | 1 | 0 | 0 | 3.32 | 0/1 |
| 702 | 18.61 | 23.6 | 2.89 | 0/1 | 2 | 21.7 | 12.7 | 2.89 | 0 |
| 703 | 38.84 | 5.76 | 1.07 | 0/1 | 3 | 2.4 | 1.2 | 1.07 | 0 |
| 704 | 26.39 | 18.4 | 9.11 | 0/1 | 4 | 7.6 | 1.6 | 9.11 | 0 |
| 705 | 12.58 | 19.25 | 7.06 | 0/1 | 5 | 0 | 0 | 7.06 | 0/1 |
| 706 | 29.58 | 9.9 | 2.66 | 0 | 6 | 0 | 0 | 2.66 | 0/1 |
| 707 | 31.09 | 21.79 | 3.87 | 0/1 | 7 | 22.8 | 10.9 | 3.87 | 0/1 |
| 708 | 22.57 | 15.65 | 6.06 | 0/1 | 8 | 30 | 30 | 6.06 | 0/1 |
| 709 | 43.08 | 8.82 | 4.47 | 0/1 | 9 | 0 | 0 | 4.47 | 0/1 |
| 710 | 12.57 | 8.45 | 7.05 | 0/1 | 10 | 5.8 | 2 | 7.05 | 0/1 |
| 711 | 48.23 | 7.13 | 8.59 | 0/1 | 11 | 0 | 0 | 8.59 | 0/1 |
| 712 | 21.06 | 25.36 | 4.84 | 0/1 | 12 | 11.2 | 7.5 | 4.84 | 0/1 |
| 713 | 37.61 | 26.48 | 9.09 | 0/1 | 13 | 0 | 0 | 9.09 | 0/1 |
| 714 | 31.51 | 11.29 | 4.21 | 0/1 | 14 | 6.2 | 1.6 | 4.21 | 1 |
| 718 | 18.89 | 29.2 | 3.11 | 0/1 | 15 | 8.2 | 2.5 | 3.11 | 1 |
| 720 | 12.17 | 18.96 | 6.74 | 0/1 | 16 | 3.5 | 1.8 | 6.74 | 1 |
| 722 | 15.36 | 21.26 | 9.29 | 0/1 | 17 | 9 | 5.8 | 9.29 | 0/1 |
| 724 | 29.37 | 4.35 | 2.5 | 0/1 | 18 | 3.2 | 0.9 | 2.5 | 0/1 |
| 725 | 33.82 | 7.55 | 6.06 | 1 | 19 | 9.5 | 3.4 | 6.06 | 0/1 |
| 727 | 43.9 | 14.81 | 5.12 | 0/1 | 20 | 2.2 | 0.7 | 5.12 | 0/1 |
| 728 | 41.18 | 7.45 | 2.95 | 0/1 | 21 | 17.5 | 11.2 | 2.95 | 0/1 |
| 729 | 35.71 | 3.51 | 7.57 | 1 | 22 | 0 | 0 | 7.57 | 0/1 |
| 730 | 43.98 | 4.07 | 5.19 | 0/1 | 23 | 3.2 | 1.6 | 5.19 | 0/1 |
| 731 | 24.38 | 16.95 | 7.5 | 0/1 | 24 | 8.7 | 6.7 | 7.5 | 0/1 |
| 732 | 48.5 | 12.72 | 8.08 | 0/1 | 25 | 0 | 0 | 8.08 | 0/1 |
| 733 | 5.98 | 25.31 | 1.79 | 0/1 | 26 | 3.5 | 2.3 | 1.79 | 0/1 |
| 734 | 7.49 | 4.8 | 2.99 | 0/1 | 27 | 0 | 0 | 2.99 | 0/1 |
| 735 | 12.45 | 13.76 | 6.96 | 0/1 | 28 | 0 | 0 | 6.96 | 0/1 |
| 736 | 35.12 | 19.28 | 7.09 | 0/1 | 29 | 2.4 | 0.9 | 7.09 | 0/1 |
| 737 | 11.03 | 12.74 | 5.82 | 0/1 | 30 | 10.6 | 1.9 | 5.82 | 0/1 |
| 738 | 46.84 | 22.32 | 7.47 | 0 | | | | | |
| 740 | 7.41 | 15.54 | 2.94 | 0/1 | | | | | |
| 741 | 31.86 | 22.34 | 4.49 | 1 | | | | | |
| 742 | 12.73 | 24.77 | 7.19 | 0/1 | | | | | |
| 744 | 19.04 | 7.71 | 3.23 | 0/1 | | | | | |
| 775 | 40.6 | 28.64 | 2.48 | 0/1 | | | | | |
| 799 | 5.27 | 19.39 | 1.21 | 0 | | | | | |

Table 6.6: Load data for the IEEE 118-bus test network

| IEEE 118-bus (1) | | | | | IEEE 118-bus (2) | | | | |
|---|---|---|---|---|---|---|---|---|---|
| $i$ | $p^i$ | $q^i$ | $w^i$ | $s^i$ | $i$ | $p^i$ | $q^i$ | $w^i$ | $s^i$ |
| 1 | 51 | 27 | 3.32 | 0/1 | 60 | 78 | 3 | 8.88 | 0/1 |
| 2 | 20 | 9 | 2.89 | 0/1 | 61 | 0 | 0 | 9.11 | 0/1 |
| 3 | 39 | 10 | 1.07 | 0/1 | 62 | 77 | 14 | 3.24 | 1 |
| 4 | 39 | 12 | 9.11 | 0/1 | 63 | 0 | 0 | 2.82 | 0/1 |
| 5 | 0 | 5 | 7.06 | 0/1 | 64 | 0 | 0 | 8.71 | 0/1 |
| 6 | 52 | 22 | 2.66 | 0/1 | 65 | 0 | 0 | 5.94 | 0/1 |
| 7 | 19 | 2 | 3.87 | 0/1 | 66 | 39 | 18 | 2.08 | 0/1 |
| 8 | 28 | 0 | 6.06 | 0/1 | 67 | 28 | 7 | 9.36 | 0/1 |
| 9 | 0 | 0 | 4.47 | 0/1 | 68 | 0 | 0 | 4.78 | 0/1 |
| 10 | 0 | 0 | 7.05 | 0 | 69 | 0 | 0 | 6.02 | 0/1 |
| 11 | 70 | 23 | 8.59 | 0/1 | 70 | 66 | 20 | 4.49 | 0 |
| 12 | 47 | 10 | 4.84 | 1 | 71 | 0 | 0 | 8.23 | 0/1 |
| 13 | 34 | 16 | 9.09 | 0/1 | 72 | 12 | 0 | 8.17 | 0/1 |
| 14 | 14 | 1 | 4.21 | 0/1 | 73 | 6 | 0 | 6.92 | 0/1 |
| 15 | 90 | 30 | 3.11 | 0/1 | 74 | 68 | 27 | 8.18 | 0/1 |
| 16 | 25 | 10 | 6.74 | 0/1 | 75 | 47 | 11 | 5.53 | 0/1 |
| 17 | 11 | 3 | 9.29 | 0/1 | 76 | 68 | 36 | 4.89 | 0/1 |
| 18 | 60 | 34 | 2.5 | 0/1 | 77 | 61 | 28 | 3.21 | 0/1 |
| 19 | 45 | 25 | 6.06 | 0/1 | 78 | 71 | 26 | 1.71 | 0/1 |
| 20 | 18 | 3 | 5.12 | 0 | 79 | 39 | 32 | 9.76 | 0/1 |
| 21 | 14 | 8 | 2.95 | 0/1 | 80 | 130 | 26 | 5.53 | 0/1 |
| 22 | 10 | 5 | 7.57 | 1 | 81 | 0 | 0 | 7.23 | 0/1 |
| 23 | 7 | 3 | 5.19 | 0/1 | 82 | 54 | 27 | 9.15 | 1 |
| 24 | 13 | 0 | 7.5 | 0/1 | 83 | 20 | 10 | 2.02 | 0/1 |
| 25 | 0 | 0 | 8.08 | 0/1 | 84 | 11 | 7 | 2.19 | 0/1 |
| 26 | 0 | 0 | 1.79 | 0/1 | 85 | 24 | 15 | 8.92 | 0/1 |
| 27 | 71 | 13 | 2.99 | 0/1 | 86 | 21 | 10 | 2.34 | 0/1 |
| 28 | 17 | 7 | 6.96 | 0/1 | 87 | 0 | 0 | 2.76 | 0/1 |
| 29 | 24 | 4 | 7.09 | 0/1 | 88 | 48 | 10 | 1.13 | 0/1 |
| 30 | 0 | 0 | 5.82 | 0 | 89 | 0 | 0 | 4.88 | 0/1 |
| 31 | 43 | 27 | 7.47 | 0/1 | 90 | 163 | 42 | 4.35 | 0 |
| 32 | 59 | 23 | 2.94 | 0/1 | 91 | 10 | 0 | 2.72 | 0/1 |
| 33 | 23 | 9 | 4.49 | 0/1 | 92 | 65 | 10 | 2.35 | 1 |
| 34 | 59 | 26 | 7.19 | 0/1 | 93 | 12 | 7 | 7.35 | 0/1 |
| 35 | 33 | 9 | 3.23 | 0/1 | 94 | 30 | 16 | 1.96 | 0/1 |
| 36 | 31 | 17 | 2.48 | 0/1 | 95 | 42 | 31 | 4.55 | 0/1 |
| 37 | 0 | 0 | 1.21 | 0/1 | 96 | 38 | 15 | 9.55 | 0/1 |
| 38 | 0 | 0 | 4.17 | 0/1 | 97 | 15 | 9 | 5.57 | 0/1 |
| 39 | 27 | 11 | 5.7 | 0/1 | 98 | 34 | 8 | 8.43 | 0/1 |
| 40 | 66 | 23 | 7.32 | 0 | 99 | 42 | 0 | 5.82 | 0/1 |
| 41 | 37 | 10 | 8.27 | 0/1 | 100 | 37 | 18 | 1.27 | 0/1 |
| 42 | 96 | 23 | 3.8 | 1 | 101 | 22 | 15 | 1.6 | 0/1 |
| 43 | 18 | 7 | 4.96 | 0/1 | 102 | 5 | 3 | 6.88 | 0/1 |
| 44 | 16 | 8 | 6.04 | 0/1 | 103 | 23 | 16 | 10 | 0/1 |
| 45 | 53 | 22 | 4.84 | 0/1 | 104 | 38 | 25 | 7.19 | 0/1 |
| 46 | 28 | 10 | 8.56 | 0/1 | 105 | 31 | 26 | 8.64 | 0/1 |
| 47 | 34 | 0 | 3.32 | 0/1 | 106 | 43 | 16 | 4.54 | 0/1 |
| 48 | 20 | 11 | 3.95 | 0/1 | 107 | 50 | 12 | 3.11 | 0/1 |
| 49 | 87 | 30 | 4.67 | 0/1 | 108 | 2 | 1 | 2.95 | 0/1 |
| 50 | 17 | 4 | 2.42 | 0 | 109 | 8 | 3 | 1.86 | 0/1 |
| 51 | 17 | 8 | 1.32 | 0/1 | 110 | 39 | 30 | 8.75 | 0 |
| 52 | 18 | 5 | 6.21 | 0/1 | 111 | 0 | 0 | 5.1 | 0/1 |
| 53 | 23 | 11 | 7.35 | 0/1 | 112 | 68 | 13 | 2.29 | 1 |
| 54 | 113 | 32 | 9.04 | 0/1 | 113 | 6 | 0 | 2.27 | 0/1 |
| 55 | 63 | 22 | 8.14 | 0/1 | 114 | 8 | 3 | 4.88 | 0/1 |
| 56 | 84 | 18 | 3.86 | 0/1 | 115 | 22 | 7 | 5.17 | 0/1 |
| 57 | 12 | 3 | 1.58 | 0/1 | 116 | 184 | 0 | 2.45 | 0/1 |
| 58 | 12 | 3 | 1.43 | 0/1 | 117 | 20 | 8 | 5.38 | 0/1 |
| 59 | 277 | 113 | 3.19 | 0/1 | 118 | 33 | 15 | 6.99 | 0/1 |

sponsive loads. We consider five instances that express different system resource flexibility levels. A case study on the modified IEEE 37-bus, 30-bus and 118-bus systems reveals that the more flexible the available restoration resource, the higher the total criticality weighted load pickup. In fact, our most advanced model outperforms previous formulations in terms of the critically weighted load pickup by 20% in the case of the modified 37-bus system, with similar number of actions taken as of lines to open, and optimal placement of the generators.

Future work directions are along two main thrusts. On the methodological side, there are possible gains in performance that can be obtained by leveraging the structure of the formulation and doing post-processing that may result in overall shorter solution times. On the policy side, our current formulation adds a parameter $\alpha$ to explicitly account for the number of actions taken, as part of a weight for the objective function. The restoration of resilient systems may have several objectives instead of a weighted one. These situations are particularly prone to arise when interdependencies with other critical infrastructures are added (see, e.g., [111,112]). In such a case, constraints can be placed on some of the objectives to build a Pareto frontier problem.

# Chapter 7

# A Heuristic Approach to the Post-disturbance Microgrid Formation Problem

## 7.1 Introduction

Microgrid formation is a potential solution in post-disaster electric grid recovery efforts. Recent works propose distribution level microgrid formation models using mixed integer linear programming techniques. However, these models can only be solved for small and medium size power systems due to their computational intractability. In this chapter we introduce a heuristic approach that allows to approximately solve the microgrid formation problem for medium to large, more realistic, instances. Furthermore, the proposed approach allows to approximately solve the stochastic version of the problem, in which the aim is to allocate extra generation capacity to the network to immunize it, as best as possible, against uncertain potential cascading failures. Our results are illustrated by solving versions of the problem on ten IEEE test cases with up to 3012 nodes.

From a conceptual point of view, the deterministic post-disturbance microgrid formation is an operation problem, whereas the uncertain microgrid formation is a planning problem. In fact, after a disturbance, the resulting network configuration is known and the failure is fully determined. The deterministic solution approach provides the best microgrid formation plan for that particular

Table 7.1: Nomenclature(Part A)

| Symbol | Description |
|---|---|
| $\pi^{\omega}$ | probability of scenario $\omega$, $\forall\ \omega \in \Omega$ |
| $b^{ij\omega}$ | switch state variable under scenario $\omega$: 1 if line $(i,j)$ is closed, 0 otherwise, $\forall\ (i,j) \in \mathcal{L},\ \omega \in \Omega$ |
| $c^{ijk\omega}$ | line-to-microgrid assignment variable under scenario $\omega$: 1 if line $(i,j)$ is assigned to microgrid $k$, 0 otherwise, $\forall\ (i,j) \in \mathcal{L},\ k \in \mathcal{K},\ \omega \in \Omega$ |
| $D^{\omega}$ | $\lvert\mathcal{K}\rvert \times \lvert\mathcal{N}\rvert$-distance matrix $D^{\omega}$, $(k,j)$-th element of $D^{\omega}$ represents the distance between the location $n(k)$ of the DG unit $k$ and node $j$ under scenario $\omega$, and $D^{j\omega}$, the $j$-th column of $D^{\omega}$, $\forall\ j \in \mathcal{N}, k \in \mathcal{K},\ \omega \in \Omega$ |
| $d^{i}$ | load dispatchability indicator: 1 if the load at node $i$ is dispatchable, 0 otherwise, $\forall\ i \in \mathcal{N}$ |
| $\delta^{ij\omega}$ | voltage slack variable for line $(i,j)$ under scenario $\omega$, $\forall\ (i,j) \in \mathcal{L},\ \omega \in \Omega$ |
| $\mathcal{K}$ | set of microgrids |
| $\mathcal{K}_{\text{fix}}$ | set of fixed Distributed Generation (DG) units, $\mathcal{K}_{\text{fix}} \subseteq \mathcal{K}$ |
| $\mathcal{K}_{\text{m}}$ | set of mobile or truck-mounted DG units, $\mathcal{K}_{\text{m}} \subseteq \mathcal{K}$ |
| $\mathcal{L}$ | set of lines |
| $\mathcal{L}_{\text{c}}^{\omega}$ | set of lines with faulted closed line switches under scenario $\omega$, $\mathcal{L}_{\text{c}}^{\omega} \subseteq \mathcal{L},\ \forall\ \omega \in \Omega$ |
| $\mathcal{L}_{\text{o}}^{\omega}$ | set of faulted open lines under scenario $\omega$, $\mathcal{L}_{\text{o}}^{\omega} \subseteq \mathcal{L},\ \forall\ \omega \in \Omega$ |
| $\mathcal{L}_{\text{c}}^{k\omega}$ | set of lines with faulted closed line switches in microgrid $k$ under scenario $\omega$, $\mathcal{L}_{\text{c}}^{k\omega} \subseteq \mathcal{L},\ \forall\ k \in \mathcal{K}, \omega \in \Omega$ |
| $\mathcal{L}_{\text{o}}^{k\omega}$ | set of faulted open lines in cluster $k$ under scenario $\omega$, $\mathcal{L}_{\text{o}}^{k\omega} \subseteq \mathcal{L}, \forall\ k \in \mathcal{K}, \omega \in \Omega$ |
| $\mathcal{L}^{k\omega}$ | set of lines under scenario $\omega$ in cluster $k$, $\mathcal{L}^{k\omega} \subseteq \mathcal{L},\ \forall\ k \in \mathcal{K}, \omega \in \Omega$ |
| $\mathcal{M}^{k\omega}$ | graph of the cluster $k$ under scenario $\omega$, $\forall\ k \in \mathcal{K}, \omega \in \Omega$ |
| $\mathcal{N}$ | set of nodes |
| $\mathcal{N}_{\text{c}}^{\omega}$ | set of nodes with faulted closed switches under scenario $\omega$, $\mathcal{N}_{\text{c}}^{\omega} \subseteq \mathcal{N},\ \forall\ \omega \in \Omega$ |
| $n(k)$ | location index of fixed DG unit $k$ |
| $\mathcal{N}_{\text{o}}^{\omega}$ | set of nodes with faulted open switches under scenario $\omega$, $\mathcal{N}_{\text{o}}^{\omega} \subseteq \mathcal{N},\ \forall\ \omega \in \Omega$ |
| $\mathcal{N}_{\text{c}}^{k\omega}$ | set of nodes with faulted closed switches in cluster $k$ under scenario $\omega$, $\mathcal{N}_{\text{c}}^{k\omega} \subseteq \mathcal{N}$, $\forall\ k \in \mathcal{K}, \omega \in \Omega$ |
| $\mathcal{N}_{\text{o}}^{k\omega}$ | set of nodes with faulted open switches in cluster $k$ under scenario $\omega$, $\mathcal{N}_{\text{o}}^{k\omega} \subseteq \mathcal{N}$, $\forall\ k \in \mathcal{K}, \omega \in \Omega$ |
| $p_{\text{d}}^{i\omega}$ | dispatched active load at node $i$ under scenario $\omega$, $\forall\ i \in \mathcal{N}, \omega \in \Omega$ |
| $Pg^{i\omega}$ | dispatched active power generation at node $i$ under scenario $\omega$, $\forall\ i \in \mathcal{N}, \omega \in \Omega$ |
| $p^{i}$ | total active load at node $i$, $\forall\ i \in \mathcal{N}$ |
| $P^{ij\omega}$ | active power flow from node $i$ to node $j$ under scenario $\omega$, $\forall\ (i,j) \in \mathcal{L}, \omega \in \Omega$ |
| $p_{\text{lb}}^{i}$ | minimum demand to serve if the dispatchable load at node $i$ is picked up, $\forall\ i \in \mathcal{N}$ |
| $P_{\text{max}}^{k}$ | active power generation capacity of DG unit $k$, $\forall\ k \in \mathcal{K}$ |
| $P_{\text{min}}^{k}$ | minimum active power of DG unit $k$, $\forall\ k \in \mathcal{K}$ |
| $p_{\text{s}}^{i\omega}$ | served active load at node $i$ under scenario $\omega$, $\forall\ i \in \mathcal{N}, \omega \in \Omega$ |
| $Qg^{i\omega}$ | dispatched reactive power generation at node $i$ under scenario $\omega$, $\forall\ i \in \mathcal{N},\ \omega \in \Omega$ |
| $q^{i}$ | total reactive load at node $i$, $\forall\ i \in \mathcal{N}$ |
| $Q^{ij\omega}$ | reactive power flow from node $i$ to node $j$ under scenario $\omega$, $\forall\ (i,j) \in \mathcal{L},\ \forall\ \omega \in \Omega$ |
| $Q_{\text{max}}^{k}$ | reactive power generation capacity of DG unit $k$, $\forall\ k \in \mathcal{K}$ |
| $Q_{\text{min}}^{k}$ | minimum reactive power of DG unit $k$, $\forall\ k \in \mathcal{K}$ |
| $q_{\text{s}}^{i}$ | served reactive load at node $i$, $\forall\ i \in \mathcal{N}$ |
| $s^{i\omega}$ | load-to-node switch state binary variable under scenario $\omega$: 1 if load at node $i$ is picked up, 0 otherwise, $\forall\ i \in \mathcal{N},\ \omega \in \Omega$ |
| $\Omega$ | set of scenarios |

Table 7.2: Nomenclature(Part B)

| Symbol | Description |
|---|---|
| $T_{\mathrm{P}}^{ij}$ | active transmission capacity of line $(i,j),\ \forall\ (i,j) \in \mathcal{L}$ |
| $T_{\mathrm{Q}}^{ij}$ | reactive transmission capacity of line $(i,j),\ \forall\ (i,j) \in \mathcal{L}$ |
| $V^{i\omega}$ | Voltage magnitude of node $i$ under scenario $\omega,\ \forall\ i \in \mathcal{N},\ \omega \in \Omega$ |
| $v^{ik\omega}$ | node-to-microgrid assignment binary variable under scenario $\omega$: 1 if node $i$ is assigned to microgrid $k$, 0 otherwise, $\forall\ i \in \mathcal{N},\ k \in \mathcal{K},\ \omega \in \Omega$ |
| $V_{\mathrm{o}}$ | nominal voltage magnitude |
| $V_{\mathrm{R}}$ | rated voltage |
| $w^i$ | criticality weight of the load at node $i,\ \forall\ i \in \mathcal{N}$ |
| $z^{ki}$ | DG-to-node assignment variable: 1 if DG unit $k$ is physically connected at node $i$, 0 otherwise, $\forall\ k \in \mathcal{K},\ i \in \mathcal{N}$ |

failure instance. On the other hand, the stochastic solution approach seeks to optimally locate fixed additional DG units within the existing grid while taking into account all potential failures that can affect the power system. In this approach, the grid operator plans for the best locations of the DG units in order to make the system robust to potential failures by using microgrid formation as a resiliency strategy.

Although the deterministic and uncertain versions described above represent two fundamentally different decision problems, from a mathematical point of view, the deterministic microgrid formation problem is a particular instance of the uncertain microgrid formation version of the problem. For the rest of this chapter, we focus on the presentation of the uncertain microgrid formation formulation with the understanding that the deterministic version is derived by reducing the set of failure scenarios to a singleton. In Section 7.5, we present illustrative examples of the effectiveness of the proposed heuristic approach when applied to these two related microgrid formation problems.

The remainder of this chapter is structured as follows. Section 7.2 describes and formulates the microgrid formation problem from both a deterministic and a stochastic point of view. Section 7.3 presents the case study set-up. Section 7.4 evaluates the proposed models on ten IEEE-based test cases and discusses the results obtained. Section 7.5 provides some concluding remarks.

## 7.2 Model and Solution Approach

### 7.2.1 Uncertain microgrid formation model

We extend the formulation in [92] to consider a problem in which the power network failure scenario is uncertain, and the aim is to allocate additional generation capacity throughout the

network (within capacity constraints), and set microgrid formation plans, in order to maximize the expected load pick up after a network failure. We assume that the information about the uncertain failures is provided in the form of a finite set of scenarios $\Omega$, with known probability of occurrence $\pi^{\omega} \forall \omega \in \Omega$. Furthermore, we represent the available additional generation capacity in the form of mobile DG units. In this way, the model can be seen as a generalization of the microgrid formation problem considered in [16]. However, in this version of the problem, it is assumed that the location of these additional generation capacity units will remain fixed regardless of the realized failure scenario. The DG units represent additional capacity added to the network to make it more resilient. In this two-stage stochastic programming, locations of DG units are first stage variables while other variables including voltages, served loads, power flow and formation of microgrids are second stage variables. All the second stage variables bear the corresponding scenario index $\omega$, for all $\omega \in \Omega$. The objective function (7.1) is the expected total criticality weighted load across all scenarios.

Constraints (7.2) and (7.3) assign DG units and nodes to microgrids. The set of constraints (7.4) through (7.6) define the load dispatch levels and (7.7) through (7.9) are node microgrid formation constraints. Nodal balance constraints (7.10) and (7.11), line flow constraints (7.12) and (7.13), generation placement and dispatch constraints (7.14) through (7.15), voltage constraints (7.16) through (7.19), and post-disturbance constraints (7.20) and (7.21) complete the formulation.

$$\max : \sum_{\omega \in \Omega} \pi^{\omega} \sum_{i \in \mathcal{N}} w^i p_{\mathrm{s}}^{i\omega} \tag{7.1}$$

subject to:

$$\sum_{i \in \mathcal{N}} z^{ki} = 1, \forall\ k \in \mathcal{K} \tag{7.2}$$

$$\sum_{k \in \mathcal{K}} z^{ki} \leq 1, \forall\ i \in \mathcal{N} \tag{7.3}$$

$$d^i p_{\mathrm{lb}}^i + (1 - d^i) p^i \leq p_{\mathrm{d}}^{i\omega} \leq p^i, \forall\ i \in \mathcal{N},\ \omega \in \Omega \tag{7.4}$$

$$\begin{aligned} & p_{\mathrm{s}}^{i\omega} \leq s^{i\omega} p^i, && \forall\ i \in \mathcal{N},\ \omega \in \Omega \\ & 0 \leq p_{\mathrm{s}}^{i\omega} \leq p_{\mathrm{d}}^{i\omega}, && \forall\ i \in \mathcal{N},\ \omega \in \Omega \\ & p_{\mathrm{s}}^{i\omega} \geq p_{\mathrm{d}}^{i\omega} - (1 - s^{i\omega}) p^i, && \forall\ i \in \mathcal{N},\ \omega \in \Omega \end{aligned} \tag{7.5}$$

$$q_{\mathrm{s}}^{i\omega} = \frac{q^i}{p^i} p_{\mathrm{s}}^{i\omega}, \forall\ i \in \mathcal{N} : p^i \neq 0,\ \omega \in \Omega \tag{7.6}$$

$$\sum_{k \in \mathcal{K}} v^{ik\omega} = 1, \forall\ i \in \mathcal{N},\ \omega \in \Omega \tag{7.7}$$

$$\begin{aligned} & v^{ik\omega} \geq z^{ki}, && \forall\ i \in \mathcal{N},\ k \in \mathcal{K},\ \omega \in \Omega \\ & c^{ijk\omega} \leq v^{ik\omega}, && \forall\ k \in \mathcal{K},\ (i,j) \in \mathcal{L},\ \omega \in \Omega \\ & c^{ijk\omega} \leq v^{jk\omega}, && \forall\ k \in \mathcal{K},\ (i,j) \in \mathcal{L},\ \omega \in \Omega \\ & c^{ijk\omega} \geq v^{ik\omega} + v^{jk\omega} - 1, && \forall\ k \in \mathcal{K},\ (i,j) \in \mathcal{L},\ \omega \in \Omega \end{aligned} \tag{7.8}$$

$$b^{ij\omega} = \sum_{k \in \mathcal{K}} c^{ijk\omega}, \forall\ (i,j) \in \mathcal{L},\ \omega \in \Omega \tag{7.9}$$

$$\sum_{j:(j,i)\in\mathcal{L}} P^{ji\omega} - \sum_{j:(i,j)\in\mathcal{L}} P^{ij\omega} + Pg^{i\omega} - p_{\mathrm{s}}^{i\omega} = 0, \forall\ i \in \mathcal{N},\ \omega \in \Omega \tag{7.10}$$

$$\sum_{j:(j,i)\in\mathcal{L}} Q^{ji\omega} - \sum_{j:(i,j)\in\mathcal{L}} Q^{ij\omega} + Qg^{i\omega} - q_{\mathrm{s}}^{i\omega} = 0, \forall\ i \in \mathcal{N},\ \omega \in \Omega \tag{7.11}$$

$$-T_P^{ij} b^{ij\omega} \leq P^{ij\omega} \leq T_P^{ij} b^{ij\omega}, \forall\ (i,j) \in \mathcal{L},\ \omega \in \Omega \tag{7.12}$$

$$-T_Q^{ij} b^{ij\omega} \leq Q^{ij\omega} \leq T_Q^{ij} b^{ij\omega}, \forall\ (i,j) \in \mathcal{L},\ \omega \in \Omega \tag{7.13}$$

$$\sum_{k \in \mathcal{K}} z^{ki} P_{\min}^{k} \leq Pg^{i\omega} \leq \sum_{k \in \mathcal{K}} z^{ki} P_{\max}^{k}, \forall\ i \in \mathcal{N},\ \omega \in \Omega \tag{7.14}$$

$$\sum_{k \in \mathcal{K}} z^{ki} Q_{\min}^{k} \leq Qg^{i\omega} \leq \sum_{k \in \mathcal{K}} z^{ki} Q_{\max}^{k},\ \forall\ i \in \mathcal{N},\ \omega \in \Omega \tag{7.15}$$

$$V^{i\omega} = V^{i\omega} + \frac{r^{ij} P^{ij\omega} + x^{ij} Q^{ij\omega}}{V_o} + \delta^{ij\omega},\ \forall\ (i,j) \in \mathcal{L},\ \omega \in \Omega \tag{7.16}$$

$$V_o \sum_{k \in \mathcal{K}} z^{ki} \leq V^{i\omega} \leq V_o, \forall\ i \in \mathcal{N},\ \omega \in \Omega \tag{7.17}$$

$$(-1 + b^{ij\omega}) V_o \leq \delta^{ij\omega} \leq (1 - b^{ij\omega}) V_o,\ \forall\ (i,j) \in \mathcal{L},\ \omega \in \Omega \tag{7.18}$$

$$(1 - \epsilon) V_R \leq V^{i\omega} \leq (1 + \epsilon) V_R,\ \forall\ i \in \mathcal{N},\ \omega \in \Omega \tag{7.19}$$

$$\begin{aligned} b^{ij\omega} &= 1, \quad \forall\ (i,j) \in \mathcal{L}_{\mathrm{c}}^{\omega},\ \omega \in \Omega \\ b^{ij\omega} &= 0, \quad \forall\ (i,j) \in \mathcal{L}_{\mathrm{o}}^{\omega},\ \omega \in \Omega \end{aligned} \tag{7.20}$$

$$\begin{aligned} s^{i\omega} &= 1, \quad \forall\ i \in \mathcal{N}_{\mathrm{c}}^{\omega},\ \omega \in \Omega \\ s^{i\omega} &= 0, \quad \forall\ i \in \mathcal{N}_{\mathrm{o}}^{\omega},\ \omega \in \Omega \end{aligned} \tag{7.21}$$

$$z^{kn(k)} = 1, \forall\ k \in \mathcal{K}_{\mathrm{fix}}. \tag{7.22}$$

We get the deterministic microgrid formation model (cf., equations (1) - (6), (9) - (19) and (20) - (24) in [92]) formulation by simply dropping the scenario index $\omega$. In other words, the scenario set $\Omega$, in the deterministic case, is reduced to a singleton. The single scenario has a probability $\pi^1 = 1$.

### 7.2.2 Heuristic Solution Approach

The microgrid formation problem, under failure scenario $\omega$ for all $\omega \in \Omega$, can be defined as a clustering problem with flow and connectivity constraints. The objective is to cluster the set of vertices $\mathcal{N}$ into $|\mathcal{K}|$ microgrids [84]. However, even with predetermined DG units locations, forming all $|\mathcal{K}|$ microgrids simultaneously using an MILP approach is computationally expensive [92] and cannot be solved for medium to large network instances. For a more tractable solution approach, we propose the heuristic approximation presented in Fig. 7.1.

To obtain an approximate solution to the problem in a reduced time, we decompose the problem into three stages: *1)* Locate the mobile DG units, *2)* Partition the network based on the DG

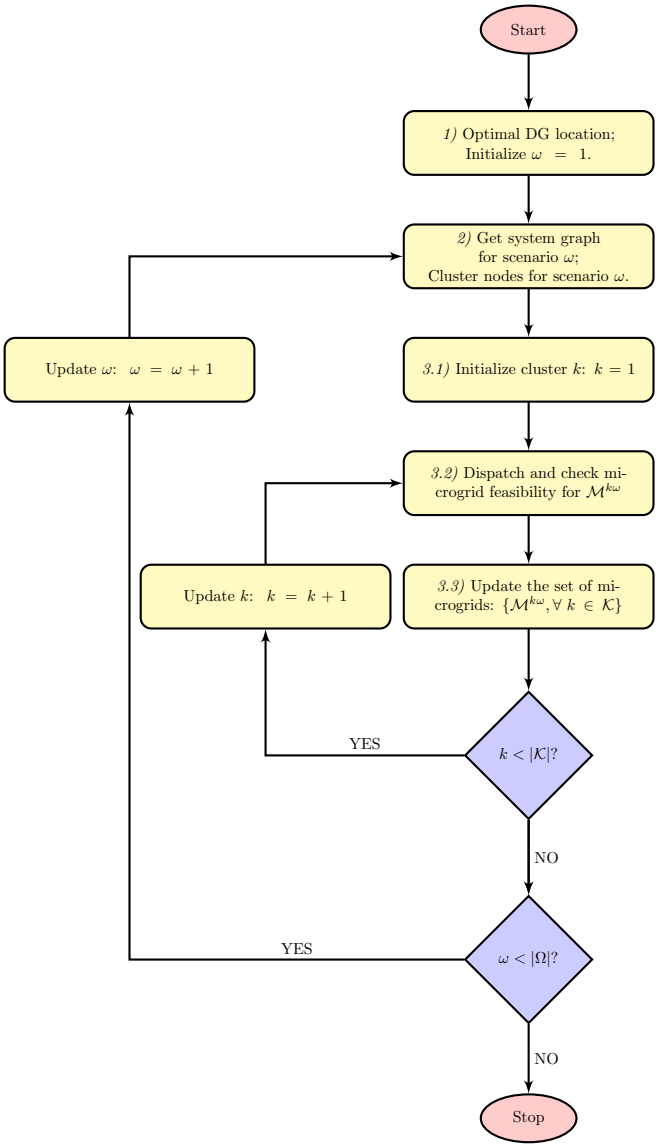


Figure 7.1: Flowchart of the microgrid formation algorithm

unit locations, and *3)* Assess operational feasibility and load pickup (comprising the steps *3.1*, *3.2* and *3.3* in Fig. 7.1).

### The DG Units Location Model

In this stage, the mobile DG units are placed, taking into account the location of fixed DG units and post-disturbance network conditions such as line and node switch outages and hardened lines. The objective is to maximize the total criticality weighted load pickup. This objective is satisfied within the boundaries of load dispatch constraints (7.4) through (7.6), nodal balance

constraints (7.10) and (7.11), line flow constraints (7.12) and (7.13), generation placement and dispatch constraints (7.14) through (7.15), voltage constraints (7.16) through (7.19), and post disturbance constraints (7.20) and (7.21). The main goal of this model is to locate mobile DG units according to the actual *load distribution* across the aftermath grid, taking into account demand responsive or dispatchable loads. Hence, the first stage model can be summarized as follows:

max : (7.1)

subject to:

Constraints (7.2)-(7.6), and (7.10)-(7.22).

There are no node clustering variables and constraints (i.e., (7.7) - (7.9)) in this first stage model. Whereas the uncertain failure MILP model of section 7.2.1 solves the DG unit placement and microgrid formation problems concurrently, the optimal DG unit location stage focuses only on locating the DG units. The DG unit locations obtained in the first stage model serve as centroids for the node clustering stage (see Fig. 7.1).

**Microgrid Formation Algorithm**

Once the first stage problem is solved, that is, the value of $z^{ki}$ is known for all $i \in \mathcal{N}$ and $k \in \mathcal{K}$, we define $n(k)$ as the bus $i$ where DG unit $k$ is located for all $k \in \mathcal{K}$. The aim of the second stage model is to cluster the non-isolated nodes into microgrids around the locations of the DG units set in the first stage. This clustering is based on the k-means concept. Nodes are clustered around DG nodes considered as centroids.

For that purpose, for each scenario $\omega \in \Omega$, we consider a $|\mathcal{K}| \times |\mathcal{N}|$-distance matrix $D^{\omega}$ such that $(k, j)$-th element of $D^{\omega}$ is the distance between the location $n(k)$ of the DG unit $k$ and the node $j$ for all $j \in \mathcal{N}$. Here, we define the term *distance* as the shortest path measured in number of edges between two nodes. For simplicity, we designate by $D^{j\omega} \in \mathbb{R}^{|\mathcal{K}|}$, the $j$-th column of $D^{\omega}$. Thus, a node $j$ is assigned to a microgrid $\mathcal{M}^{k\omega}$ if the condition of equation (7.23) is satisfied, for all $k \in \mathcal{K}$. The graph of the microgrid $\mathcal{M}^{k\omega}$ is defined by the sets of nodes and lines $\mathcal{N}^{k\omega} \subseteq \mathcal{N}$ and $\mathcal{L}^{k\omega} \subseteq \mathcal{L}$, respectively (see equations (7.24) and (7.25)).

$$k = \text{argmin}\{D^{j\omega}\}. \tag{7.23}$$

$$\mathcal{N}^{k\omega} = \{j \in \mathcal{N} : k = \text{argmin}\{D^{j\omega}\}\}, \tag{7.24}$$

$$\mathcal{L}^{k\omega} = \{(i,j) \in \mathcal{L} : i \in \mathcal{N}^{k\omega} \text{ and } j \in \mathcal{N}^{k\omega}\}. \tag{7.25}$$

This stage yields a set of microgrids $\mathcal{M}^{k\omega}$ that are used in the feasibility study in the next stage, for all $k \in \mathcal{K}$ and $\omega \in \Omega$.

**Dispatch and Feasibility Assessment**

It is important to assess how feasible the microgrids formed in the second stage are, under power systems operation constraints, in order to determine the corresponding generation dispatch and load pickup. At this stage, the model presented in (7.1) through (7.22) is customized as (7.26) through (7.43) to decide which load to serve within each microgrid $\mathcal{M}^{k\omega}$, that is, (7.26) - (7.43) is solved for all $k \in \mathcal{K}$ and $\omega \in \Omega$.

$$\max : \sum_{i \in \mathcal{N}^{k\omega}} w^i p_{\text{s}}^{i\omega} \tag{7.26}$$

subject to:

$$\sum_{i \in \mathcal{N}^{k\omega}} z^{ki} = 1, \tag{7.27}$$

$$d^i p_{\text{lb}}^i + (1 - d^i)p^i \leq p_{\text{d}}^{i\omega} \leq p^i, \forall\ i \in \mathcal{N}^{k\omega} \tag{7.28}$$

$$\begin{aligned} & p_{\text{s}}^{i\omega} \leq s^{i\omega} p^i, && \forall\ i \in \mathcal{N}^{k\omega} \\ & 0 \leq p_{\text{s}}^{i\omega} \leq p_{\text{d}}^{i\omega}, && \forall\ i \in \mathcal{N}^{k\omega} \\ & p_{\text{s}}^{i\omega} \geq p_{\text{d}}^{i\omega} - (1 - s^{i\omega})p^i, && \forall\ i \in \mathcal{N}^{k\omega} \end{aligned} \tag{7.29}$$

$$q_{\text{s}}^{i\omega} = \frac{q^i}{p^i} p_{\text{s}}^{i\omega}, \forall\ i \in \mathcal{N}^{k\omega} : p^i \neq 0 \tag{7.30}$$

$$\sum_{j:(j,i) \in \mathcal{L}^{k\omega}} P^{ji\omega} - \sum_{j:(i,j) \in \mathcal{L}^{k\omega}} P^{ij\omega} + Pg^{i\omega} - p_{\text{s}}^{i\omega} = 0, \forall\ i \in \mathcal{N}^{k\omega} \tag{7.31}$$

$$\sum_{j:(j,i) \in \mathcal{L}^{k\omega}} Q^{ji\omega} - \sum_{j:(i,j) \in \mathcal{L}^{k\omega}} Q^{ij\omega} + Qg^{i\omega} - q_{\text{s}}^{i\omega} = 0, \forall\ i \in \mathcal{N}^{k\omega} \tag{7.32}$$

$$-T_P^{ij} b^{ij\omega} \leq P^{ij\omega} \leq T_P^{ij} b^{ij\omega}, \forall\ (i,j) \in \mathcal{L}^{k\omega} \tag{7.33}$$

$$-T_Q^{ij} b^{ij\omega} \leq Q^{ij\omega} \leq T_Q^{ij} b^{ij\omega}, \forall\ (i,j) \in \mathcal{L}^{k\omega} \tag{7.34}$$

$$z^{ki} P_{\text{min}}^k \leq Pg^{i\omega} \leq z^{ki} P_{\text{max}}^k, \forall\ i \in \mathcal{N}^{k\omega} \tag{7.35}$$

$$z^{ki}Q^k_{\min} \leq Qg^{i\omega} \leq z^{ki}Q^k_{\max}, \forall\ i \in \mathcal{N}^{k\omega} \tag{7.36}$$

$$V^{i\omega} = V^{j\omega} + \frac{r^{ij}P^{ij\omega} + x^{ij}Q^{ij\omega}}{V_o} + \delta^{ij\omega}, \quad \forall\ (i,j) \in \mathcal{L}^{k\omega} \tag{7.37}$$

$$V_o z^{ki} \leq V^{i\omega} \leq V_o, \forall\ i \in \mathcal{N}^{k\omega} \tag{7.38}$$

$$(-1 + b^{ij\omega})V_o \leq \delta^{ij\omega} \leq (1 - b^{ij\omega})V_o, \forall\ (i,j) \in \mathcal{L}^{k\omega} \tag{7.39}$$

$$(1-\epsilon)V_R \leq V^{i\omega} \leq (1+\epsilon)V_R, \quad \forall\ i \in \mathcal{N}^{k\omega} \tag{7.40}$$

$$\begin{aligned} b^{ij\omega} &= 1, \quad \forall\ (i,j) \in \mathcal{L}^{\omega}_{\mathrm{c}} \\ b^{ij\omega} &= 0, \quad \forall\ (i,j) \in \mathcal{L}^{\omega}_{\mathrm{o}} \end{aligned} \tag{7.41}$$

$$\begin{aligned} s^{i\omega} &= 1, \quad \forall\ i \in \mathcal{N}^{\omega}_{\mathrm{c}} \\ s^{i\omega} &= 0, \quad \forall\ i \in \mathcal{N}^{\omega}_{\mathrm{o}} \end{aligned} \tag{7.42}$$

$$z^{kn(k)} = 1, \forall\ k \in \mathcal{K}_{\mathrm{fix}}.^{1} \tag{7.43}$$

There are two main differences between the formulation presented by (7.26) through (7.43) and the single scenario version of (7.1)–(7.22) (see also (1) - (6), (9) - (19) and (20) - (24) in [92]): ($a$) this model deals with only one microgrid at a time whereas the model in [92] concurrently solves multiple microgrids, and ($b$) no node-to-microgrid variable is needed since all nodes considered in one round (i.e., $i \in \mathcal{N}^{k\omega}$) are all part of the same partition.

## 7.3 Case Study

In order to evaluate the effectiveness of our proposed methodology, we present a series of case studies in this section. We generate failure scenarios and compare our proposed heuristic approach with the MILP solution approach, that is solving (7.1) - (7.22) directly with a MILP solver.

### 7.3.1 Scenario Generation Using Cascading Descent System

To generate the potential failure scenarios, we use the cascading failure model proposed in [113]. The steps to generate the cascading failure scenarios are as follows:

[1] In the stochastic heuristic formulation, all DG unit locations found in 7.2.2 are fixed. Thus, after the step ($a$) in Fig. 7.1, $\mathcal{K}_{\mathrm{fix}} \equiv \mathcal{K}$. However, in the deterministic formulation, $\mathcal{K}_{\mathrm{fix}}$ remains unchanged. The DG units are allowed to "move" in the dispatch and feasibility analysis phase (step $c$).

1. Initially set loads, generators outputs, and power flows in order to maximize criticality weighted load under OPF constraints with the full power system.

2. Let the lines be broken with:

$$\text{Prob}\{\text{line } (i,j) \text{ becomes outaged}\} = h_1 \max\left\{\frac{|P^{ij}|}{T_{\text{P}}^{ij}}, \frac{|Q^{ij}|}{T_{\text{Q}}^{ij}}\right\}, \tag{7.44}$$

   where $h_1$ is a positive number. Reference [113] suggests using $h_1 = 0.001$ for lines that are not overloaded and $h_1 = 0.3$ for lines that are overloaded. Instead of two values for $h_1$, we use a uniform value for all the lines in the network as shown in Table 7.5.

3. Reset loads, generators outputs, and power flows to adjust to line outages.

4. Let the lines be broken according to rule (7.44).

5. If the system is balanced, stop and use remaining lines to get one scenario. If not, go back to step 3.

From (7.44) we know that lines with higher fractional load are more likely to fail. This is reasonable as lines with high load experience thermal stress and are more likely to be outaged. Steps 1-5 give us the dynamics of a cascade and how line outages interact with new power flow to continue the cascading process. The scenario set obtained feeds the uncertain microgrid formation model.

In our experiments, we simulate the above cascading descent system 1000 times to get the possible scenarios set. Repeated scenarios are collected into a single one with an appropriate cumulative probability value. Because we only care about disruptive scenarios, only scenarios in which at least one line has failed are considered.

### 7.3.2 Case Data and Analysis

To evaluate the effectiveness of the proposed methodology for the microgrid formation problem, we compare in Tables 7.3 and 7.4 the solution obtained by the heuristic approach outlined in Section 7.2.2 (designated by *Heur.*) to those obtained from directly solving the two-stage stochastic MILP presented in Section 7.2.1. We consider 10 test cases. These cases are adapted from MATPOWER case files to reflect post-disturbance scenarios [102]. In each scenario, there are line outages, generator outages, and line and node switch failures. The network size varies from 30 to 3012 buses. For the deterministic version (see Table 7.3), the singleton post-disaster scenario sets considered in the 30-bus and 118-bus systems are the same as the failure cases studied in [92].

To evaluate the performance of the proposed heuristic, we consider the criticality weighted load served (i.e., the objective function), the computation time, and the resource allocation efficiency (RAE). The latter metric is defined as the portion of the total available restoration resource (TARR) that is used to serve loads in the resulting microgrid configuration. TARR is taken here as the total available DG unit's capacity. The total load served (TLS) is a byproduct of the resource allocation models. The resource allocation efficiency is given by:

$$\text{RAE}(\%) = \frac{\text{TLS}}{\text{TARR}} \times 100. \tag{7.45}$$

## 7.4 Results and Discussion

We discuss our findings with regard to the use of our heuristic approach to approximately solve both the deterministic and uncertain versions of the microgrid formation problem. The models are implemented in `Python`, solved using `Gurobi 7.0.2` and tested on an Intel computer Core i7-4770HQ with 2.20 GHz frequency and 16 GB RAM memory. Unless otherwise stated, the MIP gap is set to 1% for the MILP models.

### 7.4.1 Deterministic Failure Cases

Table 7.3 compares the MILP approach (i.e., solving the singleton version of (7.1) - (7.22)) to the proposed heuristic (*Heur.*) for each of the study cases from 30 to 3012-bus systems across three performance metrics, namely, *computation time*, *objective value*, and *total load served* (TLS or interchangeably RAE).

Across all 10 cases, the MILP approach is more computationally expensive than the heuristic. The computation time for the MILP approach tends to increase very rapidly with the network size. The MILP is even unsolvable for the 2383-bus and 3012-bus cases because time limit is reached. In these two cases, Table 7.3 provides the upper bounds reached in 10 hours of computation. A 2%-suboptimal solution is achieved in 3 hours on the 1354-bus system. On the other hand, the largest solution time of the heuristic is less than 15 minutes. Fig. 7.3 compares the solution times.

When it comes to the criticality weighted load pickup (the objective value), the MILP solution is optimal and provides an upper bound to the heuristic which achieves a suboptimal solution in less computation time. The average optimality gap found across the test cases 30 through 300-bus is 7.82%, with a maximum of 24.92% in the 57-bus case and a minimum of 0% in the 30-bus case.

Table 7.3: Case study results: Deterministic formulation

| Case | Time (s) | | Objective | | TLS (kW)[1] | | TARR[2] |
|---|---|---|---|---|---|---|---|
| | MIP | Heur | MIP | Heur | MIP | Heur | (kW) |
| 30-bus | 1.37 | 0.10 | 691.25 | 691.25 | 135.90 | 135.90 | 150.00 |
| 39-bus | 0.49 | 0.10 | 5,240.60 | 4,945.18 | 724.00 | 747.60 | 750.00 |
| 57-bus | 23.15 | 0.11 | 5,078.68 | 3,813.00 | 983.10 | 724.10 | 1,000.00 |
| 89-bus | 18.27 | 0.35 | 9,322.83 | 8,001.45 | 1,100.00 | 1,050.00 | 1,100.00 |
| 118-bus | 61.00[3] | 0.44 | 8,325.31 | 7,796.58 | 1,245.00 | 1,203.00 | 1,250.00 |
| 145-bus | 51.21 | 0.76 | 8,251.80 | 7,425.26 | 1,146.00 | 1036.42 | 1,150.00 |
| 300-bus | 15.56 | 5.10 | 16,587.60 | 16,330.50 | 1,850.00 | 1,801.00 | 1,850.00 |
| 1354-bus | 11,079.48 | 43.44 | 29,817.50[3] | 29,845.70 | 3,084.30 | 3,085.00 | 3,085.00 |
| 2383-bus | 36,000.00 | 868.23 | 28,887.19[4] | 28,017.90 | * | 3,107.78 | 3,340.00 |
| 3012-bus | 36,000.00 | 864.31 | 31,249.49[4] | 30,248.90 | * | 3,397.27 | 3,400.00 |

[1] Total load served
[2] Total available restoration resource or total DG capacity
[3] Best integer solution at 2% optimality gap
[4] Best upper bound

Table 7.4: Case study results: Stochastic formulation

| Case | Time (s) | | Objective | | TLS (kW) | | TARR |
|---|---|---|---|---|---|---|---|
| | MIP | Heur | MIP | Heur | MIP | Heur | (kW) |
| 30-bus | 160.60 | 0.81 | 621.37 | 543.20 | 113.34 | 95.07 | 150.00 |
| 39-bus | 1,229.24 | 1.68 | 6,457.12 | 6021.40 | 749.19 | 724.18 | 750.00 |
| 57-bus | 165.84 | 3.21 | 4,163.26 | 3,752.62 | 764.84 | 687.70 | 1,000.00 |
| 89-bus | 7,383.33 | 11.80 | 9,629.49 | 7,767.20 | 1,053.70 | 862.21 | 1,100.00 |
| 118-bus | 36,000.00 | 94.20 | 9,765.13[1]- 10,330.13[2] | 9,127.50 | * | 1,160.18 | 1,250.00 |
| 145-bus | 36,000.00 | 155.31 | 4,730.72[1]- 10,227.78[2] | 8,542.64 | * | 1,086.37 | 1,150.00 |
| 300-bus | 6,335.08 | 68.18 | 16,404.90 | 16,303.00 | 1,833.00 | 1,833.00 | 1,850.00 |

[1] Best lower bound
[2] Best upper bound

There is a tighter variation in the resource allocation efficiency (cf., (7.45)) metric. From Fig. 7.2, we can see that the RAE gap between the MILP and the heuristic solutions is on average 5.09% with a maximum of 25.90% in the 57-bus case. In terms of RAE, the heuristic outperforms the MILP model in cases 39 and 1354-bus.[2] Overall, the MILP solution achieves 97.82% RAE whereas the proposed heuristic achieves 92.73% on cases 30 through 1354-bus, and 93.48% across all 10 cases.

### 7.4.2 Uncertain Failure Cases

Table 7.4 compares the stochastic MILP approach (i.e., solving (7.1)-(7.22)) to the proposed stochastic heuristic approach for cases from 30 to 300-bus systems across three performance metrics, namely, *computation time*, *objective value*, and *total load served*. Table 7.5 provides the number of

[2]Since RAE is not the objective function, this does not mean that *Heur.* is optimal.

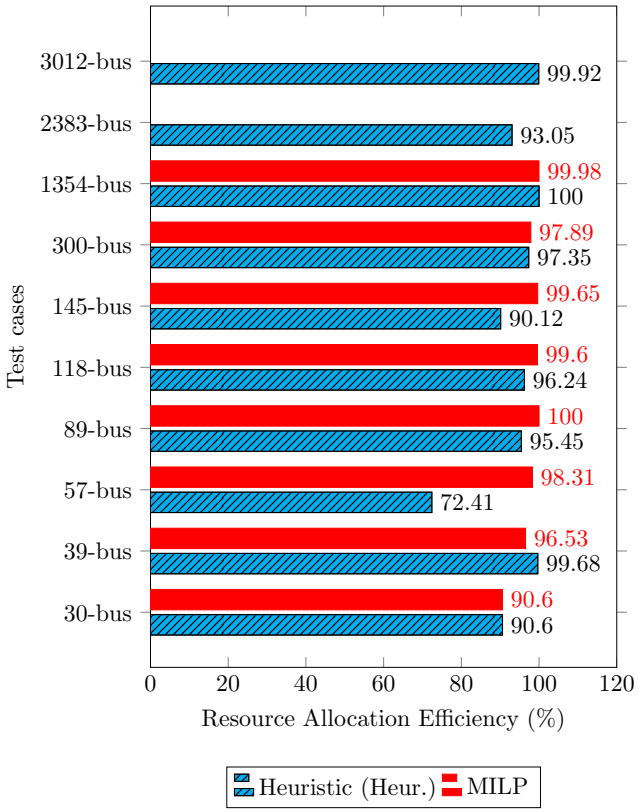


Figure 7.2: Resource allocation comparison: Deterministic formulation

scenarios and corresponding parameters for each case.

For all of these 7 cases, the stochastic MILP approach is much more computationally expensive than the stochastic heuristic approach. For the 145-bus system, the solver does not converge even in 10 hours with the stochastic MILP approach whereas we can get a sub-optimal solution with the stochastic heuristic in 155.31 seconds.

When comparing criticality weighted load pickup, the stochastic MILP approach offers an upper bound for the stochastic heuristic approach with less computational time. The average optimal objective gap is 9.83%, with a maximum of 19.34% in the 89-bus system and a minimum of 0.08% in the 300-bus system.

When considering RAE, none of the approaches is outstanding. This is reasonable as the location assignment of additional DG units is based on various scenarios. Moreover, the power system is heavily sabotaged in some scenarios. However from Fig. 7.4, we see that the RAE of the stochastic heuristic approach is close to the stochastic MILP approach which is much more computationally expensive. The average gap between these two approaches is 8.33%, with a maximum of 17.42% in the 89-bus system and a minimum of 0% in the 300-bus system.

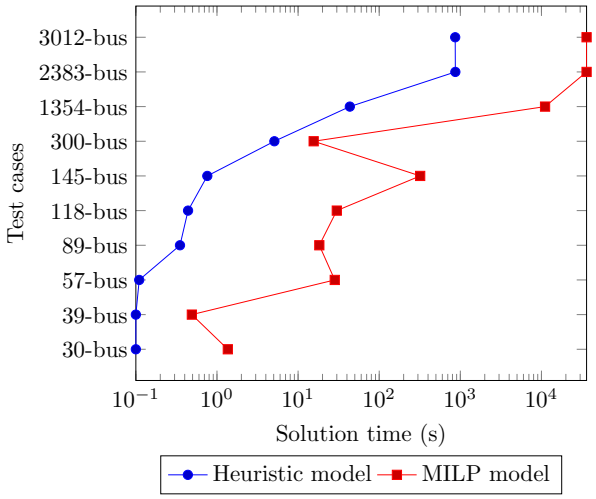


Figure 7.3: Solution time comparison: deterministic formulation

Table 7.5: Information of Scenarios

| Case | No. of scenarios | $h$ value |
|---|---|---|
| 30-bus | 8 | 0.10 |
| 39-bus | 14 | 0.10 |
| 57-bus | 13 | 0.10 |
| 89-bus | 19 | 0.10 |
| 118-bus | 8 | 0.05 |
| 145-bus | 6 | 0.05 |
| 300-bus | 5 | 0.05 |

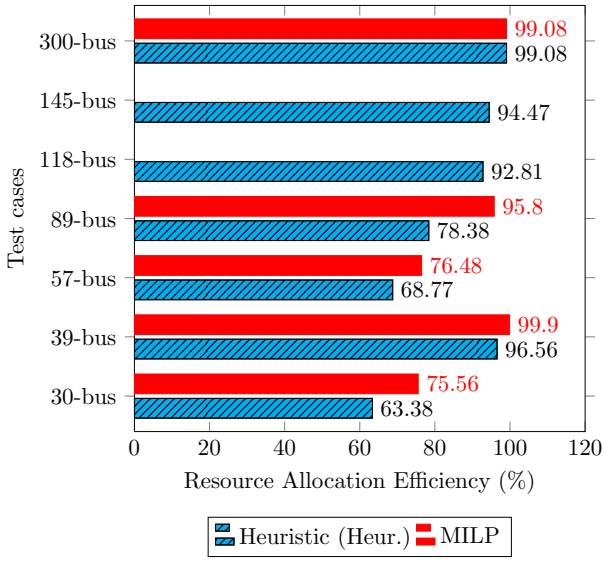


Figure 7.4: Resource allocation comparison: Stochastic formulation

## 7.5 Conclusion

In this chapter, we approach the post-disaster grid recovery problem using microgrid formation from two perspectives. We propose a deterministic or after-the-matter model, and a stochastic or

before-the-matter model. The first solves an operations problem whereas the second deals with a planning problem. More importantly, for both versions of the problem, we propose a heuristic method that makes the solution process tractable. The heuristic approach reaches 8%-suboptimal solution on average, 10 to 100s times faster than the traditional MILP approach, and achieving 93% resource allocation efficiency on average. The stochastic heuristic approach reaches 10%-suboptimal solution on average, 50 to 150 times faster than the stochastic MILP approach. For both large and small systems, stochastic MILP is much more computational expensive compared to the stochastic heuristic approach. In future work we envision to include the restoration time and task scheduling in the post-disaster grid recovery optimization problem. This would take into account interdependencies among all critical infrastructures (e.g., bridges, roads, towers and poles) that may affect the restoration process.

# Chapter 8

# Conclusion

This dissertation work has demonstrated that all grid participants share a vital role in maintaining grid reliability and resiliency. Chapters 2 through 4 concentrate on how to design retail pricing mechanisms that implicitly beckon end-users to undertake and active role in shaping their demand after a desired supply profile. In fact, our proposed Minimax pricing scheme has much potential for electricity peak demand management. In addition to improving the load factor and reducing the peak demand, it lowers the consumers's daily bill, providing enough incentive for consumers to adopt it. Case studies prove that Minimax pricing outperforms well-known schemes such as Time-of-Use and Real-time pricing. Chapter 3 pinpoints the importance of load aggregation in reliable grid operation under dynamic retail pricing. It clearly proves that under Minimax, massive load aggregation is a win-win game. By pooling more deferrable loads together, demand response programs or third party group load control systems are likely to experience more flexibility and achieve an increased reliability. Chapter 4 generalizes the concept presented in Chapter 2 into a scheme designated by GenMinimax. Consumers, under GenMinimax, have the opportunity or the power to reduce their energy rate by reducing or increasing their demand because the energy rate is not only time dependent, it is also demand dependent. Case studies show that consumers are able to follow closely the reference supply profile sent by a single aggregator as a solution to her own profit maximization problem given anticipated market conditions, with 5% maximum error and less than 2% average error. Clearly, price responsiveness of demand is key under the future smart grid paradigm where higher renewable penetrations are expected. Future work should concentrate on implementing the proposed schemes in quasi-realistic settings in order to derive behavioral parameters that would potentially hinder their expected impacts and engineer ways to hedge against

possible drawbacks.

In Chapter 5, we note that there is a value in introducing a short-term reserve market for both the system operator and renewable energy farms. The system operator gains in securing additional generation capacity to pull from whenever necessary for balancing purposes. The simulation case study shows that there is a financial incentive for renewable energy farms to participate in the short-term reserve market. In the particular case studied, the induced risk range increase does not result in profit decrease. The profit increased by 5%. As we witness more renewable grid penetration, in addition to long-term capacity contracts, short-term reserve markets would be critical for a reliable system operation. Future work may use a comprehensive data-driven approach to better calibrate the two-stage stochastic model proposed in order to derive more realistic practical insight for the short-term reserve market design.

In Chapters 6 & 7, the post-disturbance grid restoration is considered. The proposed microgrid formation model aims to restore critical loads after a large external disturbance, while satisfying post-disaster and operational constraints within each microgrid. The model applies to general power network topologies, including radial and meshed configurations, and integrates demand responsive loads as well as mobile emergency generation units. Case studies with different flexibility levels across several electric network cases reveal that the more flexible the available restoration resource, the higher the total criticality weighted load pickup. Chapter 7 proposes a heuristic algorithm purposed at reducing the solution time of the microgrid formation problem. It also introduces a stochastic or before-the-matter model that is designed to deal with the restoration problem in its emergency preparedness version. The heuristic approach reaches 8%-suboptimal solution on average, 10 to 100s times faster than the traditional MILP approach, and achieving 93% resource allocation efficiency on average. The stochastic heuristic approach reaches 10%-suboptimal solution on average, 50 to 150 times faster than the stochastic MILP approach. For both large and small systems, stochastic MILP (Chapters 6) is much more computational expensive compared to the stochastic heuristic approach. In this area, future directions should consider interdependencies among critical infrastructures that might affect the power systems. In addition, inter-temporal features along with the cranking process of conventional generation units need to be accounted for.

# Bibliography


[1] E. O. of the President, "Economic benefits of increasing electric grid resilience to weather outages-august 2013."

[2] M. E. Baran and F. F. Wu, "Network reconfiguration in distribution systems for loss reduction and load balancing," *IEEE Transactions on Power delivery*, vol. 4, no. 2, pp. 1401–1407, 1989.

[3] U. E. I. Administration, "Electric power annual 2010 technical report," Nov 2011.

[4] A. Mishra, D. Irwin, P. Shenoy, J. Kurose, and T. Zhu, "Smartcharge: cutting the electricity bill in smart homes with energy storage," in *Proceedings of the 3rd International Conference on Future Energy Systems: Where Energy, Computing and Communication Meet.* ACM, 2012, p. 29.

[5] D. Cauchon, "Household electricity bills skyrocket," *USA Today*, 2011.

[6] I. Koutsopoulos, V. Hatzi, and L. Tassiulas, "Optimal energy storage control policies for the smart power grid," in *Smart Grid Communications (SmartGridComm), 2011 IEEE International Conference on.* IEEE, 2011, pp. 475–480.

[7] T. Carpenter, S. Singla, P. Azimzadeh, and S. Keshav, "The imapct of electricity pricing schemes on storage adoption in ontario," in *Proceedings of eEnergy*, May 2012.

[8] S. Govindan, A. Sivasubramaniam, and B. Urgaonkar, "Benefits and limitations of tapping into stored energy for datacenters," in *Computer Architecture (ISCA), 2011 38th Annual International Symposium on.* IEEE, 2011, pp. 341–351.

[9] O. E. Board, "Electricity prices," 2012. [Online]. Available: http://www.ontarioenergyboard.ca/OEB/Consumers

[10] S. G. I. Clearinghouse, "Legistration and regulation," 2011. [Online]. Available: http://www.sgiclearinghouse.org/Legistration?q=node/1705

[11] M. Ilic, J. W. Black, E. Fumagalli, P. Visudhiphan, and J. L. Watz, "Understanding demand: The missing link in efficient electricity markets," *Energy Lab. Pub., Tech. Rep*, 2001.

[12] H. Parmesano, "Rate design is the no. 1 energy efficiency tool," *The Electricity Journal*, vol. 20, no. 6, pp. 18–25, 2007.

[13] M. H. Albadi and E. El-Saadany, "Demand response in electricity markets: An overview," in *IEEE power engineering society general meeting*, vol. 2007, 2007, pp. 1–5.

[14] D. S. Kirschen, "Demand-side view of electricity markets," *Power Systems, IEEE Transactions on*, vol. 18, no. 2, pp. 520–527, 2003.

[15] P. Gas, "Electric company,commercially available aggregator programs in california, 2011."

[16] L. Gkatzikis, I. Koutsopoulos, and T. Salonidis, "The role of aggregators in smart grid demand response markets," *Selected Areas in Communications, IEEE Journal on*, vol. 31, no. 7, pp. 1247–1257, 2013.

[17] S. Barsali, M. Ceraolo, R. Giglioli, and D. Poli, "Aggregation and management of the demand in a deregulated electricity market," in *Power Tech Conference Proceedings, 2003 IEEE Bologna*, vol. 4. IEEE, 2003, pp. 4–pp.

[18] B. J. Kirby, "Spinning reserve from responsive loads," ORNL, Tech. Rep., 2003.

[19] E. Hirst and B. Kirby, *Retail-load participation in competitive wholesale electricity markets*. Citeseer, 2001.

[20] E. Hirst, "Barriers to price-responsive demand in wholesale electricity markets," *Edison Electric Institute*, 2002.

[21] S. Borenstein, M. Jaske, and A. Rosenfeld, "Dynamic pricing, advanced metering, and demand response in electricity markets," 2002.

[22] A. Faruqui, S. Sergici, and L. Akaba, "The impact of dynamic pricing on residential and small commercial and industrial usage: New experimental evidence from connecticut." *Energy Journal*, vol. 35, no. 1, 2014.

[23] S. Borenstein and S. P. Holland, "On the efficiency of competitive electricity markets with time-invariant retail prices," National Bureau of Economic Research, Tech. Rep., 2003.

[24] K. S. Sedzro, M. C. Chuah, and A. J. Lamadrid, "Minimax: an incentive-driven pricing scheme in the electricity retail market," in *Modeling and Simulation of Cyber-Physical Energy Systems (MSCPES), 2015 Workshop on*. IEEE, 2015, pp. 1–6.

[25] G. Dutta, K. Mitra *et al.*, "Dynamic pricing of electricity: A survey of related research," Indian Institute of Management Ahmedabad, Research and Publication Department, Tech. Rep., 2015.

[26] S. Borenstein, "The long-run efficiency of real-time electricity pricing," *The Energy Journal*, pp. 93–116, 2005.

[27] K. Spees and L. B. Lave, "Demand response and electricity market efficiency," *The Electricity Journal*, vol. 20, no. 3, pp. 69–85, 2007.

[28] J. McDonald and K. Lo, "Dynamic price structures and consumer load reaction," in *Metering Apparatus and Tariffs for Electricity Supply, 1990., Sixth International Conference on*. IET, 1990, pp. 6–10.

[29] C. Triki and A. Violi, "Dynamic pricing of electricity in retail markets," *4OR*, vol. 7, no. 1, pp. 21–36, 2009.

[30] F. Wolak, "Designing a competitive wholesale market that benefits costumers," *Dept. of Economics, University of Stanford, working paper*, 2001.

[31] Z. Zhou, F. Zhao, and J. Wang, "Agent-based electricity market simulation with demand response from commercial buildings," *IEEE Transactions on Smart Grid*, vol. 2, no. 4, pp. 580–588, 2011.

[32] J. M. López-Lezama, A. Padilha-Feltrin, J. Contreras, and J. I. Muñoz, "Optimal contract pricing of distributed generation in distribution networks," *IEEE Transactions on Power Systems*, vol. 26, no. 1, pp. 128–136, 2011.

[33] R. Fernández-Blanco, J. M. Arroyo, and N. Alguacil, "A unified bilevel programming framework for price-based market clearing under marginal pricing," *IEEE Transactions on Power Systems*, vol. 27, no. 1, pp. 517–525, 2012.

[34] G. E. Asimakopoulou, A. L. Dimeas, and N. D. Hatziargyriou, "Leader-follower strategies for energy management of multi-microgrids," *IEEE transactions on smart grid*, vol. 4, no. 4, pp. 1909–1916, 2013.

[35] B. Colson, P. Marcotte, and G. Savard, "An overview of bilevel optimization," *Annals of operations research*, vol. 153, no. 1, pp. 235–256, 2007.

[36] S. Dempe, "Annotated bibliography on bilevel programming and mathematical programs with equilibrium constraints," 2003.

[37] S. J. Kazempour, A. J. Conejo, and C. Ruiz, "Strategic bidding for a large consumer," *IEEE Transactions on Power Systems*, vol. 30, no. 2, pp. 848–856, 2015.

[38] B. F. Hobbs, C. B. Metzler, and J.-S. Pang, "Strategic gaming analysis for electric power systems: An mpec approach," *IEEE transactions on power systems*, vol. 15, no. 2, pp. 638–645, 2000.

[39] R. Herranz, A. M. San Roque, J. Villar, and F. A. Campos, "Optimal demand-side bidding strategies in electricity spot markets," *IEEE Transactions on power systems*, vol. 27, no. 3, pp. 1204–1213, 2012.

[40] A. G. Thomas, P. Jahangiri, D. Wu, C. Cai, H. Zhao, D. C. Aliprantis, and L. Tesfatsion, "Intelligent residential air-conditioning system with smart-grid functionality," *IEEE Transactions on Smart Grid*, vol. 3, no. 4, pp. 2240–2251, 2012.

[41] M. Parvania, M. Fotuhi-Firuzabad, and M. Shahidehpour, "Optimal demand response aggregation in wholesale electricity markets," *IEEE Transactions on Smart Grid*, vol. 4, no. 4, pp. 1957–1965, 2013.

[42] C. Chen, S. Kishore, Z. Wang, M. Alizadeh, and A. Scaglione, "How will demand response aggregators affect electricity markets?a cournot game analysis," in *Communications Control and Signal Processing (ISCCSP), 2012 5th International Symposium on.* IEEE, 2012, pp. 1–6.

[43] J. L. Mathieu, M. Kamgarpour, J. Lygeros, G. Andersson, and D. S. Callaway, "Arbitraging intraday wholesale energy market prices with aggregations of thermostatic loads," *IEEE Transactions on Power Systems*, vol. 30, no. 2, pp. 763–772, 2015.

[44] K. S. Sedzro, A. J. Lamadrid, and M. C. Chuah, "The value of aggregation under minimax pricing scheme in the electricity retail market," in *Power and Energy Society General Meeting (PESGM), 2016.* IEEE, 2016, pp. 1–5.

[45] J. P. Fershee, "Changing resources, changing market: The impact of a national renewable portfolio standard on the us energy industry," *Energy Law Journal*, vol. 29, no. 1, 2008.

[46] D. A. Halamay, T. K. Brekken, A. Simmons, and S. McArthur, "Reserve requirement impacts of large-scale integration of wind, solar, and ocean wave power generation," *IEEE Transactions on Sustainable Energy*, vol. 2, no. 3, pp. 321–328, 2011.

[47] H. Holttinen, "Optimal electricity market for wind power," *Energy Policy*, vol. 33, no. 16, pp. 2052–2063, 2005.

[48] G. N. Bathurst, J. Weatherill, and G. Strbac, "Trading wind generation in short term energy markets," *IEEE Transactions on Power Systems*, vol. 17, no. 3, pp. 782–789, 2002.

[49] J. Usaola and J. Angarita, "Bidding wind energy under uncertainty," in *2007 International Conference on Clean Electrical Power.* IEEE, 2007, pp. 754–759.

[50] I. Marti, G. Kariniotakis, P. Pinson, I. Sanchez, T. Nielsen, H. Madsen, G. Giebel, J. Usaola, A. M. Palomares, R. Brownsword *et al.*, "Evaluation of advanced wind power forecasting models–results of the anemos project," in *European Wind Energy Conference, EWEC 2006*, 2006, pp. 9–pages.

[51] Y. V. Makarov, C. Loutan, J. Ma, and P. De Mello, "Operational impacts of wind generation on california power systems," *IEEE Transactions on Power Systems*, vol. 24, no. 2, pp. 1039–1050, 2009.

[52] E. D. Castronuovo and J. P. Lopes, "On the optimization of the daily operation of a wind-hydro power plant," *IEEE Transactions on Power Systems*, vol. 19, no. 3, pp. 1599–1606, 2004.

[53] J. Matevosyan and L. Soder, "Minimization of imbalance cost trading wind power on the short-term power market," *IEEE Transactions on Power Systems*, vol. 21, no. 3, pp. 1396–1404, 2006.

[54] J. M. Morales, A. J. Conejo, and J. Pérez-Ruiz, "Short-term trading for a wind power producer," *IEEE Transactions on Power Systems*, vol. 25, no. 1, pp. 554–564, 2010.

[55] A. Botterud, J. Wang, R. Bessa, H. Keko, and V. Miranda, "Risk management and optimal bidding for a wind power producer," in *IEEE PES General Meeting*. IEEE, 2010, pp. 1–8.

[56] P. Pinson, C. Chevallier, and G. N. Kariniotakis, "Trading wind generation from short-term probabilistic forecasts of wind power," *IEEE Transactions on Power Systems*, vol. 22, no. 3, pp. 1148–1156, 2007.

[57] N. C. Petruzzi and M. Dada, "Pricing and the newsvendor problem: A review with extensions," *Operations Research*, vol. 47, no. 2, pp. 183–194, 1999.

[58] C. J. Dent, J. W. Bialek, and B. F. Hobbs, "Opportunity cost bidding by wind generators in forward markets: Analytical results," *IEEE Transactions on Power Systems*, vol. 26, no. 3, pp. 1600–1608, 2011.

[59] E. Y. Bitar, R. Rajagopal, P. P. Khargonekar, K. Poolla, and P. Varaiya, "Bringing wind energy to market," *IEEE Transactions on Power Systems*, vol. 27, no. 3, pp. 1225–1235, 2012.

[60] R. Campbell, "Weather-related power outages and electric system resiliency. congressional research service," in *Library of Congress*, 2012.

[61] A. M. Salman, Y. Li, and M. G. Stewart, "Evaluating system reliability and targeted hardening strategies of power distribution systems subjected to hurricanes," *Reliability Engineering & System Safety*, vol. 144, pp. 319–333, 2015.

[62] N. C. for Environmental Information, "Billion-dollar weather and climate disaster: Overview."

[63] N.-A. E. R. Corporation, "State of reliability 2015."

[64] R. Billinton, L. Salvaderi, J. D. McCalley, H. Chao, T. Seitz, R. N. Allan, J. Odom, and C. Fallon, "Reliability issues in today's electric power utility environment," *IEEE Transactions on Power Systems*, vol. 12, no. 4, pp. 1708–1714, Nov 1997.

[65] D. T. Ton and W. P. Wang, "A more resilient grid: The us department of energy joins with stakeholders in an r&d plan," *IEEE Power and Energy Magazine*, vol. 13, no. 3, pp. 26–34, 2015.

[66] P. J. Maliszewski and C. Perrings, "Factors in the resilience of electrical power distribution infrastructures," *Applied Geography*, vol. 32, no. 2, pp. 668 – 679, 2012. [Online]. Available: http://www.sciencedirect.com/science/article/pii/S0143622811001524

[67] W. Yuan, J. Wang, F. Qiu, C. Chen, C. Kang, and B. Zeng, "Robust optimization-based resilient distribution network planning against natural disasters," *IEEE Transactions on Smart Grid*, vol. 7, no. 6, pp. 2837–2848, 2016.

[68] Edison, "Before and after the storm," Edison Electric Institute, Tech. Rep., 2014.

[69] M. Panteli and P. Mancarella, "Modeling and evaluating the resilience of critical electrical power infrastructure to extreme weather events," *IEEE Systems Journal*, vol. PP, no. 99, pp. 1–10, 2015.

[70] S. Ma, B. Chen, and Z. Wang, "Resilience enhancement strategy for distribution systems under extreme weather events," *IEEE Transactions on Smart Grid*, 2016.

[71] R. Sarkar, A. Gusrialdi, and Z. Qu, "An adaptive restorative method for resilient power distribution networks," in *Power and Energy Society General Meeting (PESGM), 2016.* IEEE, 2016, pp. 1–5.

[72] M. Choobineh and S. Mohagheghi, "Emergency electric service restoration in the aftermath of a natural disaster," in *Global Humanitarian Technology Conference (GHTC), 2015 IEEE.* IEEE, 2015, pp. 183–190.

[73] C.-C. Liu, S. J. Lee, and S. Venkata, "An expert system operational aid for restoration and loss reduction of distribution systems," *IEEE Transactions on Power Systems*, vol. 3, no. 2, pp. 619–626, 1988.

[74] F. Ren, M. Zhang, D. Soetanto, and X. Su, "Conceptual design of a multi-agent system for interconnected power systems restoration," *IEEE Transactions on Power Systems*, vol. 27, no. 2, pp. 732–740, 2012.

[75] T. Nagata and H. Sasaki, "A multi-agent approach to power system restoration," *IEEE Transactions on power systems*, vol. 17, no. 2, pp. 457–462, 2002.

[76] D. S. Kirschen and T. L. Volkmann, "Guiding a power system restoration with an expert system," *IEEE Transactions on Power Systems*, vol. 6, no. 2, pp. 558–566, 1991.

[77] Z. Wang and J. Wang, "Self-healing resilient distribution systems based on sectionalization into microgrids," *IEEE Transactions on Power Systems*, vol. 30, no. 6, pp. 3139–3149, 2015.

[78] H. Farzin, M. Fotuhi-Firuzabad, and M. Moeini, "Enhancing power system resilience through hierarchical outage management in multi-microgrids," *IEEE Transactions on Smart Grid*, vol. 7, no. 6, pp. 2869–2879, 2016.

[79] G. Davis, A. F. Snyder, and J. Mader, "The future of distribution system resiliency," in *Power Systems Conference (PSC), 2014 Clemson University*. IEEE, 2014, pp. 1–8.

[80] Z. Tan, R. Fan, Y. Liu, and L. Sun, "Microgrid black-start after natural disaster with load restoration using spanning tree search," in *Power and Energy Society General Meeting (PESGM), 2016*. IEEE, 2016, pp. 1–5.

[81] H. Gao, Y. Chen, Y. Xu, and C.-C. Liu, "Resilience-oriented critical load restoration using microgrids in distribution systems," *IEEE Transactions on Smart Grid*, vol. 7, no. 6, pp. 2837–2848, 2016.

[82] J. P. Lopes, C. Moreira, F. Resende *et al.*, "Microgrids black start and islanded operation," in *15th Power systems computation conference (PSCC), Liege*, 2005.

[83] P. Murinelli Pesoti, E. V. de Lorenci, A. C. Zambroni de Souza, K. L. Lo, and B. I. Lima Lopes, "Robustness area technique developing guidelines for power system restoration," *Energies*, vol. 10, no. 1, p. 99, 2017.

[84] C. Chen, J. Wang, F. Qiu, and D. Zhao, "Resilient distribution system by microgrids formation after natural disasters," *IEEE Transactions on Smart Grid*, vol. 7, no. 2, pp. 958–966, 2016.

[85] S. Lei, J. Wang, C. Chen, and Y. Hou, "Mobile emergency generator pre-positioning and real-time allocation for resilient response to natural disasters," *IEEE Transactions on Smart Grid*.

[86] N. Abi-Samra, J. McConnach, S. Mukhopadhyay, and B. Wojszczyk, "When the bough breaks: Managing extreme weather events affecting electrical power grids," *IEEE Power and Energy Magazine*, vol. 12, no. 5, pp. 61–65, 2014.

[87] X. Liu, M. Shahidehpour, Y. Cao, Z. Li, and W. Tian, "Risk assessment in extreme events considering the reliability of protection systems," *IEEE Transactions on Smart Grid*, vol. 6, no. 2, pp. 1073–1081, 2015.

[88] L. Che, M. Khodayar, and M. Shahidehpour, "Only connect: Microgrids for distribution system restoration," *IEEE Power and Energy Magazine*, vol. 12, no. 1, pp. 70–81, 2014.

[89] S. Liu, Y. Hou, C.-C. Liu, and R. Podmore, "The healing touch: Tools and challenges for smart grid restoration," *IEEE Power and Energy Magazine*, vol. 12, no. 1, pp. 54–63, 2014.

[90] R. Eskandarpour, H. Lotfi, and A. Khodaei, "Optimal microgrid placement for enhancing power system resilience in response to weather events," in *North American Power Symposium (NAPS), 2016*. IEEE, 2016, pp. 1–6.

[91] U. D. of Energy, "Hurricane irma and hurricane harvey event summary."

[92] K. S. A. Sedzro, A. J. Lamadrid, and L. F. Zuluaga, "Allocation of resources using a microgrid formation approach for resilient electric grids," *IEEE Transactions on Power Systems*, 2017.

[93] Y. Wang, C. Chen, J. Wang, and R. Baldick, "Research on resilience of power systems under natural disasters: A review," *IEEE Transactions on Power Systems*, vol. 31, no. 2, pp. 1604–1613, 2016.

[94] D. N. Trakas and N. D. Hatziargyriou, "Optimal distribution system operation for enhancing resilience against wildfires," *IEEE Transactions on Power Systems*, 2017.

[95] A. Gholami, T. Shekari, F. Aminifar, and M. Shahidehpour, "Microgrid scheduling with uncertainty: the quest for resilience," *IEEE Transactions on Smart Grid*, vol. 7, no. 6, pp. 2849–2858, 2016.

[96] W. Su, J. Wang, and J. Roh, "Stochastic energy scheduling in microgrids with intermittent renewable energy resources," *IEEE Transactions on Smart Grid*, vol. 5, no. 4, pp. 1876–1883, 2014.

[97] V. Mohan, J. G. Singh, and W. Ongsakul, "An efficient two stage stochastic optimal energy and reserve management in a microgrid," *Applied Energy*, vol. 160, pp. 28–38, 2015.

[98] A. Mishra, D. Irwin, P. Shenoy, and T. Zhu, "Scaling distributed energy storage for grid peak reduction," in *Proceedings of the fourth international conference on Future energy systems*. ACM, 2013, pp. 3–14.

[99] R. Chang and C. Lu, "Feeder reconfiguration for load factor improvement," in *Power Engineering Society Winter Meeting, 2002, IEEE.*

[100] M. Pipattanasomporn, M. Kuzlu, S. Rahman, and Y. Teklu, "Load profiles of selected major household appliances and their demand resposne opportunities," in *IEEE Transaction on SmartGrid*, vol. 5, March 2014.

[101] D. E. M. Bondy, G. T. Costanzo, K. Heussen, and H. W. Bindner, "Performance assessment of aggregation control services for demand response," in *Innovative Smart Grid Technologies Conference Europe (ISGT-Europe), 2014 IEEE PES.* IEEE, 2014, pp. 1–6.

[102] R. D. Zimmerman, C. E. Murillo-Sánchez, and R. J. Thomas, "Matpower: Steady-state operations, planning, and analysis tools for power systems research and education," *IEEE Transactions on power systems*, vol. 26, no. 1, pp. 12–19, 2011.

[103] H. Lu, W. Jeon, T. Mount, and A. J. Lamadrid, "Can energy bids from aggregators manage deferrable demand efficiently?" in *System Sciences (HICSS), 2015 48th Hawaii International Conference on.* IEEE, 2015, pp. 2530–2539.

[104] J. Fortuny-Amat and B. McCarl, "A representation and economic interpretation of a two-level programming problem," *Journal of the operational Research Society*, pp. 783–792, 1981.

[105] P. Faria and Z. Vale, "Demand response in electrical energy supply: An optimal real time pricing approach," *Energy*, vol. 36, no. 8, pp. 5374–5384, 2011.

[106] M. H. Albadi and E. El-Saadany, "A summary of demand response in electricity markets," *Electric power systems research*, vol. 78, no. 11, pp. 1989–1996, 2008.

[107] O. E. Board, "Electricity prices," *Ontario Energy Board*, 2012.

[108] L. V. Snyder and Z.-J. M. Shen, *Fundamentals of supply chain theory.* John Wiley & Sons, 2011.

[109] W. H. O. Institution, "Historical data for station 32012 - woods hole stratus wave station."

[110] A. Lamadrid, D. Shawhan, C. Murillo-Sanchez, R. Zimmerman, Y. Zhu, D. Tylavsky, A. Kindle, and Z. Dar, "Stochastically optimized, carbon-reducing dispatch of storage, generation, and loads," *Power Systems, IEEE Transactions on*, vol. 30, no. 2, pp. 1064 – 1075, 2015.

[111] L. Dueñas-Osorio and A. Kwasinski, "Quantification of lifeline system interdependencies after the 27 february 2010 mw 8.8 offshore maule, chile, earthquake," *Earthquake Spectra*, vol. 28, no. S1, pp. S581–S603, 2012. [Online]. Available: http://dx.doi.org/10.1193/1.4000054

[112] D. Martinelli, G. P. Cimellaro, V. Terzic, and S. Mahin, "Analysis of economic resiliency of communities affected by natural disasters: The bay area case study," *Procedia Economics and Finance*, vol. 18, pp. 959–968, 2014. [Online]. Available: http://www.sciencedirect.com/science/article/pii/S2212567114010235

[113] D. Bienstock, *Electrical Transmission System Cascades and Vulnerability: An Operations Research Viewpoint*. SIAM, 2015.

# Vita

Born on Saturday (*which is why he's named Kwami*) October 24, 1981 in Mission-Tove (South Togo, West Africa) to an elementary school principal Yaovi Misadzi M. Sedzro and a seamstress Adzo Fidelia Sedzro, Kwami Senam A. Sedzro is the youngest of a 10-kid family. He attended the Public Primary School of Mission-Tove (EPP Mission-Tove) from 1988 to 1994, the Middle School of Mission-Tove/Kovie (CEG MTK) from 1994 to 1998 and the Tsevie High School (Lytse) from 1998 to 2001. After his Baccalaureate degree in 2001, Kwami joined the prestigious High National College for Engineers (ENSI, the only one engineering college in the country back then) of the University of Lome where he obtained his Bachelor and Master of Science in Electrical Engineering in July 2006 and his Master in Engineering Sciences (with concentration in Electrical Engineering) in April 2010. Before enrolling at Lehigh University in 2013, Kwami Sedzro served as: Electrical Systems Engineer at System Africa 2000 (2006 - 2007), Adjunct Professor at High National College for Engineers (2007 - 2013), and Senior Energy Consultant at K&P Group (2009 - 2013). During his soon-to-end journey at Lehigh, he earned a Master of Engineering in Energy Systems in 2014 and joined the P.C. Rossin College of Engineering (Lehigh University) from where he is expecting a PhD in Electrical Engineering.

Kwami Sedzro is a P.C. Rossin fellow, a recipient of the prestigious Fulbright Scholarship Award and of the Dean's Doctoral Assistantship.

His passion for power and energy systems led him as a Research Assistant to: LONG Lab where he developed and implemented a multiple AC source interconnection system as an Add-on to the existing DOE's IREP DC microgrid, WiNS Lab where he designed Minimax (a novel retail pricing scheme to increase reliability and efficient grid operation), and PORT Lab where he worked on grid resiliency and reliability solutions such as GenMinimax, post-disaster grid restoration and renewable market integration. Kwami also lent his expertise and thirst to learn to leading companies. He worked for PJM (a Regional Transmission Organization serving 13 US. states and

Washington DC) as an intern in Summer 2016 (Outage Analysis Technologies department) and in Summer 2017 (Generation department). During his time at PJM, Kwami developed power system and data integrity management, and abnormality detection tools. Furthermore, he was involved in energy efficiency auditing and consulting with B. Braun Medical Inc. and many other companies.

Besides all the above, along with his supportive wife Perla, Kwami holds a full-time position: he is father of three adorable boys (Othniel, Nathan and Ethan) and a precious girl (Alva).